Aus dem Zentrum für Biomaterialentwicklung,
Institut für Polymerforschung,
GKSS Forschungszentrum GmbH

Physical Crosslinking of Gelatin: A Supramolecular Approach to Biomaterials

Dissertation
zur Erlangung des akademischen Grades
"doctor rerum naturalium"
(Dr. rer. nat.)
in der Wissenschaftsdisziplin
"Materialien in den Lebenswissenschaften"

eingereicht an der
Mathematisch-Naturwissenschaftlichen Fakultät
der Universität Potsdam

von
Alessandro Zaupa
aus Cassano Magnago, Italien

Potsdam, den 10.11.2010

Published online at the
Institutional Repository of the University of Potsdam:
URL http://opus.kobv.de/ubp/volltexte/2011/5288/
URN urn:nbn:de:kobv:517-opus-52888
http://nbn-resolving.de/urn:nbn:de:kobv:517-opus-52888

Gutachter: Prof. Dr. Andreas Lendlein, Universität Potsdam
Prof. Dr. Klaus von der Mark, Universität Erlangen-Nürnberg
Prof. Prof. Dr. Gerd Multhaup, Freien Universität Berlin

Tag der Annahme der Dissertation: 10.11.2010
Tag der Disputation: 07.06.2011

This work was partially financed by the
Deutschen Forschungsgemeinschaft (DFG)
Through the SFB 760 subproject B5

Physical Crosslinking of Gelatin: A Supramolecular Approach to Biomaterials

Summary

The ageing societies and the change of lifestyle led to an increase in the number of patients who suffer from injuries and degenerating diseases resulting in tissue damage or malfunctioning. The undisturbed biological repair mechanisms often leads to scarring, and in many cases, a full functional regeneration of tissue is not achieved. Regenerative Medicine aims to support the biological regeneration while preventing scarring. One approach in this context is material induced autoregeneration, where a biomaterial temporarily substitutes for the extracellular matrix (ECM) at a defect site, and is subsequently replaced by functional neotissue. Key properties that a biomaterial should address include mechanical properties close to the substituted tissue, specific adhesion of cells, and tailorable degradability. Generally the use of biopolymers from the ECM as basis for such biomaterials is highly desirable but challenging due to difficulties in tailoring and controlling the material properties.

In this study, a knowledge-based approach was used to investigate the systematic variation of material properties of gelatin by introducing functional groups engaging in specific physical interactions using a combination of modeling studies and synthetic methods.

Gelatin was selected as non-immunogenic and degradable derivative of the ECM component collagen, and control of material properties was achieved by incorporation of aromatic residues derived from tyrosine, which can potentially form π-π interactions as well as hydrogen bonds even under physiological conditions and enable the formation of a supramolecular organization to obtain stable physically crosslinked networks. Thereby, a material consisting only of biologically derived compounds was designed which aimed at ensuring low cytotoxicity and high biocompatibility.

Molecular models of gelatin-based materials formed the basis for the knowledge-based design of a physically cross-linked polymer system. The molecular dynamics (MD) simulations using the second generation forcefield CFF91 of models with 0.8 wt.-% or 25 wt.-% water content were validated by comparison of the calculated structural properties with pre-available experimental data for pure gelatin such as density, backbone conformation angle distribution, and X-ray scattering spectra. The models for the modified gelatin were then used as predictive tools to study chain organization, cross-link formation, and their influence on the swelling behavior. The introduced tyrosine derived side groups, desaminotyrosine (DAT) and desaminotyrosyl tyrosine (DATT), led to the reduction of the residual helical conformation and to the formation of physical net-points by π–π interactions and hydrogen bonds. A key result of the simulations was the prediction that increasing the number of aromatic functions attached to the gelatin chain leads to an increase in the number of physical netpoints observed in the simulated bulk packing models, which by comparison with the Flory-Rehner model suggested reduced equilibrium swelling by factor 6 of the functionalized materials in water. This prediction was confirmed by the afterwards performed experimental work. The reduction and control of the equilibrium degree of swelling in water is a key criterion for the applicability of functionalized gelatins e.g. as matrices for induced autoregeneration of tissues. The functionalized gelatins could be synthesized by chemoselective coupling of the free carboxylic acid groups of DAT and DATT to the amino groups of gelatin. At 25 wt.-% water content, the simulated and experimentally determined elastic mechanical properties (e.g. Young Modulus) were in the same order of magnitude and were not influenced by the degree of aromatic modification. The experimental equilibrium degree of swelling in water decreased with increasing the number of inserted aromatic functions (from 2800 vol.-% for pure gelatin to 300 vol.-% for the DATT modified gelatin). The measured mechanical properties Young's modulus, elongation at break, and maximum tensile strength for the gels

in their equilibrium state of swelling, however increased with the number of introduced aromatic modifier groups.

The single and triple helical organization of protein chains strongly influences the mechanical properties of gelatin-based materials. A chemical method for obtaining different degrees of helical organization in gelatin is the chemical functionalization described above, while a physical method for achieving the same goal is the variation of the drying conditions of gelatin solutions. Therefore, it was explored how the introduction of DAT and DATT linked to amino groups of gelatin influenced the kinetics and thermodynamic equilibrium of the renaturation process of single and triple helices following different drying conditions. Drying at a temperature above the helix-to-coil transition temperature of gelatin ($T > T_c$, called v_{short} treatment) generally resulted in gelatins with relatively lower triple helical content ($X_{c,t}$ = 1 – 2 %) than lower temperature drying ($T < T_c$, called v_{long} treatment) ($X_{c,t}$ = 8 – 10 %), where the DAT(T)-functional groups generally disrupted helix formation. While different helical contents affected the thermal transition temperatures only slightly, the mechanical properties were strongly affected for swollen hydrogels (E = 4 – 13 kPa for samples treated by v_{long} and E = 120 – 700 kPa for samples treated by v_{short}). Altogether, the functionalization of gelatin with DAT or DATT strongly reduced the tendency of the materials to form triple helices, which however could be fine tuned by altering drying conditions in the production of films. In this way, the mechanical properties of the materials could be tailored in two ways.

Combining gelatins functionalized with DAT or DATT with hydroxyapatite (HAp) led to the formation of composite materials with much lower swelling ratio than of the pure matrices. Shifts of IR bands related to the free carboxyl groups could be observed in the presence of HAp, which suggested a direct interaction of matrix and filler that formed additional physical crosslinks in the material. In tensile tests and rheological measurements, the composites equilibrated in water had increased Young's moduli (from 200 kPa up to 2 MPa) and tensile strength (from 57 kPa up to 1.1 MPa) compared to the matrix polymers without affecting the

elongation at break. Furthermore, an increased thermal stability from 40 °C to 85 °C of the networks could be demonstrated. The differences of the behavior of the functionalized gelatins to pure gelatin as matrix suggested an additional stabilizing bond between the incorporated aromatic groups to the hydroxyapatite as supported by the IR results. The composites can potentially be applied as bone fillers

.

Physikalische Quervernetzung von Gelatine: Ein supramolekularer Zugang zu Biomaterialien

Zusammenfassung

Der Anstieg der Lebenserwartung und die Änderungen des Lebensstils haben zu einer Zunahme an Patienten geführt, die an Verletzungen und degenerativen Erkrankungen leiden, die zu Gewebeverletzungen und –veränderungen führen. Die unbeeinflussten biologischen Reparatur-Mechanismen, soweit sie in den entsprechenden Patienten noch funktionieren, führen häufig zu Narbenbildung, so dass keine vollständige Regeneration des betreffenden Gewebes erreicht wird. Die Regenerative Medizin zielt darauf ab, die biologische Regeneration zu unterstützen, während die Ausbildung von Narbengewebe unterdrückt werden soll. Ein Ansatz dabei ist die Material-Induzierte Autoregeneration, bei der ein Biomaterial temporär Funktionen der extrazellulären Matrix (ECM) an einer Defektstelle übernimmt, und dann im Laufe der Zeit durch funktionales Neo-Gewebe ersetzt wird. Schlüsseleigenschaften, die das Biomaterial besitzen sollte, sind dabei mechanische Eigenschaften ähnlich dem Gewebe, dass ersetzt wird, Möglichkeiten zur spezifischen Adhäsion von Zellen, und einstellbare Abbaubarkeit. Im Allgemeinen ist die Verwendung von Biopolymeren aus der ECM als Basis für solche Materialien sehr wünschenswert, aber schwierig zu realisieren, da die Eigenschaften dieser Biopolymere schwer einzustellen und zu kontrollieren sind.

In dieser Arbeit wurde ein wissensbasierter Ansatz gewählt, um die systematische Variation der Materialeigenschaften von funktionalisierter Gelatine zu untersuchen. Dies sollte erreicht werden, in dem Gruppen in Gelatine eingeführt werden, die spezifische, nicht-kovalente Bindungen eingehen sollten, und die entsprechenden Systeme mit Molekular Modellirung und synthetisch-experimentellen Methoden untersucht werden.

Gelatine wurde als nicht-immunogenes und abbaubares Derivat der ECM-Komponente Kollagen ausgesucht. Die Kontrolle der Materialeigenschaften sollte durch die Funktionalisierung mit aromatischen Gruppen, die von Tyrosin abgeleitet sind, erreicht werden, da diese Gruppen potentiell π–π-Wechselwirkungen und Wasserstoffbrücken-bindungen auch unter physiologischen Bedingungen eingehen können und somit die Ausbildung supramoleuklarer Aggregate ermöglichen sollten, so dass physikalisch quervernetzte Netzwerke erzeugt werden. Dabei werden ausschließlich aus der Natur abgeleitete Moleküle benutzt, was im Hinblick auf Zytotoxizität und Biokompatibilität von besonderer Bedeutung ist.

Molekulare Modelle der Gelatine-basierten Materialien waren die Grundlage des wissensbasierten Ansatzes der physikalisch quervernetzten Polymersysteme. Die Moleküldynamik (MD) Simulationen wurden mit einem Kraftfeld zweiter Generation (CFF91) an Modellen mit 0.8 Gew.-% und 25 Gew.-% Wassergehalt durchgeführt. Die Validierung der Modelle erfolgte durch Vergleich der errechneten mit experimentellen Daten wie z.B. der Dichte, Bindungswinkeln des Proteinrückgrats sowie Röntgenstreuungsspektren. Die Modelle wurden dann zur Vorhersage der molekularen Organisation der Polymerketten, Formierung physikalischer Netzpunkte, und Berechnung der mechanischen Eigenschaften eingesetzt. Die zur Funktionalisierung der Gelatine eingesetzten Gruppen Desaminotyrosin (DAT) und Desaminotyrosyltyrosin (DATT) führten beide zu einer Verminderung der Helikalisierung, die sonst typischerweise in Gelatine auftritt, wobei stattdessen die Ausbildung physikalischer Netzpunkte durch π–π-Wechselwirkungen und Wassertstoffbrückenbindungen, wie gewünscht, auftrat. Ein Schlüsselergebnis der Simulationen war, dass mit zunehmender Zahl an aromatischen Gruppen auch eine Zunahme der physikalischen Netzpunkte beobachtet werden konnte. Ein Vergleich mit dem Flory-Rehner-Model legte dabei nahe, dass eine Reduktion des Quellungsgrads in Wasser bis zu Faktor 6 zu erwarten war. Diese Vorhersage wurde später durch experimentelle Befunde

bestätigt. Die Reduktion und Kontrolle des Gleichgewichtsquellungsgrades war ein wichtiges Kriterium für die Anwendbarkeit der Materialien z.B. als Matrices für die induzierte Autoregeneration.

Die funktionalisierten Gelatinen konnten durch chemoselektive Reaktion der Aminogruppen der Gelatine mit den freien Carboxylatgruppen von DAT und DATT erreicht werden. Materialien mit 25 Gew.-% Wassergehalt hatten in der Simulation und im Experiment mechanische Eigenschaften derselben Größenordnung (z.B. E-Moduln im unteren GPa-Bereich). Der Quellungsgrad der Materialien im Experiment nahm mit zunehmender Zahl an aromatische Gruppen ab (von 2800 Vol.-% auf 300 Vol.-%), wobei der Elastizitätsmodul, die Bruchdehnung sowie die Zugfestigkeit zunahmen.

Die Organisation der Proteinketten von Gelatine-basierten Materialien in Einzel- und Tripelhelikale Bereiche hat einen starken Einfluss auf die mechanischen Eigenschaften des Materials. Die oben beschriebene Funktionalisierung der Gelatine ist eine chemische Methode, um die helikale Organisation zu beeinflussen oder zu unterdrücken, während die genaue Kontrolle der Trocknungsbedinguungen von Gelatine-basierten Materialien eine physikalische Methode mit demselben Ziel ist. Daher wurde untersucht, wie die Inkorporierung von DAT und DATT als Seitenketten der Gelatine das kinetische und thermodynamische Gleichgewicht des Renaturierungsprozesses der Ketten in Einzel- und Tripelhelices abhängig von den Trocknungsbedingungen beeinflusst. Trocknung von Gelatine-basierten Materialien oberhalb der Helix-Knäuel-Übergangstemperatur ($T > T_c$, hier als v_{short}-Behandlung bezeichnet) führt im Allgemeinen zu einem relativ geringeren Anteil an tripelhelikalen Bereichen ($X_{c,t}$ = 1 – 2 %) als Trocknung bei tieferer Temperatur ($T < T_c$, hier als v_{long}-Behandlung bezeichnet) ($X_{c,t}$ = 8 – 10 %), wobei die Seitengruppen die Helixausbildung unterdrückten. Während unterschiedliche Anteile an helikalen Bereichen die thermischen Übergänge nur wenig beeinflussten, wurden die mechanischen Eigenschaften insbesondere von Materialien im Gleichgewichtsquellungszustand stark beeinflusst (E = 4 –

13 kPa für Materialien, die mit v_{long} behandelt wurden, und E = 120 – 700 kPa für Materialien, die mit v_{short} behandelt wurden). Zusammengefasst führte die Funktionalisierung von Gelatine mit DAT oder DATT zu einer stark verminderten Helixausbildungstendenz, die jedoch durch Variation der Trocknunsgbedingungen noch fein abgestimmt werden konnte. Somit konnten die mechanischen Eigenschaften von Filmen aus funktionlisierter Gelatine mit zwei unabhängigen Methoden eingestellt werden.

Die Kompositierung der mit DAT oder DATT funktionalisierten Gelatine mit Hydroxyapatiten (HAp) gab Materialien mit deutlich verringerter Quellung. Verschiebung von Banden der freien Carboxylgruppen in IR-Spektren in der Gegenwart von HAp legte eine direkte Interaktion der Matrix und des HAp nahe, wodurch zusätzliche physikalische Netzpunkte im Material entstanden. In Zugdehnungsexperimenten und rheologischen Untersuchungen zeigten die Komposite im Gleichgewichtsquellungszustand erhöhte Elastizitätsmoduln (von 200 kPa auf bis zu 2 MPa) und Zugfestigkeit (von 57 kPa auf bis zu 1.1 MPa) im Vergleich zu den Matrixmaterialien alleine, wobei die Bruchdehnung nicht beeinflusst wurde. Darüber hinaus konnte die Übergangstemperatur T_c deutlich gesteigert werden (von ca. 40 °C auf > 85 °C). Da für reine Gelatine eine solche Änderung nicht zu finden war, unterstützt dieser Befund den Schluss, dass zusätzliche stabilisierende Bindungen zwischen den aromatische Gruppen und dem HAp auftreten. Die Komposite können potentiell zur Behandlung von Knochendefekten eingesetzt werden.

To my parents

Statement of Originality

I, Alessandro Zaupa, formally submit the dissertation entitled “Physical Crosslinking of Gelatin: A Supramolecular Approach to Biomaterials” to the Department of Mathematics and Natural Sciences of the University of Potsdam, Germany, for the acquirement of the academic degree of Doctor of natural sciences (Dr. Rer. Nat.) in Materials for Life Science.

I hereby certify that this submission is entirely my own original work and that, to the best of my knowledge and belief, it contains no material previously published or written by another person, except where due reference is made in the thesis itself. Most of the experiments presented in Chapter 6 were performed by Axel Löbus in his diploma thesis. In that context I supervised the work in the lab and helped with the design and setting up of the experiments as well as with the analysis evaluation of the data. No other sections of this dissertation have been previously submitted for a degree or other qualification to any other University or Institution. Any contribution made to the research by others, with whom I have worked at GKSS or elsewhere, is explicitly acknowledged in the thesis.

Alessandro Zaupa,

Potsdam, 10.11.2010

CONTENTS

List of Symbol and Abbreviation

a.u.	arbitrary unit
DAT	Desaminotyrosine (hydroxyphenyl propionic acid)
DATT	Deseminotyrosyl-Tyrosine
DCM	Dichloromethane
DIPEA	Diisopropylethylamine
DMSO	Dimethyl sulfoxide
E	Young's modulus
E_c	Compressive modulus
ε_b	Elongation at break
ECM	extracellular matrix
EDC	1-ethyl-3-(3-dimethyl-aminopropyl) carbodiimide
ESI	Electron Spray Ionization
Et_2O	Diethyl ether
EtOH	Ethanol
Fmoc	Fluoren-9-ylmethyloxycarbonyl
MALDI-TOF	Matrix Assisted Laser Desorption Ionization – Time of Flight
MD	Molecular Dynamics
MeCN	Acetonitrile
MeOH	Methanol
MS	Mass spectrometry
NMP	*N*-Methylpyrrolidone
NMR	Nuclear Magnetic Resonance
PBC	Periodic Boundary Conditions
RDF	Radial Distribution Function
Q	Degree of Swelling
QSAR	Quantitative Structure Activity Relationships
RP-HPLC	reversed phase high performance liquid chromatography
SAXS	Small Angle X-ray Scattering
SD	Steepest Descent
σ_{max}	Maximum tensile strength
TLC	Thin Layer Chromatography
TNBS	2,4,6-trinitro-benzensulfonic acid
*t*Bu	*tert.*-Butyl
TFA	trifluoro acetic acid
TIPS	Triisopropylsilyl
TM-DSC	Temperature Modulated Differential Scanning Calorimetry
TNBS	2,4,6-trinitro-benzensulfonic acid
WAXS	Wide Angle X-ray Spectrometry

Amino acid code

Amino acid	Three letter code	One letter code
Alanine	Ala	A
Arginine	Arg	R
Asparagine	Asn	N
Aspartic acid	Asp	D
Cysteine	Cys	C
Glutamine	Gln	Q
Glutamic acid	Glu	E
Glycine	Gly	G
Histidine	His	H
Hydroxylysine	Hyl	-
Hydroxyproline	Hyp	-
Isoleucine	Ile	I
Leucine	Leu	L
Lysine	Lys	K
Methionine	Met	M
Phenylalanine	Phe	F
Proline	Pro	P
Serine	Ser	S
Threonine	Thr	T
Tryptophan	Trp	W
Tyrosine	Tyr	Y
Valine	Val	V

List of Tables

List of Figures

1 Introduction

The change in living conditions during the twentieth century has brought several major benefits to the welfare and health of humankind. However, the increased life expectancy, the change of lifestyle, and the growing world population lead to a substantial increase in patients who suffer from tissue damage and malfunctioning because of degenerative diseases and injuries. The difficulties in conventional treatment as well as the increasing mismatch between supply and demand for organs and tissues for transplantation[1] has driven the development of the field of regenerative medicine. The growth and repair of human tissues follow different biological paths, so that in most cases even under ideal conditions scarring occurs as a consequence of repair of damaged tissues. In some cases, tissues damage results in critical, i.e. non self-healing, defects, so that clinical intervention is necessary to restore a level of tissue function.

Regenerative medicine is an interdisciplinary field which has emerged more than two decades ago that uses various therapeutic strategies, such as the use of biomaterials, the use of cells, or a combination of biomaterials and cells to permit the full functional regeneration of damaged tissue by supporting the endogenous regeneration. The use of degradable biomaterials to induce tissue autoregeneration is especially promising in case of critical size, i.e. non-healing defects. Once implanted, the material shall act as a temporary substitute of the extracellular matrix enabling the ingrowths of new tissue by attracting cells from the

surrounding environment and providing suitable conditions for cell proliferation. The construct shall then progressively degrade as the formation of neotissue progresses. A thorough understanding of the clinical needs, the biological processes, as well as the chemistry and mechanics of the involved materials is necessary to reach this goal.

Despite many important achievements, biomaterial-based clinical applications have demonstrated only partial success.[2, 3]

Each biomedical application requires materials with tailored properties such as mechanical and thermal properties, water uptake and swelling behavior, as well as degradation behavior.[4-7] While early polymer were adopted from other areas of science and technology without specific redesign for medical use and were investigated only after the accidental findings of biocompatibility, e.g. poly(methylmethacrylate), the specific and goal-oriented development of materials and material constructs is now predominating.[8]

Polymer systems, whose macroscopic properties can be adjusted in a wide range by only slightly changing their chemical structures, were developed to meet this demand.[9-11] The variation of the type of monomers,[12] and of the polymer architecture[10, 13] permit controlled material properties and degradation behavior. An attractive strategy for obtaining tunable polymer systems with multiple functions is to enable defined but reversible physical interactions along the polymer chains. In biopolymers, such physical interactions control their self-organization under physiological conditions,[14] which among other factors depends on the electronic properties of the repeating units[15] as well as the possibility to form hydrogen bonds in an aqueous environment.[16, 17]

In material induced autoregeneration, the material temporarily functions as an artificial extracellular matrix (ECM), which should then be replaced over time by neo-tissue consisting of regio-specific cells and their self-produced, native ECM. Therefore, in the ideal case the development of new biomaterial must be driven towards the exact knowledge of cell function

on the one hand, and, on the other hand, toward the knowledge of interactions and signals that cells must receive from the environment so they can behave as in natural tissues.

1.1 Hydrogels in biomedical applications and Regenerative Medicine

During the past decade, there has been a substantial paradigm shift in the design criteria of modern biomaterials.[18] Current developments integrate principles from cell and molecular biology to mimic certain aspects of the natural ECM. Hydrogels show in some case innate structural similarities to the extracellular matrix presenting an extensive framework for cellular proliferation and survival and have since received a lot of attention.

Hydrogels are three-dimensional crosslinked networks formed by a hydrophilic polymer that can retain large volumes of water, causing the network to swell in solution. Although the initial mechanical properties of hydrogels cannot match those of solid polymers, they are thought to encourage accelerated tissue formation, such that the natural matrix soon supplements and assumes much of the hydrogel's mechanical responsibility.[19] Biological sources such as agarose,[20] alginate,[21] chitosan, hyaluronan,[22, 23] fibrin, and collagen,[23] and hydrophilic polymers such as poly(ethylene oxide),[24, 25] poly(vinyl alcohol) (PVA), polyacrylates such as poly(2-hydroxyethyl methacrylate), and their derivatives have also attracted interest for tissue regeneration.[26]

Several molecular parameters can be used to quantitatively describe the network structure of hydrogels. The extent of swelling and the content of water retained are largely dependent on the hydrophilicity of the polymer chains and the crosslinking density, which directly affect the mechanical properties and the effective solute transport properties. The crosslinks can be formed by either covalent or physical bond between the polymer segments, such as ionic bonds, hydrogen bonds, van der Waals forces, and hydrophobic interactions.[27]

1.2 The Extracellular Matrix (ECM)

The extracellular matrix (ECM) is a complex multimaterial system consisting of macromolecules that surround and support cells in animal and human tissue (Figure 1.1). In additionally to the main ECM component, water, two main classes of extracellular macromolecules make up the matrix: (1) polysaccharides from the class of glycosaminoglycans (GAGs), which are usually found covalently linked to proteins in the form of proteoglycans, and (2) fibrous proteins, including collagen, elastin, fibronectin, and laminin, which have structural and adhesive functions.

Proteoglycans are composed of about 95% polysaccharides and about 5% proteins. The protein core is associated with one or more varieties of glycosaminoglycan (GAG) chains. GAG chains are unbranched polysaccharides made from disaccharides of an amino sugar and another sugar (see inset Figure 1.1). Hyaluronic acid, chondroitin sulfate, keratan sulfate, dermatan sulfate and heparan sulfate are some examples of GAGs. At least one component of the disaccharide has a negatively charged sulfate or carboxylate group, so the GAGs tend to repel each other and other anions while attracting cations and facilitating interactions with water.[28] In connective tissue proteoglycans form a highly hydrated "ground substance" in which the fibrous proteins are embedded. The polysaccharide gel is responsible to resist compressive forces on the matrix while permitting the rapid diffusion of nutrients, metabolites, and hormones between the blood and the tissue cells. The collagen fibers both strengthen and help organize the matrix, and rubber-like elastin fibers give it resilience. Finally, many matrix proteins help cells attach in the appropriate locations.

The supramolecular organization of these macromolecules is dictated by the mutual cell control and self-organization properties of the molecular constituents.[29, 30] The variations in their relative amounts and the way in which they are organized in the ECM give rise to an

amazing diversity of forms, each adapted to the functional requirements of the particular tissue.

In bone and cartilage for example, the ECM forms the basis for highly organized structures over different length scales. Bone is strengthened by the nucleation of hydroxyapatite into the nanodimensional gaps between collagen molecules to form a calcified outer layer filled with osteons, or Haversian systems each supplied by their own vasculature. The osteocytes within these systems are surrounded by a dense network of aligned collagen I fibers, which provide templates for the self-assembly of hydroxyapatite crystals. Cartilage, by contrast, is a non-vascular, turgid network, which supports chondrocytes spaced 10–200 mm apart. Hydrophilic proteoglycans, such as aggrecan, interwoven between a network of collagen II fibres, provide a shock-absorbing matrix. In addition to a structural role, the ECM presents cells with instructive cues needed to maintain cell phenotype and behavior.

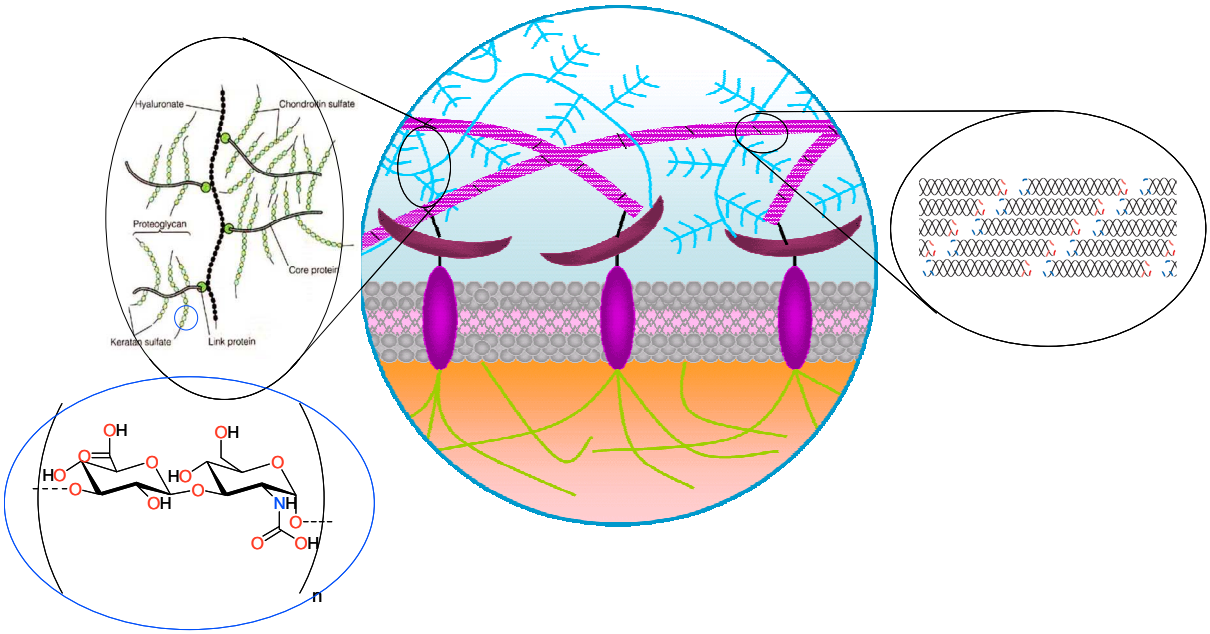

Figure 1.1. Overview of the macromolecular organization of the extracellular matrix with a diagram of proteoglycan structure associate with a hyaluronate backbone (right) and fibrillar organization of collagen (left).

1.2.1 Collagen

Collagen, the most abundant protein present in mammals, is a dynamic fibrillar system that undergoes self-organized helicalization processes during its biosynthesis.[31] There are at least 30 different collagen genes dispersed throughout the human genome. These 30 genes generate proteins that combine in a variety of ways to create over 20 different types of collagen fibrils. Types I, II and III are the most abundant types and form fibrils of similar structure. Type IV collagen forms a two-dimensional net-like structure and is a major component of the basal lamina. Collagens are predominantly synthesized by fibroblasts, but epithelial cells also synthesize these proteins. The typical feature of collagen is its long, stiff, triple helical structure, in which collagen polypeptide chain called α-chains, are wound around one another in a ropelike superhelix. The single chains of collagen contain the highly repetitive triad $(Gly\text{-}Xaa\text{-}Yaa)_n$, with Xaa being mostly proline (Pro) and Yaa predominantly hydroxyproline (Hyp), that gives rise to a left-handed helical conformation ('polyproline type II'), which is more elongated than typical α-helices as there are less hydrogen bonds because of the larger number of imino acids.[32, 33, 31] The structural organization of collagen molecule can be observed for example by using different X-ray scattering techniques that permit to analyze the intra- and intermolecular as well as intra- and interfibrillar interactions (Figure 1.2b).

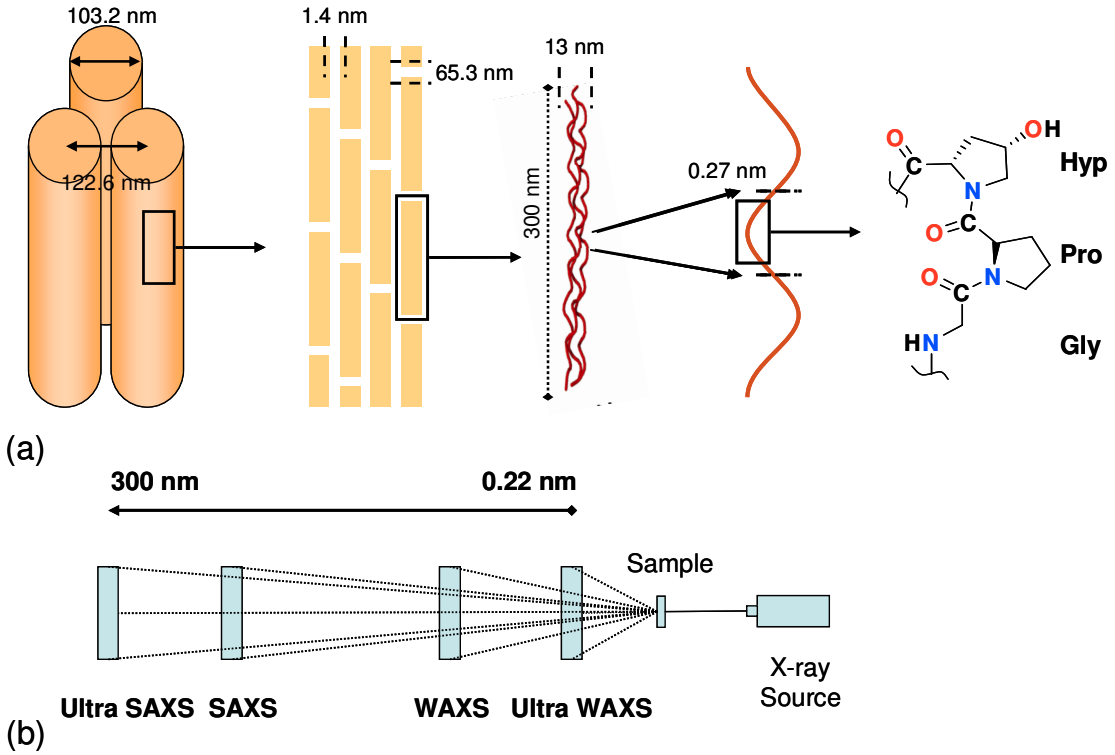

Figure 1.2. Collagen hierarchy from the microscopic to the molecular (a). From left to right: fibril packing, microfibril packing, collagen triple helix, helical rise per residue distance, collagen sequence. Diagram is for bovine hide and is not to scale. (b) Illustration of sample to detector distances covering UWAXS and USAXS scattering angles and the range of structural definition that can be obtained by the different examination.

The self-assembly of collagen is strongly dependent on hydrophobic interactions within the physiological environment, and takes place over multiple steps from the expression of pro-collagen proteins to their assembly into triple-helical fibres.[34]

The triple helix formation and stabilization relies on weak, cooperative forces and is dependent on the amino acid sequence. Specifically, hydroxyproline, hydroxylysine, lysine, aspartic acid and glutamic acid tend to stabilize the triple helix, while aromatic amino acids destabilize the helix.[35, 36] The strong influence of the amino acid side chains on the formation of the triple helices is also evidenced by failed assembly of the collagen chains in hereditary, even lethal, diseases due to the exchange of single amino acids.[37, 38]

After being secreted into the extracellular space, these collagen molecules assemble into higher-order structure depending on the collagen type. Collagen type I for example, as found

in bone, self organizes into collagen fibrils which are thin structures (10–300 nm in diameter) many hundreds of micrometers long. Collagen fibrils further aggregate into larger, cable-like bundles, several micrometers in diameter, which can be seen in the light microscope as collagen fibers (Figure 1.2). Interestingly, the assembly of collagen fibrils during their biosynthesis is controlled by aromatic residues present at the non-helical regions at both ends of a collagen molecule, known as telopeptides, which increase the kinetics of fibril self association.[39]

Collagen[40, 41] as an ECM component is applied in biomedicine e.g. as heart valves and vascular grafts.[42, 43] However, collagen materials show significant shrinkage in physiological environments[44-46] and have raised concerns due to immunogenic responses.[47] Attempts to covalently crosslink collagen[48-51] did only lead to slight variation of mechanical properties, which may be because of intra- rather interfibrillar reactions. Interfibrillar crosslinking techniques[52-54] have drawn some attention, but have not yet found wide-spread acceptance.

1.3 Gelatin

Gelatin is the product of the partial hydrolysis of collagen consisting of a polydisperse mixture of polypeptide chains with a molecular weight distribution generally ranging from 10-400 kDa.[55, 56] The degradation process leads to the removal of crosslinks and glycostructures, and to the denaturation of the triple helical quaternary structures that are typical for collagen. Gelatin is mainly an amorphous material in which extended helical structures of 100-200 residues in length form a physical network and coexist with flexible random coils regions (Figure 1.3).[57, 58] The physical networks obtained by cooling a gelatin solution at temperatures below 35 °C are disordered and their properties vary considerably from batch to batch. The variability of chemical composition of the biopolymer, the molecular weight, the polydispersity, the modifications of the environment such as pH,

presence of ions, additives such as sugars, polyols, etc., the thermal history, or the passage of time itself have been shown to substantially influence the mechanical and thermal properties of these physical gels.[59, 60, 17, 61] Gelatin can be dissolved in water and forms low viscosity solutions at temperatures above ca. 35 °C (helix-to-coil transition, T_c). On a molecular level, this dissolution occurs because the cooperative interactions between the gelatin chains are disrupted at $T > T_c$, leading to the formation of random single coils. Cooling of such gelatin solutions to $T < T_c$ results again in physically crosslinked gels that, following certain drying conditions, possess locally regions re-associated collagen-like triple helices.[62-64] Generally, low molecular weight gelatin or materials obtained by drying at $T > T_c$ result in amorphous materials with lower triple helical contents and lower gel stability, which are less elastic[64-66] than dried materials produced from higher molecular weight gelatins or those dried at $T < T_c$.[67] However, gelatin is highly hygroscopic[68] and may easily undergo structural changes during (re)wetting or during storage, which affect its helical content, thermal transitions, and mechanical properties.[65, 69]

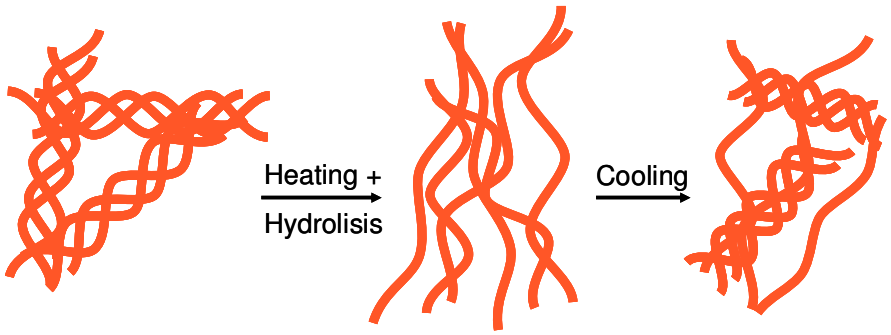

Figure 1.3. Denaturation process of collagen to obtain gelatin: the thermal treatment and hydrolytic degradation lead to the irreversible breakdown of the triple helix structure. Random gelatin coils are thereby formed, which can partially renaturate on cooling.

1.3.1 Gelatin hydrogels: state of the art and challenges

Numerous studies have revealed that gelatin-based scaffolds and microspheres have a high degree of biological functional groups, and have some potential for applications in tissue

regeneration. Gelatin has been shown to be proangiogenic[70] and non-immunogenic,[47, 71] with lower levels of cytotoxicity.[72] Gelatin is currently used in pharmaceuticals,[73] wound dressings[74] and adhesives in clinics due to its permitting good cell viability and lacking of antigenicity.[47, 71] One of the main practical advantages of gelatin with respect to collagen is the broader spectra of processing technique that can be used to obtain porous sponges as well as hydrogels. In order to ensure adequate materials, structural integrity, and controlled, reproducible gel properties *in-vivo,* gelatin is usually chemically crosslinked.[73] Different strategies can be used to specifically tailor the hydrogel properties. The formation of zero-length crosslink can be obtained by chemical reaction between free amino and carboxylic groups mediated by carbodiimide[75, 76] or enzymes such as tranglutaminase.[77, 78] Bi- or polyfunctional crosslinking agents like glutaraldehyde,[79-81] genipin,[82, 77] oxidized chondroitin sulfate,[83, 84] dextran dialdehyde,[72] or hexamethylene diisocyanate,[85, 86] permit to insert a spacer that, according to its length and properties, influence the mesh size of the final product. Physical methods like photo-crosslinking can also be used after functionalization of gelatin chain with methacrylate or phenolic groups.[87] The mechanical properties of the obtained materials vary strongly depending on helical content and the obtained degree of cross-linking, that are strongly affected by the processing method and gelatin source.[80, 79] In the swollen state, gelatin gels typically have Young's moduli in the range of 10 to 125 kPa, depending on the crosslinking density and Bloom index. However, covalent crosslinking involves additional difficulties to remove unreacted crosslinker that is usually toxic and may affect the integrity of additional substances incorporated into the gel, like growth factors or cytokines.[88] On the other hand the introduction of strongly physically interacting functional groups at the side chain of gelatin might lead to the formation of a reversibly physically crosslinked network with reduced swelling behavior and increased mechanical properties.[89]

1.4 Supramolecular Self-assembly

Supramolecular chemistry is a highly interdisciplinary field of science covering the chemical, physical, and biological features of chemical species of higher complexity, that are interacting by means of intermolecular (non-covalent) bonding interactions. These forces include metal coordination, electrostatic effects, hydrogen bonding, π-π interactions, van der Waals forces, and hydrophobic forces.[90] In biological systems the molecular interplay within tissues leans heavily towards weak interactions. These lower energy molecular couplings are responsive, adaptive, and can enable the rapid assembly and disassembly of protein inducing conformational changes and structural remodelling.[91] Proteins are defined by their amino acid sequences which control their complex secondary and tertiary structural organization. Typical secondary structures of proteins include α-helices, β-sheets and random coils. Lipids, with their structural variety, form a large subset of biological materials with various properties. In water, hydrophobic effects lead to membrane formation in the form of micelles, liposomes, and bilayers. DNA and RNA self-assemble into two helical chains each coiled round the same axis due to strong multiple H-bond interaction, where aromatic pi-stacking helps in stabilizing the structure.

Synthetic polymers have recently been reported that combine the benefits of chemical design and the self-assembly properties seen in biological macromolecules by integrating non-covalent recognition motifs into artificial polymers, which have lead to responsive architectures. Supramolecular polymers can form highly crosslinked networks, resulting in gels and processable materials.[92, 93] For example, Holmes et al. used the associative properties of small molecules containing aromatic functions to form supramolecular hydrogels for the production of scaffolds to enable neurons growht.[94]

One advantage of supramolecular complexes is that they can be easily broken by increasing the temperature or changing other environmental conditions (pH or polarity of the

solvent), but are reformed after cooling or restoring the starting conditions. The reversible nature of the related netpoints widens the spectrum of processing techniques and would avoid the removal of unreacted crosslinker from the final material, thereby increasing the biocompatibility of the same.[90, 88, 89, 95] Aromatic ring systems can, for example, interact with each other with an energy similar to the hydrogen bond (~5 kJ•mol^{-1})[96] and, due to their hydrophobicity, can be a suitable choice for gelatin functionalization.

In supramolecular chemistry, an aromatic interaction (or π-π interaction) is a noncovalent interaction between organic compounds containing aromatic moieties. π-π interactions are caused by intermolecular overlapping of p-orbitals in π-conjugated systems, and become stronger as the number of π-electrons increases. In literature, many examples can be found that show the capability of aromatic ring systems to stabilize material conformation in aqueous environment. For example polystyrene macromolecules grafted to the backbone of soluble poly(vinyl-pyrrolidone) permit the formation of stable hydrogels thanks to the network points created by the hydrophobic aromatic moieties of polystyrene.[97] Mahler et al. reported the efficient self-assembly of an aromatic dipeptide, Fmoc-Phe-Phe, to form a hydrogel with high stability over a broad range of temperatures and pH values with good biomechanical characteristic comparable to the one of uncrosslinked gelatin.[98] In addition, aromatic moieties found in proteins are involved in aromatic pairs, where about 60 percent of aromatic side chains form networks of two or more interacting rings participating in the stabilization of protein conformation.[15]

1.5 Composite hydrogels

Nature uses composites to generate materials that exhibit high mechanical stability combined with elasticity. In these composites, inorganic micro- or nano-sized fillers are distributed in a (bio)polymer matrix that binds the filler together and protects the filler from damage by stress

distribution.[99] The increase of material properties of the composites depends on i) the original properties of the matrix, ii) the filler content, iii) the filler size and form, and iv) the interaction between filler and matrix.[100] In technical applications, fillers with high aspect ratios such as layered silicates or carbon nanotubes are often used as they already show strong effects even when only small weight percentages of filler is incorporated.[101, 102] However, particulate fillers with small aspect ratios are important for mimicking biological materials. Biomineral fillers important in biological composite materials include calcium phosphates, calcium carbonates, and silica. In vertebrates, calcium phosphates represent the most important class. Hydroxyapatite (HAp), in form of carbonate containing calcium phosphates, is present in bone, teeth, and tendons and has also been applied as an implanted biomaterial.[103, 104]

It has been shown that the biocompatibility of materials in contact with osteoblasts in cell culture and with bone in the living system can be increased by incorporating calcium phosphates such as tricalciumphosphate or HAp.[105, 106] One observation in this respect is the better contact between bone and implant,[107] as these interactions at the interface are important in bone and implant remodeling processes.[108] The natural matrix in bone is mainly collagen I, which therefore has been investigated extensively. Composites of HAp dispersed in collagen or other matrices can be prepared by incorporating pre-fabricated calcium phosphate or carbonated-HAp particles into the respective matrix. In addition to films, composite scaffolds have also been prepared.[109, 110]

The interaction between matrix and filler generally has a strong effect on the maximum tensile strength of the composite. On the one hand, particle size and surface area play an important role for the interactions between matrix and filler, where nanoparticles often have a stronger effect on material properties than microparticles.[111] On the other hand, specific chemical functionalization of the filler may increase the interaction between filler and

matrix.[112, 113] Modeling studies have shown that in biological composites matrices seem to specifically interact with their fillers.[114-116]

1.6 Molecular modeling

Molecular modeling is a computer based theoretical approach that can be used to elucidate the dependencies between molecular and macroscopic properties of a material. It can also be utilized to predict static and dynamic properties of single molecules, molecular aggregates and, within its theoretical limits, it can be considered as an investigation method of existing or hypothetical materials. Molecular modeling techniques are particularly useful in the evaluation of properties which cannot be directly measured by experiments, as well as in the molecular design of new materials, avoiding synthesis and characterization of compounds which, finally, are found to be not satisfactory. Molecular dynamic simulations have largely been used to generate representative structure of polymeric materials to study chain organization,[117] swelling and diffusion processes,[118] as well as to estimate the mechanical properties of materials.[119, 120] Collagen and gelatin systems have been widely investigated by computational methods to elucidate the folding mechanism,[121, 122] and the interactions of collagen-like peptides with small molecules such as gallic acid or calcium ions.[122, 123, 114]

The complete mathematical description of a molecule should consider both quantum mechanical and relativistic effects, where molecules are considered as collection of nuclei and electrons. Although recent developments demonstrated quantum mechanical calculations to be successful in describing atomistic and molecular interactions, these methods are not of practical use in the description of macromolecular systems, e.g. polymers, where the number of atoms can easily reach several thousands, resulting in extremely high time consuming calculations, even with the most modern hardware state-of-art.

Forcefield based (FF) methods (see Appendix A), on the other hand are based on empirical data that implicitly incorporate all relativistic and quantum effects. Molecules are considered to be built up of soft sphere (atoms) and bonds. Bond interactions are described via mechanical analogues (like springs and torsion rods), while non-bonded interactions are calculated using van der Waals- and Coulomb terms. The dynamic of atoms are then treated by classical mechanics methods, for instance using the Newton's equations of motion. The computational cost of FF calculation is dominated by the evaluation of non-bonded interactions, and the magnitude of the relative energies decay rapidly with increasing interatomic distance. Its simplicity makes it a useful tool for analysis of macromolecular system, however two main limitations has to be considered. On the one hand, the success of the methods depends on the parameterization set employed by the force field and on the other the quality of the results should be always evaluated by comparing them with experimental data.

2 Aim of the Ph. D. Thesis

The goal of this project was to develop a knowledge-based design for the realization of physically-crosslinked gelatins using a combination of modeling studies and synthetic methods. The functionalized gelatins should be intended for use in induced autoregeneration, which could be important for bone regenerative implants. By using such a strategy to investigate physically-crosslinked gelatins, several detailed goals are outlined here that should be met to ensure their applicability in a clinical setting. First, several novel gelatins bearing varying degrees of physical crosslinks or degrees of functionalization should be proposed, which should be the starting point and focus throughout this thesis. During this design, one key aspect was to choose chemical groups that would maintain material biocompatibility and degradability. Second, molecular models of these gelatin-based materials should be developed by the construction and molecular dynamic simulation of atomistic chain packing models and be validated by comparison with experimental data from the literature. These models should then be used as predictive tools for the efficient design and evaluation of the proposed novel materials. The next steps outline the synthesis and characterization of the materials, which should then be performed in order to verify the results from the modeling and to investigate structure-property relationships. Third, the synthetic process should be scaled up to prepare reasonable amounts of materials for material testing. Fourth, the physically crosslinked gelatin-based biomaterials should be tested in comparison with unmodified gelatin in terms of physical properties pertinent to the *in vivo* environment, such as swelling properties, mechanical and

thermal properties. Tailoring of the materials as well by chemical functionalization as by physical treatment of the materials has to be addressed, explored, and understood by comparing molecular and macroscopic properties of the systems. Ideally, all of the physically crosslinked materials should display predictable, tailorable, yet applicable mechanical properties that are similar to the ECM under physiological conditions. As a final aim, the physically crosslinked gelatins should be used to investigate their potential as matrix for composites with hydroxyapatite in view of its potential application in bone regeneration.

3 Strategies and Concepts

The overall success of an artificial biomaterial scaffold in contact with a biological system depends on several properties like compatibility and biofunctionality that should fulfill regiospecific requirements. For example, to support endogenous regeneration the artificial construct should interact with surrounding cells and tissues, as well as with blood and immune system. Therefore, the design of a new biomaterial for applications in regenerative therapy should aim at providing essential properties and characteristics of the extracellular matrix, near or within the targeted implant site in terms of signaling pathway and macroscopic properties. Amongst the most important factors, the material's mechanical properties and degradation behavior, which shall be substituted over time by neo-tissue, the material's wettability, and the cell-material interactions (e.g. through peptidic adhesion sequences), have to be taken into account. The selection of a starting material is therefore of paramount importance. A natural biopolymer present in the ECM, such as collagen or hyaluronic acid can be advantageous in such a setting, but achieving controlled and tailored material properties in unfunctionalized biopolymers is often difficult due to the inherent variability between production batches. For this reason, a feasible option is to choose a tailorable material that derives from an ECM-derived polymer, such as gelatin, which through a standardized production process already has some reproducibility.[124] The mechanical properties of gelatin-based systems are at least partially influenced by the dynamic processes

of internal helical (re)organization.[125, 65, 69] The most efficient method of achieving predictable and stable mechanical properties of gelatin therefore depends also on controlling this self-organization by using chemical functionalization, which may result in chemically-crosslinked (thermosets) or physically-crosslinked networks (thermoplastics). The main advantage of creating gelatin-based thermoplastic materials includes the ability to (re)process the materials following their formation. Moreover, potentially toxic reactive groups often used in synthesizing thermosets would be avoided.

The starting point was to transfer typical material design strategies used for synthetic polymers to explore the potential of side chain functionalization of gelatin in order to develop a defined polymer system with tailorable properties by enabling specific non-covalent interaction.[11, 126, 127] The side chain functionalization shall inhibit typically observed trimerization of gelatin chains to collagen-type triple helices,[55, 57] which in unfunctionalized gelatin is thermodynamically driven,[128] by steric hindrance and altered properties of groups engaged in hydrogen bonding. Two physically interacting groups were selected for the specific functionalization of the lysine gelatin side chains to create supramolecular networks (Figure 3.1). The amino acid-derived desaminotyrosine (DAT) and desaminotyrosyl tyrosine (DATT), which have previously been used to trigger physical interactions in synthetic polymer networks,[129, 130] can interact by two different mechanisms: aromatic π-π interactions and hydrogen bonds via the phenolic group (as H-bond donor or acceptor) and have been shown to be non-toxic.[130] Therefore, these side groups should interact and create netpoints within these physically crosslinked networks, which would differ in the number of aromatic clusters. According to literature,[131, 72, 75] the nucleophilic reactivity of amino groups is much higher when compared to hydroxyl groups, thereby making a chemoselective functionalization of the amino groups feasible. The amino groups on lysine residues and protein chain ends are selectively targeted via the free carboxylic acid group of DAT and DATT.

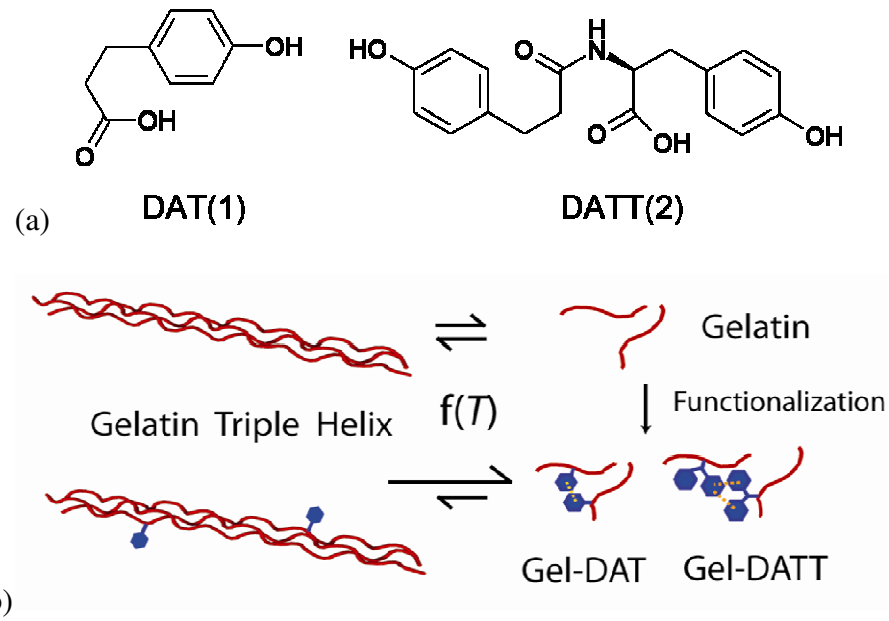

Figure 3.1. Structures of desaminotyrosine (DAT, 1) and desaminotyrosyl-tyrosine (DATT, 2) (a). Aim of this work was to establish if functionalization of gelatin with 1 or 2 would enable the formation of specific physical netpoints and simultaneously influences the balance between triple helical and amorphous chain organization in the materials (b).

Molecular modeling investigations were used to explore the potential of side-chain functionalization to tailor the material properties by enabling specific non-covalent interactions. Molecular simulations studies shall provide a tool for gaining an insight into the relations between the molecular structure (e.g. physical crosslink density) of the modified gelatins and some important macroscopic properties (e.g. equilibrium degree of swelling, solubility parameters, and Young's modulus) before expensive and time-consuming laboratory activities are conducted. The starting points were low hydration models with only 0.8 wt.-% water contents and wet models with 25 wt.-% water contents to investigate the influence of water. This water content is a compromise between the computational effort necessary when increasing the number of atoms in the model and the equilibrated swollen state, which is relevant in Regenerative Medicine.

To create a correlation between molecular structure and macroscopic properties, gelatin models were constructed as atomistic bulk systems under periodic boundary conditions similarly to what was previously demonstrated for polymeric systems (cf. section 0).[117, 132-135]

Specifically, the local interactions occurring within the gels, such as π-stacking and hydrogen bonding, which should be involved in the interchain self-assembling process, are of great interest for the modeling studies in terms of the fractional free volume distribution and chain mobility.

The generated models would then need to be validated in terms of structural resemblance (e.g. X-ray scattering spectra, dihedral angle distribution, density) by comparison with experimental data. Previous to the work described in this thesis, this was only possible for pure gelatin. The hypothesis then was that model construction and equilibration strategies working for gelatin would also be useful for creating packing models for DAT- and DATT modified gelatin. Based on the positive results from these models (to be outlined below) subsequently the corresponding "real" DAT- and DATT-functionalized gelatins had to be synthesized, processed into films and comprehensively characterized in terms of their potential as regenerative materials (mechanical properties, thermal properties, degree of renaturation, etc.). Specifically, X-ray spectroscopy, differential scanning calorimetry, and tensile testing could be used to characterize these novel systems. Important aspects of these materials include their helical contents, which should be inhibited by the interacting aromatic side chain moieties, and their swelling capacities, which should be reduced due to the increase of physical crosslinks. These factors are prerequisites in successfully applying gelatin-based materials in Regenerative Medicine. Last but not least suitable properties of the real materials could be used for an "a posteriori" conformation of the quality of the related atomistic packing models.

Given that these functionalized gelatins are thermoplastic biopolymer-based networks, they are (re)processable and dynamic in nature. Specifically, varying the drying conditions of gelatin films affects the renaturation process of gelatin chains, which determines the final bulk material properties. Therefore, an accurate study of the influence of the processing condition on the structural and mechanical properties of the material have to be pursued to study the

influence of introduced functional groups on the renaturation process of gelatin. One treatment should involve drying films below the gelation temperature ($T < T_c$), which would favor helix formation, while a second treatment involved drying casted films above gelation temperature ($T > T_c$), which would hinder the formation of helices. Because the treatment procedures (v) achieve different time periods of chain mobility in the gelatin samples,[34] the lower temperature treatment procedure will be denoted as v_{long} treatment since longer times are required for film formation, and the higher temperature treatment procedure as v_{short} treatment since shorter times are required for film formation. In addition, the absolute humidity (a.h.) of the drying chamber shall be varied during film formation of v_{long} treated samples to obtain further control of helical (re)formation.

The obtained materials should further be tested in combination with hydroxyapatite fillers to create polymer composite materials in view of its application in the regeneration of bone tissue. Therefore, it was explored whether the composite material macroscopic properties could be altered by changing the interaction of filler and matrix *via* the systematic variation of polymer properties, which would result in the development of a polymer composite system. By using the aromatically functionalized gelatins as a matrix, an increased number of groups which potentially can interact with ions on the surface of the filler is present.[136, 137] As the particle size and surface area play an important role for the interaction between matrix and filler,[138, 139] nanoparticles were selected in this investigation. The goal of the study was to investigate the interactions between matrix and filler in detail as well as how the addition of particles affects the overall material properties, where the water uptake and swelling, mechanical properties, and the thermal transitions of the composites compared to the pure matrix were of particular interest. Because of the intended application, all mechanical properties should be determined under conditions relevant to potential biomedical applications, i.e. under equilibrium swelling.

In the following Chapters (4 to 6) the results of the work are described and discussed in detail, followed by a conclusion in Chapter 7. Chapter 4 discusses the molecular modeling studies, chapter 5 discusses the synthesis of the functionalized materials, their processing and characterization as well as a comparison between models and experiments, and chapter 6 describes the application of the materials as matrices for hydroxyapatite composites.

4 Gelatin bulk atomistic model: simulation details and validation of the models

In this chapter, details of the gelatin model systems are provided. The atomistic models were developed from the biomolecule of the real gelatin materials. The general and the specific conditions employed for the different models are justified and the methodology used for their equilibration is described in detail. The validation of the equilibrated models of pure gelatin models is carried out by comparison between specific properties experimentally determined and taken from the literature, and the corresponding values calculated for the simulated models. Furthermore, the models are used as predictive tool for molecular chain organization and prediction of bulk material properties. The theoretical basis of the applied methodology is described in detail in section 8.1 and Appendix A.

4.1 Detailed atomistic bulk models of gelatin

Gelatin molecules were generated using the Discovery Studio software,[140] from a 276 aa sequence taken from the collagen Type I molecule (GenBankTM accession No. AAF23130). Special attention was paid in selecting the protein sequence so that the content of the different amino acids is close to the average described in the literature, especially the lysine residues needed for functionalization.[141] In Table 4.1 the composition of the used gelatin chain is compared with the experimental data determined for the α-chain of pig skin collagen

type I.[142] This specific sequence was selected according to the typical gelatin source that is obtained by acid degradation of pig skin.

Table 4.1: Amino acid composition of the simulated 276 aa gelatin and pig skin gelatin.[142]

	Model		Exp,[142]
AA	**No res,**	**mol-%**	**mol-%**
Gly	**92**	**33,3**	**32,9**
Pro	**29**	**10,5**	**13,2**
Hyp	**32**	**11,6**	**9,1**
Ala	**40**	**14,5**	**11,2**
Val	**5**	**1,8**	**2,5**
ILe	**1**	**0,4**	**1**
Leu	**4**	**1,5**	**2,3**
Phe	**3**	**1,1**	**1,4**
Trp	**0**	**0**	**0**
Ser	**10**	**3,6**	**3,5**
Thr	**5**	**1,8**	**1,8**
Tyr	**0**	**0**	**0,3**
Met	**1**	**0,4**	**0,4**
Cys	**0**	**0**	**0**
Asn	**5**	**1,8**	**1,6**
Gln	**6**	**2,2**	**2,5**
Lys	**10**	**3,6**	**2,7**
Hyl	**0**	**0**	**0,6**
Arg	**13**	**4,7**	**4,9**
His	**0**	**0**	**0,4**
Asp	**5**	**1,8**	**2,9**
Glu	**15**	**5,4**	**4,8**
Total	**276**	**100**	**100**

In the models, DAT and DATT were attached through an amide bond to the amino group of each lysine residues of the selected gelatin chain, as this corresponds to a synthetically feasible scheme of functionalization.

An initial gelatin chain was constructed in a helical conformation, where the dihedral angles φ and ψ were set to -65° and 170°, respectively, corresponding to the mean values of a typical collagen chain.[143] After a short equilibration, combination of minimization step and NVT molecular dynamic (MD), the optimized chain was packed into bulk models using the Amorphous Cell module of the Material Studio Modeling Environment.[144] NVT means conditions of constant particle number N, constant volume V and constant temperature T for a

given model. A bulk model is a cubic cell under three-dimensional periodic boundary conditions, which represents a part cut out of the interior of a natural gelatin specimen (cf. Appendix A).

As it is well known that gelatin properties are highly dependent from its hydration state,[65, 69, 145] two different water swollen stages were considered, specifically 0.8 wt.-% and 25 wt.-% of water. The models with 0.8 wt.-% water content (_0.8) correspond to the experimentally easily reachable 'dry' state (e.g. in vacuum over phosphorous pentoxide),[65] in which the remaining water molecules are tightly bound to the polypeptide chains. This low hydration state was selected to better analyze the non covalent interaction energies generated by the introduced functional groups as lower effect of water molecules is observed. The models with 25 wt.-% water content (_25) correspond to the water content of the gelatin films used for experimental purposes (see Chapter 5). In this state, not only a monomolecular layer of water molecules around the peptide backbone is present, but there are some tightly bound water molecules and some freely moveable water molecules that permit a higher mobility of the chain. Furthermore, by using the same water content in all models as in the experimental measurements, a standardization of the models enabling a better comparison with the experimental data was envisioned.

In Table 4.2 the specific parameters for the generated bulk models are reported. For each system, three independent models were realized to increase the statistical significance of the results.

Table 4.2. Samples of gelatin bulk models. Values are the average over three bulk models. The names of the models refer to pure gelatin (Gel), DAT functionalized gelatin (DAT-Gel), and DATT functionalized gelatin (DATT-Gel) respectively.

System ID	N° atoms	N° Aromatic rings	N° Water molecules	Cell dimension [Å]	Density [g·cm^{-3}]
Gel_0.8	3331	3	11	32.28 ± 0.4	1.233 ± 0.001
DAT-Gel_0.8	3544	13	12	32.82 ± 0.08	1.228 ± 0.001
DATT-Gel_0.8	3734	23	13	33.49 ± 0.04	1.191 ± 0.001
Gel_25	4648	3	450	35.63 ± 0.03	1.187 ± 0.004
DAT-Gel_25	4848	13	480	36.05 ± 0.33	1.196 ± 0.006
DATT-Gel_25	5222	23	508	37.15 ± 0.04	1.187 ± 0.002

4.2 General equilibration process for the bulk models of gelatin

The obtained models were subjected to an equilibration strategy similar to those reported in the literature by our group[132, 118, 133, 146] which led to reasonable results for other polymer systems. Specific equilibration procedure is described in section 8.1:

- Minimum image periodic boundary conditions in the three dimension.
- *Verlet Velocity* integration method.
- Non-bonded interaction:
  - Cutoff of 15 Å.
  - Group based summation method.
- Minimization: first using the *steepest descent* method, followed by the *Polak-Ribiere conjugated gradient*.
- Van-der-Waals tail correction for the pressure of 18 Å in the NPT-MD simulations (isothermal-isobaric ensemble, where the number of atoms N, the pressure P, and the temperature T, remain constant along the simulation).
- Dynamic time step of 1 fs (if not specified otherwise).

- *Berendsen* or *velocity scaling* as temperature control method, with a temperature window of 10 K.
- *Andersen* control method for pressure.

Figure 4.1 shows the equilibrated structure of the pure gelatin models with water contents of 0.8 wt.- % and 25 wt.- %, respectively, at 303 K obtained from the equilibration procedure described in section 8.1.3. The cell sizes are proportional to the real cell lengths and only the gelatin chains are shown in the figure, after all water molecules were removed for clarity.

For the evaluation of the obtained system it was made sure that the kinetic and potential energies as well as the model pressure and density of the respective models as a function of simulation time are only fluctuating randomly about constant mean values (see Figure 4.2) before any averaging of properties was performed. The results presented in the following section are calculated as a average values obtained from the final 2 ns of the NPT dynamics

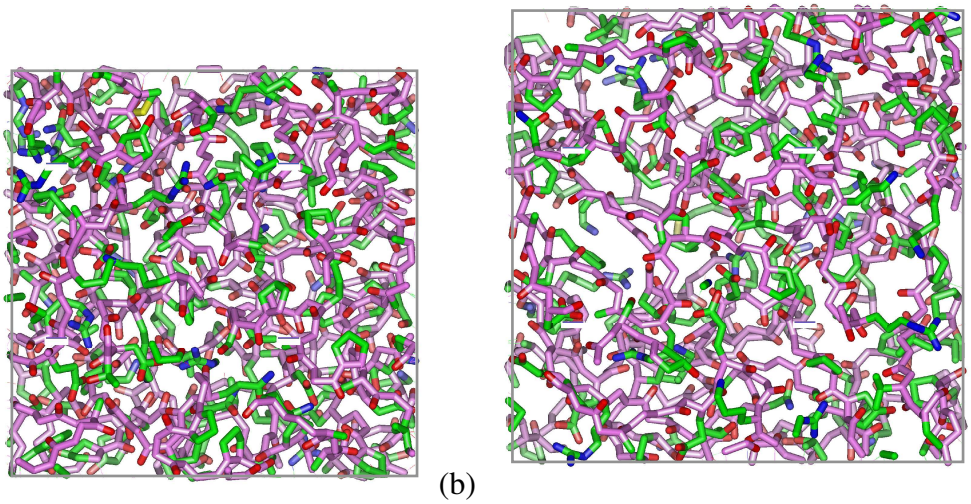

Figure 4.1. Snapshots of final structures of pure gelatin models with water contents of 0.8 (a) and 25 wt % (b) at 303 K. Water molecules and hydrogen atoms are not shown. The backbone is represented in magenta, side chain carbons are represented in green, oxygens in red and nitrogens in blue.

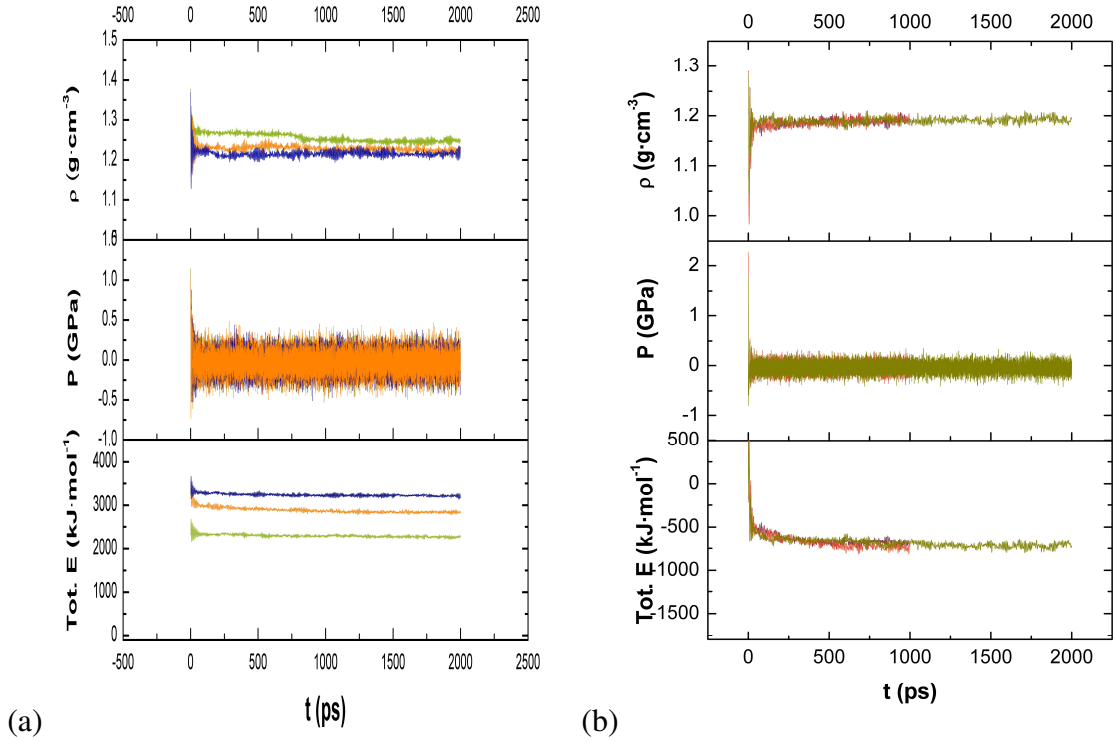

Figure 4.2. Example of MD simulation data recorded for a pure gelatin with 0.8 wt.-% (a) and 25 wt.-% H_2O content (b). Total energy, in (kJ·mol^{-1}), pressure in (GPa), and density in (g·cm^{-3}).

4.3 Validation of pure gelatin model

For validation of the models and evaluation of the selected forcefield, the generated pure gelatin structures were compared against experimental data (from the literature and self-determined). The average densities of the models during the NPT dynamic at 1 Bar were sufficiently similar (at maximum 3% lower) to the respective experimental values obtained via pycnometric measurements (see Table 4.2). Here it needs to be considered that gelatin as a natural biopolymer can show quite some variability in its properties including low degrees of three-dimensional order which tend to increase the density in comparison to the completely amorphous state realized in the models.

The statistical distribution of the dihedral angles of the peptide backbone φ, ψ, and ω (see Figure 4.3) are plotted in Figure 4.4. The two main points here are that on the one hand the ω values are close to 0° and ±180°, correctly showing the *cis* and *trans* amide bonds in peptide chains, which reflect the partial double bond character of amide bonds. The torsional angles φ

(N-C-Cα-C) and ψ (C-Cα-C-N), on the other hand show a more statistical distribution that correlates with the simulated amorphous structure. Nevertheless certain features of the typical collagen conformation are retained as indicated by the main peaks around -77° for φ and around 160° for ψ, as can be seen in Figure 4.4. This is comparable to the situation of e.g. polyethylene, where amorphous packing models (as a literature known amorphous reference material) show a global maximum for trans conformers which are defining the helical structure of PE chains in the orthorhombic crystalline state. The reason simply is that the defining conformational angles in highly ordered states normally also show the highest Boltzmann probabilities in amorphous systems. Summarizing the mentioned results at least qualitatively confirm the suitability of the used force field to model the peptidic structures in gelatin.

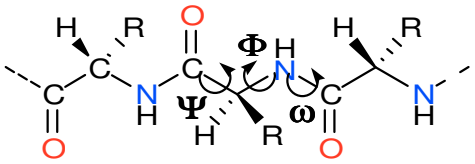

Figure 4.3. The backbone dihedral angles of protein.

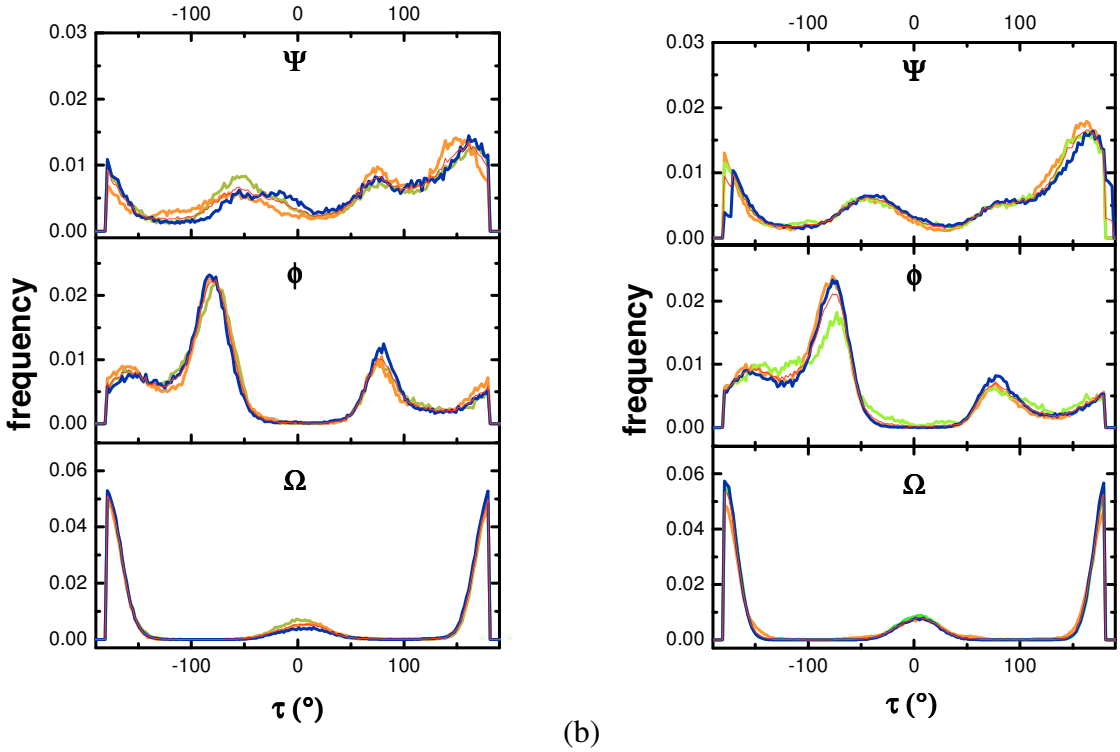

(a) (b)

Figure 4.4. Peptide torsional angles Ω, Φ, and ψ for the pure gelatin models with (a) 0.8 wt.-% and (b) 25 wt.-% water content. The distribution is shown for all the three packing models (blue, orange, green) and the averaged curve (red).

In Figure 4.5, calculated WAXS spectra for the different models are depicted for 2θ = 5° to 50° at a wavelength of 1.5418 Å (CuK_α radiation). Curves are shown as an average over the three packing models. Gelatin models with 0.8 wt.-% water contents show a broad scattering peak corresponding to a totally amorphous material (The visible ripples below 10° are artifacts of the limited model size). The peak is situated at 2θ = 19.85° (d = 4.47 Å) which is also observed in the natural material at a slightly different position (2θ = 22.4°, d = 3.97 Å), indicating that the average distance between two adjacent chain segments in the completely amorphous models is a bit larger than in real dry gelatin. While the general shape of the simulated and measured WAXS patterns is quite similar (Figure 5b) pure "real" gelatin shows a certain triple helical content as indicated by the peak at about 7°. This is a sign of a certain level of renaturation in the "real" case. Since these triple helical regions act as crosslinkers the slightly closer average distance between chain segments of the amorphous regions (cf. above

discussed positions of the main WAXS peak) in real gelatin in comparison of the completely amorphous models can be explained.

Figure 4.5b depicts the simulated WAXS data for the case of 25 wt.-% absorbed water. While there is no qualitative difference to the "dry" patterns the observable lower overall intensity level of the models containing 25 wt.-% of water is due to the screening effect of the bulk water molecules in the model.

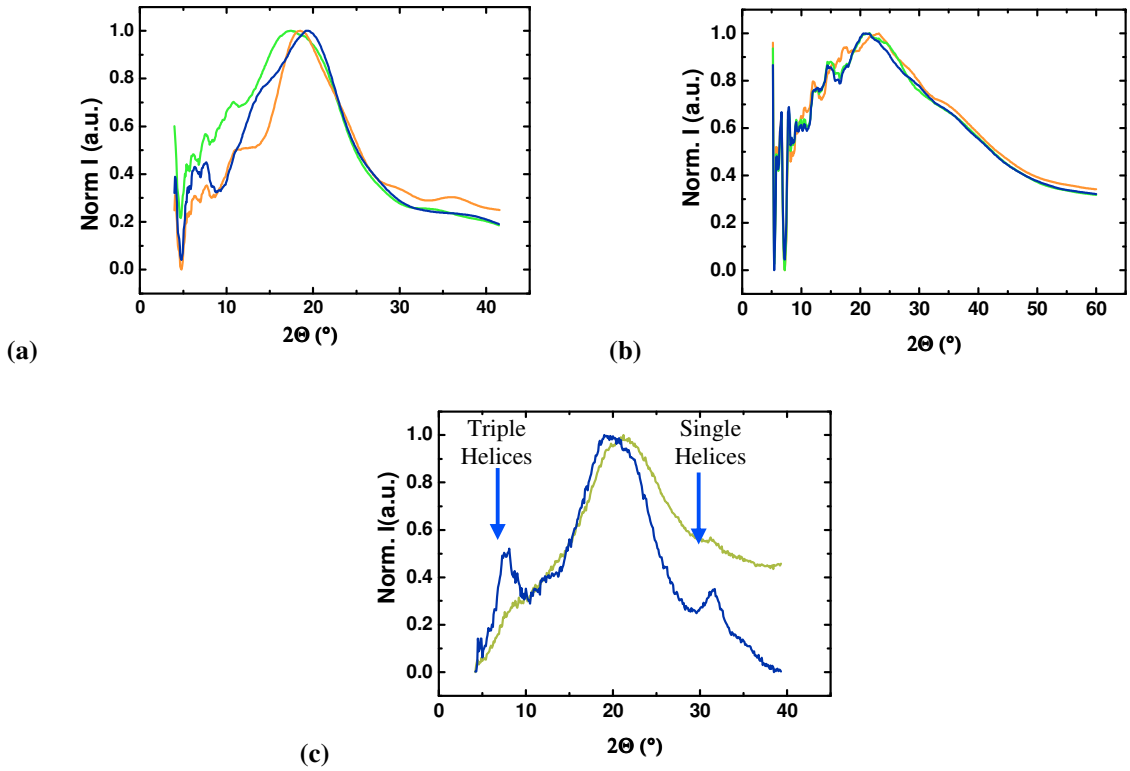

Figure 4.5. Calculated WAXS spectra of the molecular models (a) 0.8 wt.-% water content, (b) 25 wt.-% water content, and (c) experimental spectra of natural helical (blue) and amorphous (green) gelatins. For models the spectra is show for all the three packing models (blue, orange, green)

4.4 Validation of the bulk models of functionalized gelatins

Models of gelatin functionalized with DAT and DATT were submitted to the same equilibration process as pure gelatin. Comparison of the average density during the last 2 ns of NPT dynamic with the experimental value obtained in a second stage along this work showed values approximately 3% lower than the experimental value (see Table 4.2). This level of coincidence is typically considered as being sufficient considering the highly

complex nature of the investigated system. Similarly to the pure gelatin, dihedral angel distribution (Figure 4.6) show the tendency to maintain the typical helical conformation of collagen as indicated by the peak around -77° for φ and around 160° for ψ, with no influence by the respective hydration state. The calculated X-ray spectra for DAT-Gel and DATT-Gel show the broad diffusion band indicating the amorphous character of the models (Figure 4.8) in both case this band is located at 2θ = 19.06° for 0.8 wt.-% models and 21.6° in hydrated models, describing the amorphous nature of the material.

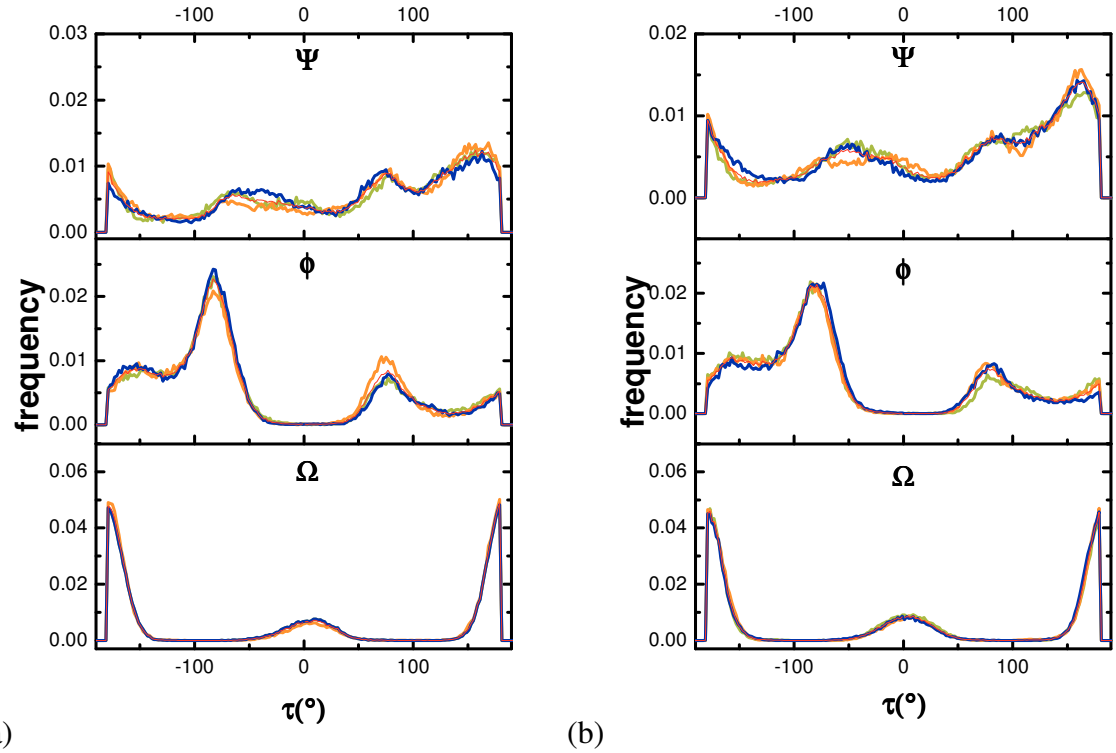

Figure 4.6. Peptide torsional angles ω, φ, and ψ for (a) DAT-Gel and (b) DATT-Gel models with 0.8 wt.-% water content. The distribution is shown for all the three packing models (blue, orange, green) and the averaged curve (red).

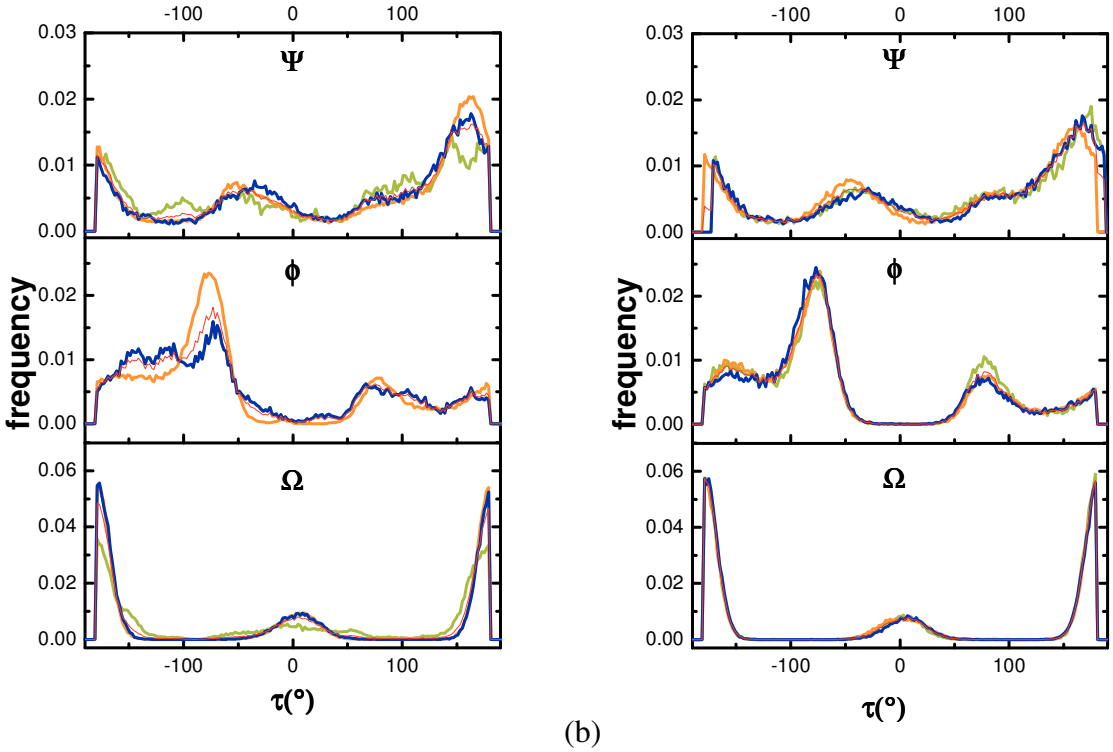

(a) (b)

Figure 4.7. Peptide torsional angles ω, φ, and ψ for the pure gelatin models with 25 wt.-% water content for (a) DAT-Gel and (b) DATT-Gel. The distribution is shown for all the three packing models (blue, orange, green) and the averaged curve (red).

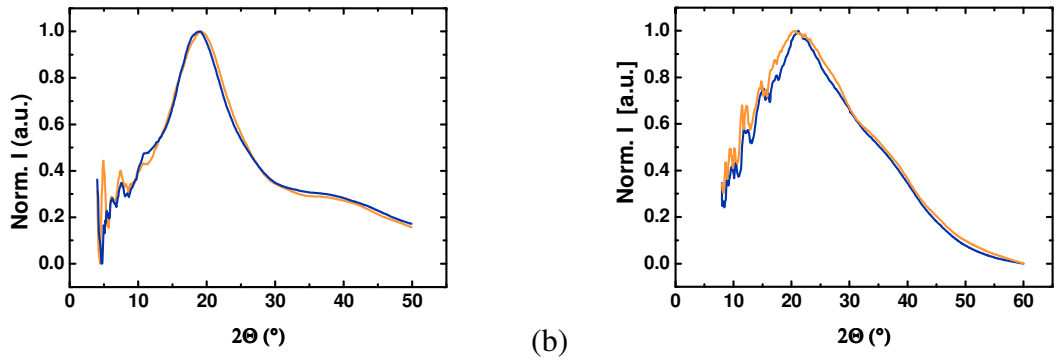

(a) (b)

Figure 4.8. Calculated X-ray scattering curve averaged over three models for functionalized DAT-Gel (blue) and DATT-Gel (orange) models with 0.8 wt.-% (a) and 25 wt.-% water content (b).

4.5 Structural analysis of the network

The validated models were further analyzed to observe the influence of introduced aromatic modifier groups. In this section, several structural properties such as chain segmental mobility, chain organization, and free volume distribution in the models among others are presented and discussed. The mentioned properties were studied in both hydration states. The presented data were obtained as an average over a large number of snapshots

extracted from the trajectory of the last 2 ns of the respective NPT MD run. Other properties, such as fractional free volume distribution and the hydrogen bond formation, were determined just for one representative snapshot for each model, and averaged over the three models representing each system.

4.5.1 Mobility of gelatin chains

The self-diffusion of the gelatin chain segment in the models with different water content was evaluated in terms of mean square displacement (MSD) of the atoms of the backbone during the last 2 ns of NPT-MD simulations with snapshots taken every 1 ps.

Figure 4.9 displays the mean squared displacement (MSD) of gelatin chain atoms of Gel, DAT-Gel and DATT-Gel, representing the mobility of the respective atoms in a given model. As expected, the presence of water had a great effect on the self-diffusion of gelatin chains, which increased with increasing water content. In models with 25 wt.-% of water, the MSD curves are considerably higher with respect to the models with just 0.8 wt.-% water content. The influence of the DAT or DATT side groups on the respective MSD curves is not straightforward. Both for the 0.8 and the 25 wt.-% water content causes the mobility decreases in the order DAT-Gel > Gel > DATT-Gel. The effects are however not too distinct and could therefore be of statistical nature.

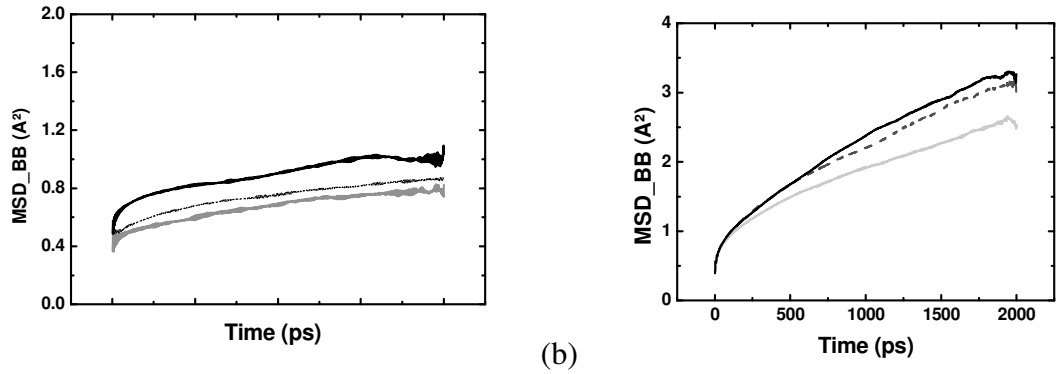

(a) (b)

Figure 4.9. Mean squared displacement for the self-diffusion of backbone atoms of gelatin chains averaged over three independent models of G(--), DAT-Gel(—), and DATT-Gel (—) at different hydration state; (a) 0.8 wt.-% and (b) 25 wt.-% H_2O content.

4.5.2 Crosslinking aromatic cluster formation

The main aim of introducing additional aromatic groups by functionalizing the lysine residues of gelatin consisted in the creation of reversible, specific noncovalent interactions between the respective aromatic rings at different functionalization sites which should lead to additional physical crosslinks. The necessary formation of aromatic interaction clusters requires certain distance and steric arrangement criteria of the participating aromatic groups. Typical are π-π stacking arrangements and edge-to-face CH/π-contacts. The distance of aromatic group centroids in both cases should not be larger than 7.5 Å to allow effective interaction.[15, 14]

In this study the effective formation of clusters was analyzed through different calculations, such as radial distribution function, detection of hydrogen bond formation, and π-π stacking arrangements along the trajectory of the data production run.

4.5.2.1 Radial distribution function

The radial distribution function, $g_{ab}(r)$, or the pair correlation function, is a measure to determine the correlation between particles within a system. This function describes the probability of finding a certain atom type *b* at a distance between *r* and *r*+*dr* from a reference atom type *a* as a function of the separation between them, *r* (see Figure 4.10).

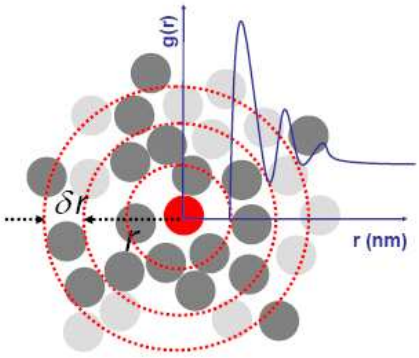

Figure 4.10.Basic scheme of the RDF including an example plot (blue line), where the red particle is the reference particle, and dark grey particles are those which are within the circular shell, dotted in red.

In this regard, the RDF between red particle (reference atom) and dark grey particle (atom of interest) is defined as:

$$g = \frac{\rho_r}{\rho} = \frac{N_r \cdot V}{N \cdot (4\pi r^2)\delta r} \qquad \text{((eq. 4.1)}$$

Where ρ_r is the number of atoms of interest in the volume element, ρ is the overall density, N_r is the number of atoms of interest inside the shell, N is the total number of atoms in the system, and V is the defined volume.

Using the RDFs it is then possible to determine the existence and degree of specific interactions like π-π interaction or hydrogen bonding. Here the RDF was used to evaluate the correlation between aromatic carbons, $g_{cc}(r)$, for distances up to 15 Å. In Figure 4.11 the RDFs for all gelatin system in the two hydration states are presented.

The curves are calculated as an average of the structure obtained from the last 2 ns of NPT simulation run, and consider only aromatic carbon belonging to different rings. The observed distances start at drastically lower values for models of functionalized gelatin than for the unmodified case. For DAT-Gel and DATT-Gel a considerable amount of the aromatic carbon-aromatic carbon distances were found below 7.5 Å permitting in principle the formation of effective aromatic stacking. The presence of water seems to only slightly influence this correlation (cf. Figure 4.11c).

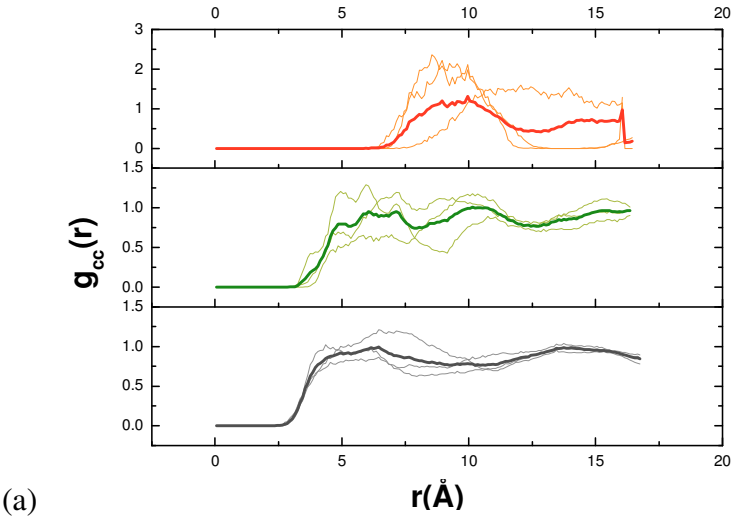

(a)

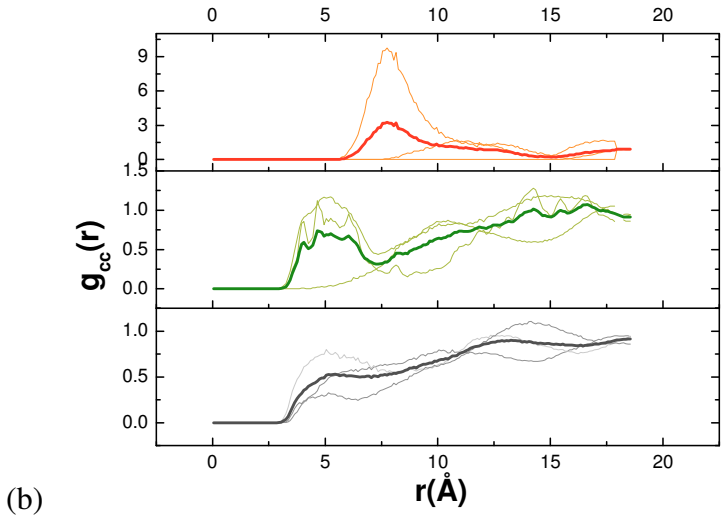

(b)

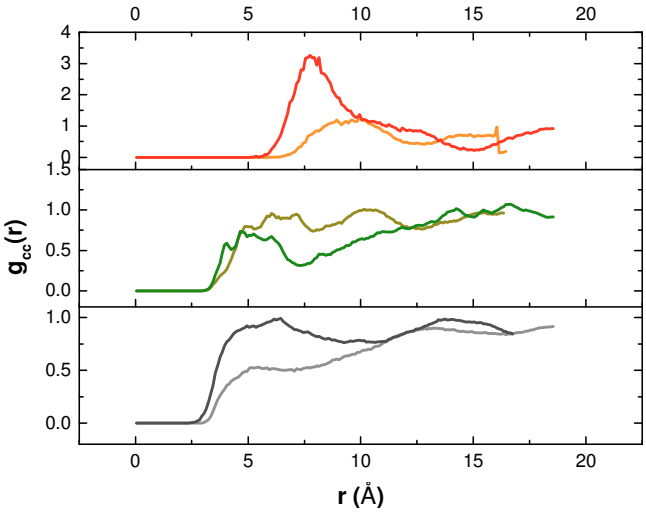

(c)

Figure 4.11. Intermolecular radial distribution function $g_{cc}(r)$, for intergroup distances between aromatic carbons for all simulated gelatin systems. Curve represent the behavior of the three independently simulated models for (from bottom to top) Gel, DAT-Gel and DATT-Gel (thin lines) and their average (thick line) for the 0.8wt.-% (a) and 25 wt.-% hydration state (b) and the averaged curve compared for the two hydration state studied (c).

4.5.2.2 Stacking of aromatic rings and hydrogen bonding

The actually created physical crosslinks are visualized for one specific packing models of each of the simulated model types at 25 wt.-% water contents (Gel_25, DAT-Gel_25, DAT-GelT_25) in Figure 4.12a-c. The frequency of such contacts between pairs of phenyl rings, not considering internal interactions between the two phenyl rings of one DATT functionalization site, were averaged over the three independent packing models created for each case. Clearly, an increased number of phenyl-phenyl cluster interactions were observed for the models with an increasing number of phenyl groups in the modifier (gelatin: 0.3 ± 0.6, DAT-Gel 1.7 ± 1.2, DATT-Gel 6 ± 1.7 contacts in 25 wt.-% models) and the close contact is maintained along the NPT run. In Figure 4.13 for the 0.8 wt.-% water containing dry models the calculated distances between centroids of aromatic groups belonging to different residues are plotted against the trajectory generated from the last 2 ns of the NPT dynamic run. The results confirm that also for the dry case with increasing number of phenyl rings in the model there are more contacts below the critical threshold for the formation of specific π-π interactions.

In the simulated functionalized gelatins was observed that 16% and 20% of the phenolic groups of DAT-Gel and DATT-Gel respectively, in addition to π-π interactions are also involved in hydrogen bonding while no such interactions were observed between the rather few aromatic units in unfunctionalized gelatin models.

Summarizing, the simulated models are predicting a trend towards the formation of physical crosslinks which is increasing for an increasing number of aromatic units per modifier molecule. I.e., the introduced phenolic groups in the functionalized gelatins can obviously undergo π-π interactions among each other and H-bond interaction from or to the polymer backbone, functional side groups, and other phenols.

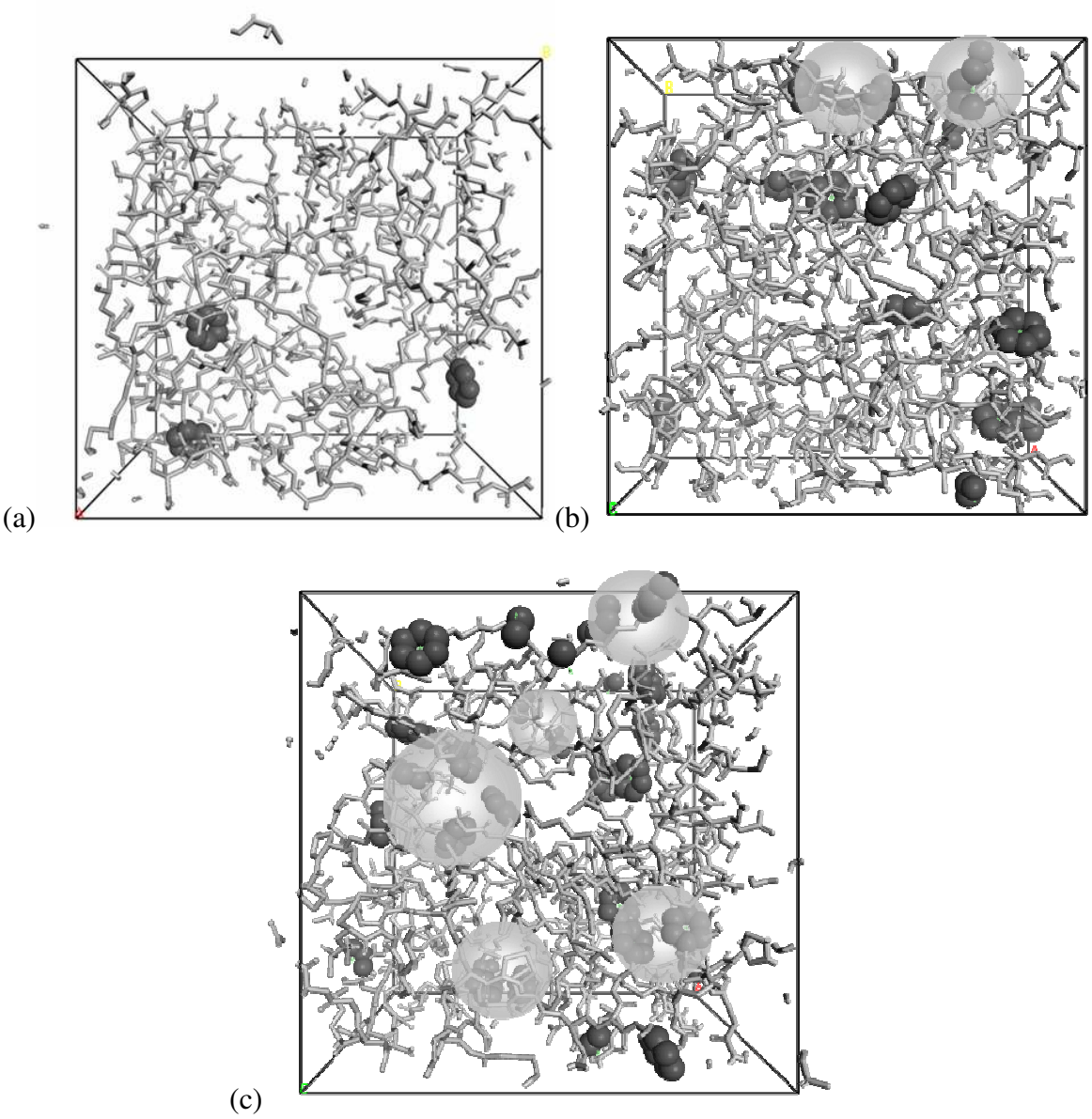

Figure 4.12. Amorphous cell structure of equilibrated models of Gel_25 (a), DAT-Gel_25 (b), and DATT-Gel_25 (c). Water molecule are removed for clarity, gelatin chains are represented by stick models except aromatic moieties (CPK representation). The aromatic rings are colored in dark gray and the formation of effective π-π interaction between phenyl groups belonging to different residues is highlighted by gray spheres.

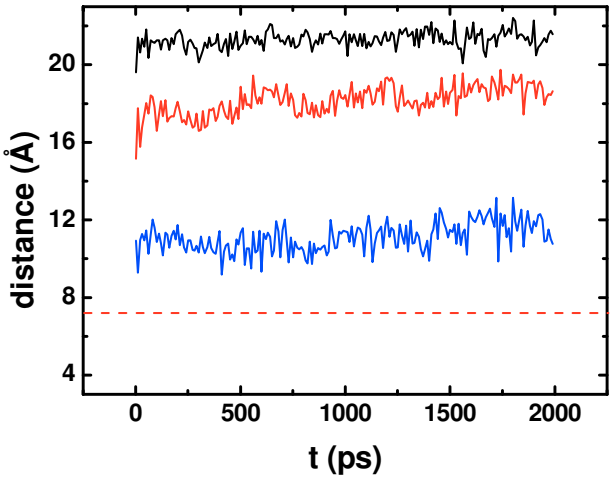

(a)

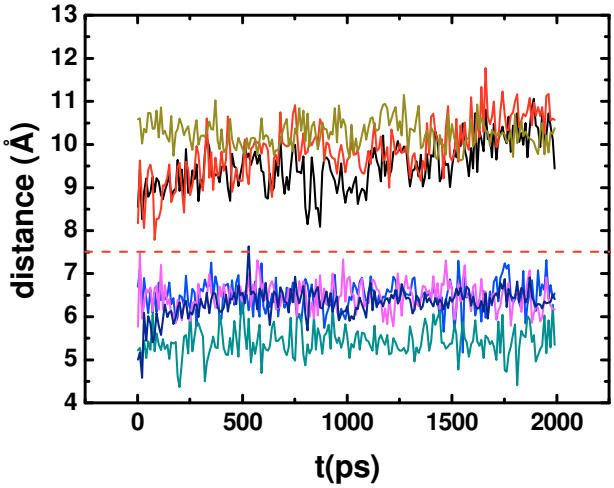

(b)

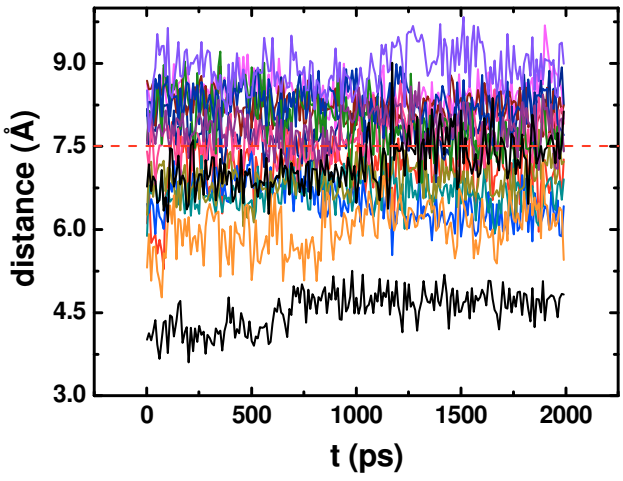

(c)

Figure 4.13. Diagram of distance between aromatic centroids belonging to different residues. Only significant centroid pairs are here represented for Gel_08 (a), DAT-Gel_08 (b), DATT-Gel_08 (c). The dotted red line indicate the range for effective aromatic π-π interactions

4.5.2.3 Characterization of free volume

One of the characteristics of the amorphous materials is the free volume existing in the bulk. The spatial distribution and overall amount of free volume is expected to have a considerable influence on material properties like water uptake and mechanical behavior. Different water contents and the presence of physical crosslinking may potentially influence the structural organization of the gelatin chain segments which in turn can have an effect on the water-accessible free volume distribution in the respective bulk polymer.

Bulk models were sliced along the x-axis in monolayer of atoms of about 4 Å in thickness (similar to computer tomography). This offers a qualitative visualization of the distribution of the free volume in the systems. Figure 4.14 shows series of monoatomic layers for the gelatin models in both hydration states, in each case only one representative model of the three generated was selected.

The amount of water accessible free volume in the 0.8 wt.-% water containing models is obviously very low and only small free volume elements are found which are isolated from each other (cf. Figure 4.14a/c/e). In the 25 wt.-% water containing cases (Figure 4.14b/d/f), the high amount of water lead to larger, often interconnected holes.

The free volume distribution could be also quantitatively characterized thanks to a calculation tool developed in-house.[133, 147] The free fractional volume accessible for water molecules was determined by overlaying a grid with a grid spacing of 0.5 Å over the cubic packing cells of interest. Then, a hard sphere with a radius of 1.1 Å or 1.4 Å, resembling a hydrogen or a water molecule, respectively, was placed on each grid point and it was checked if an overlap with any gelatin atom occurred.

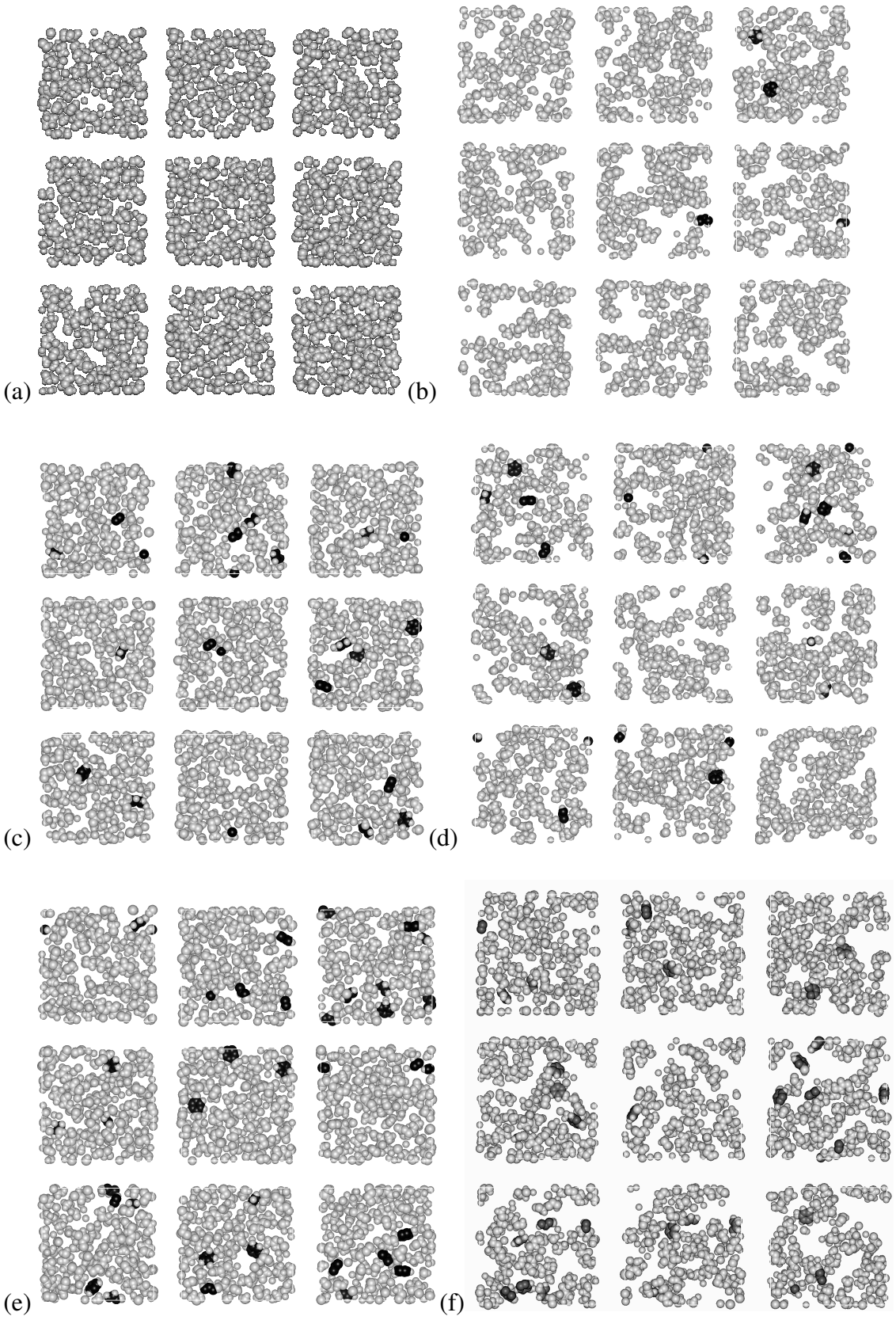

Figure 4.14. Representation of the free volume of the equilibrated models of unfunctionalized gelatins (a, b), DAT-Gel (c, d), DATT-Gel (e, f). With 0.8 wt.-% (a, c, e) and 25 wt.-% (b, d, f) H_2O content as a series of about 4.0 Å thick slices cut perpendicularly to the x-axis after removal of water molecules. The aromatic groups are highlighted in black.

The result of each particle insertion is a classification of the respective grid point as "occupied" or "free". If the grid point is considered "free", not occupied by gelatin atoms, than the surrounding lattice cube of 0.5 Å side length belongs to the accessible free volume of the model. Subsequently, the connectivity of the free grid point is checked and connected free grid points are collected into groups, which represent the individual holes. A simple topological criterion to determine the connectivity considers that every point of a group has at least one direct neighbor that is also a member of this group. This approach permits to identify holes which may have a complex geometry and large volume. The linear dimensions of the final holes are here expressed as the radius of a sphere of equal volume. For the examination of the free accessible volume all the water molecules are removed and the atoms of gelatin are represented by hard spheres with radii derived from the Van der Waals radii of respective atoms.

On this basis in Figure 4.15 the relative amount of free volume (y-axis) is displayed as a function of the respective cavity radius (x-axis). This examination is for all cases performed for the final snapshot of the respective NPT-MD data production run after all the water molecules were removed. The distributions were averaged over the three models existing for each system.

The increase of the water accessible free volume content in the models containing 25 wt.-% water compared to the models with 0.8 wt.-% water content is clearly visible, as observed previously in Figure 4.14. While in the 0.8 wt.-% water content models the free volume is organized in relatively small isolated holes, in the 25 wt.-% water content models a trend towards a more or less continuous hole-phase parallel to smaller holes can be seen. A similar situation was observed for ultra-high free volume polymers.[147] On the other hand, the effect of the aromatic modifiers on the free volume distributions of the respective models for both water contents is negligible.

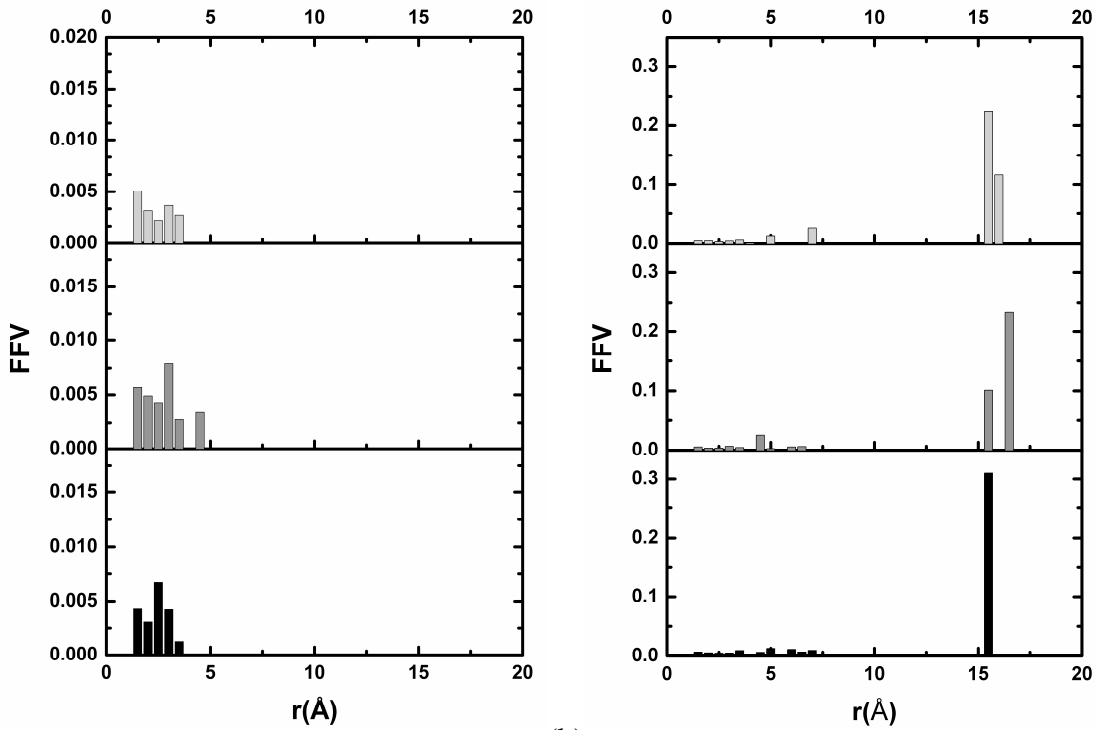

(a) (b)

Figure 4.15. Free fractional volume accessible to H_2O in the individual unmodified gelatin models at different hydration states. (a) Models with 0.8 wt.-% H_2O and (b) models with 25 wt.-% H_2O. Top: Gel (■), middle: DAT-Gel (■), bottom: DATT-Gel (■).

In the following the use of the models for predicting bulk thermomechanical material properties is discussed.

4.6 Macroscopic properties of the network

4.6.1 Mechanical properties

Mechanical properties of the models were determined by a static method developed by Theodorou and Suter (values see Table 4.3). The simulated values for Young's modulus E, compressive modulus E_c and shear modulus G were similar for all models of one specific hydration state, and there were also no significant differences between the models containing 25 wt.-% and 0.8 wt.-% of water, because the static method used for the calculation considers

the system in its glassy state and does not consider entropic variations that can be expected to have a higher contribution in the swollen models.

Table 4.3. Summary of calculated Young's modulus E, compressive modulus Ec, and shear modulus G for Gel, DAT-Gel, and DATT-Gel at 0.8 and 25 wt.-% water content.

System ID	E [GPa]	E_c [GPa]	G [GPa]
Gel_08	6.39 ± 0.63	5.81 ± 0.67	2.43 ± 0.24
DAT-Gel_08	6.31 ± 0.60	5.30 ± 0.02	2.43 ± 0.27
DATT-Gel_08	6.40 ± 0.19	5.59 ± 0.16	2.44 ± 0.09
Gel_25	6.67 ± 0.44	5.82 ± 0.08	2.55 ± 0.19
DAT-Gel_25	6.43 ± 0.26	5.89 ± 0.27	2.44 ± 0.03
DATT-Gel_25	6.65 ± 0.06	5.71 ± 0.11	2.54 ± 0.03

4.6.2 Prediction of equilibrium swelling capability of the network

More pronounced effects of aromatic functionalization are expected to be found in contact with water where the aromatic moieties tend to form clusters. The aromatic crosslink density was then used to predict the degree of swelling Q using the Flory-Rehner model.

The density of elastic network chains (ν/V) was used and was calculated according to the number of cluster (μ) found in the models and the average functionality of the network crosslinks (Φ) using the formula

$$\frac{\upsilon}{V} = \frac{\mu \cdot \phi}{2 \cdot V \cdot 10^{-21} \cdot N_A} \qquad \text{((eq. 4.2)}$$

The obtained values were utilized to approximate the degree of equilibrium swelling $Q = 1/\nu_s$ using the Flory-Rehner equation:[148]

$$\frac{\upsilon}{V} = \frac{\left[\ln(1-\upsilon_s) + \upsilon_s + \chi_1 \cdot \upsilon_s^2\right]}{V_1\left[\upsilon_s^{1/3} - \frac{2\upsilon_s}{\phi}\right]} \qquad \text{((eq. 4.3)}$$

with $\chi_1 = 0.49$ being the Flory polymer-solvent interaction parameter for isoelectric gelatin and V_1 being the molar volume of the solvent (V_1=18 mL/mol for water).

These results of the calculation are reported in Table 4.4, showing a reduction of a factor 6 for DATT-Gel respect to pure amorphous gelatin (zero crosslink density).

Table 4.4. Density of chain segments between two crosslinks ν/V and swelling degree Q(ν/V) obtained from application of the Flory-Rehner equation Q (ν/V) to the simulated models.

System ID	ν/V [cm^{-3}]	Q (ν/V)	Q (ν/V) [Vol. %]
G_25	$0.3 \cdot 10^{-7}$	162	16200
DAT-Gel_25	$2.2 \cdot 10^{-7}$	33	3300
DATT-Gel_25	$4.1 \cdot 10^{-7}$	27	2700

4.6.3 Calculation of solubility parameters

The cohesive energy density offers an insight into the strength of intermolecular forces, and in the case of a polymer it is closely related with its solubility in a defined solvent. In atomistic simulations, the CED is defined as the increase in energy per mole of material when all intermolecular forces are eliminated. The overall energy of the system with periodic boundary conditions is calculated first, and this value is subtracted from the respective energy calculated for the parent chain when the periodic boundary conditions are removed. The cohesive energy density is a parameter derived from the heat of vaporization and thus it can be considered a numerical value of the van der Waals (vdW) and electrostatic forces holding the molecules of a system together. A higher CED (and δ) is associated with higher physical interactions between the functionalized gelatin chains with polar solvents. The calculated values (Table 4.5) show a slight decrease of the solubility parameter with the introduction of additional aromatic moieties by modifying the lysine groups of gelatin. In this context, the electrostatic interaction energies are reduced more than the vdW contribution to the overall value. The overall decrease of the solubility parameter indicates a slight trend towards a more hydrophobic system.

Table 4.5. Calculated solubility parameters.

	Solubility parameter δ $[(J \bullet cm^{-3})^{1/2}]$	Electrostatic $[(J \bullet cm^{-3})^{1/2}]$	vdW Energy $[(J \bullet cm^{-3})^{1/2}]$
Gel_0.8	25.02 ± 3.61	17.98 ± 4.66	17.19 ± 1.34
DAT-Gel_0.8	24.10 ± 0.35	15.49 ± 0.28	18.46 ± 0.23
DATT-Gel_0.8	23.51 ± 0.11	14.78 ± 0.21	18.28 ± 0.31

4.6.4 Summary

Atomistic molecular modeling could be utilized to obtain an improved insight into structural features of gelatin and aromatically functionalized gelatins as amorphous bulk materials. Using NPT-MD simulations, well equilibrated bulk models of amorphous gelatin could be prepared and the influence of supramolecular aggregation of the introduced aromatic groups on the structural features and bulk properties of the respective materials could be investigated. The modeling of gelatin-based materials in the amorphous state was successfully implemented and gave results in the same order of magnitude (e.g. Young's modulus) and trend (decreased swelling) of the later obtained experimental data. This on the one hand indicates a sufficient quality of the models and on the other hand shows the predictive potential of the chosen computer aided modeling approach.

It could be proven from the models that the applied functionalization of gelatin side chains with aromatic moieties leads to a self-assembling process by formation of aromatic clusters. This process is based on specific, non-covalent interactions between the π-electron systems of the involved aromatic units and by hydrogen bonds from and to the phenolic OH-groups. Experimental measurements showed that already in the present case relatively low concentration of the introduced modifier groups led to a dramatic reduction of swelling capacity that could be qualitatively correlated to the amount of aromatic cluster observed in the models using the Flory-Rehner equation (see section 5.4.3).

The limited variation observed on some other bulk properties e.g. elastic moduli and fractional free volume distribution suggest that just modifying the 3 mol-% of lysine groups on native gelatin will not result in more dramatic changes of macroscopic properties in the dry state.

5 Synthesis and characterization of gelatin networks

In this chapter the syntheses and characterization of the physically crosslinked gelatin hydrogels are described. Gelatin was functionalized using the two different amino acid-derived compounds, DAT and DATT, which were introduced in the Strategies and Concepts (Chapter 3). Here, detailed descriptions of the synthetic path to DATT as well as the functionalization of gelatin are given. Subsequent sections in this chapter provide descriptions of the characterization of the material that aimed at understanding the influence of introduced groups on the renaturation process of gelatin, the gel stability, and the mechanical properties in the dry state and swollen state.

5.1 Synthesis of Desaminotyrosyl-tyrosine

An efficient synthesis of DATT (4) was realized in two steps. The first step was used to obtain the *tert*-butyl ester of DATT *via* the formation of an amide bond between H-L-Tyr-OtBu and EDC-activated DAT (Figure 5.1). The second step involved the deprotection of the tBu groups with trifluoroacetic acid (TFA) to give DATT with a free carboxylic acid in 53% over two steps after chromatographic purification. DATT was characterized by NMR and ESI-MS, which confirmed its high purity. The reaction was easily scaled up to produce 15 g batches of DATT.

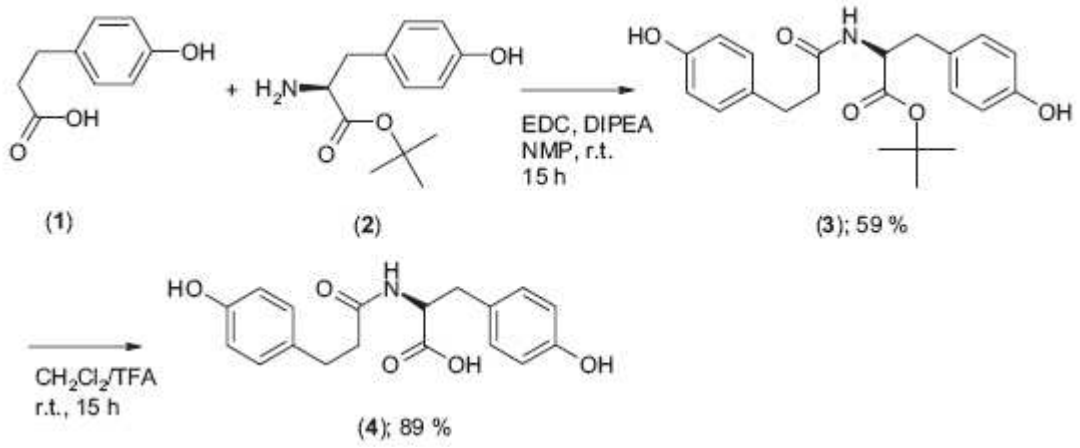

Figure 5.1. Synthetic route to DATT (4).

5.2 Polymer analogous reaction: synthesis of DAT- and DATT-Gels

Gelatin contains approximately 2.9 % lysine and 0.8-1.5% hydroxylysine residues.[142] On the basis of this amino acid composition, 1 gram of gelatin has 0.3 mmol of free amino groups, which are available for covalent attachment with activated DAT(T) functionalities. Indeed, this value was verified in the starting material used for these studies using TNBS measurements. First, DAT or DATT were reacted with NHS in the presence of EDC and DIPEA in DMSO to obtain the succinimidyl ester of the relative acid (DAT(T)-NHS) (see Figure 5.2). The activated DAT(T)-NHS is then able to react with the amino groups in gelatin to form covalent amide linkages. Then, DAT(T)-NHS was reacted with gelatin to obtain DAT-Gel (6) and DATT-Gel (7) as white powders following drying.

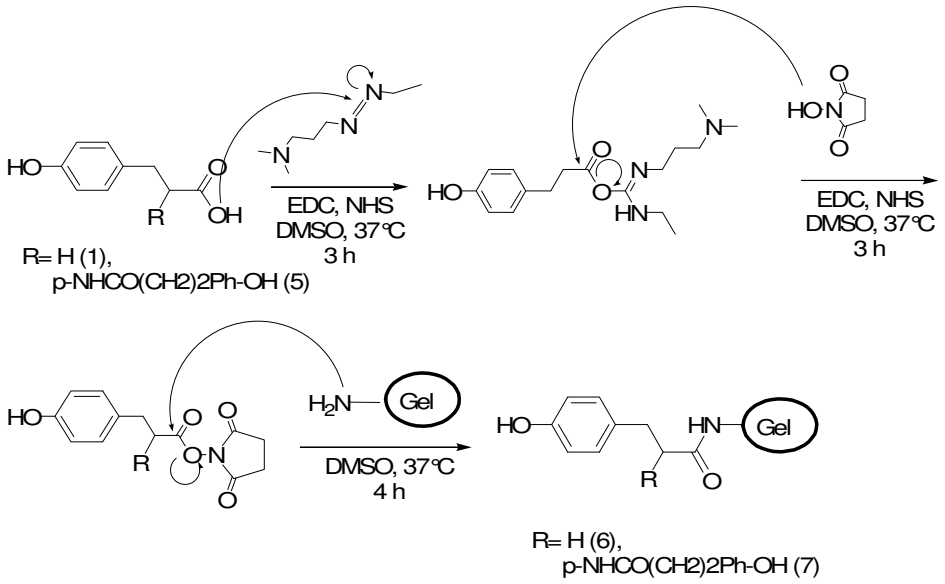

Figure 5.2.Mechanism of reaction of DAT and DATT with gelatin.

The degrees of functionalization for DAT-Gel and DATT-Gel by a polymer analogous reaction were determined by two independent methods, both of which resulted in similar values: ^{1}H NMR analyses and a colorimetric assay based on the reaction of free amino groups with TNBS. ^{1}H NMR calibration curves were obtained by mixing gelatin and DAT(T) at various concentration levels. The ^{1}H NMR peaks of gelatin (δ = 0.6 – 0.9 ppm) that corresponded to the methyl groups of the apolar amino acid residues leucine, valine, and isoleucine as well as the peaks that corresponded to the aromatic function (δ = 6.5 – 7.5 ppm) were integrated (Figure 5.3). The calibration curves were linear and gave R^2 values of 0.97 ± 0.001 and 0.98 ± 0.003 for DAT and DATT, respectively, for six data points. On the basis of ^{1}H NMR calibration data, DAT(T)-Gel was found to have 0.26 ± 0.02 mmol of DAT groups and 0.27 ±0.02 mmol of DATT per gram of gelatin, which corresponded to 80 ± 10 mol-% degree of functionalization with respect to gelatin lysine residues for DAT and 91 ± 3 mol-% degree of functionalization for DATT, both of which are good yields for polymer analogous reactions. These values were confirmed by the colorimetric assay based on the reaction of free amino groups with TNBS.[149]

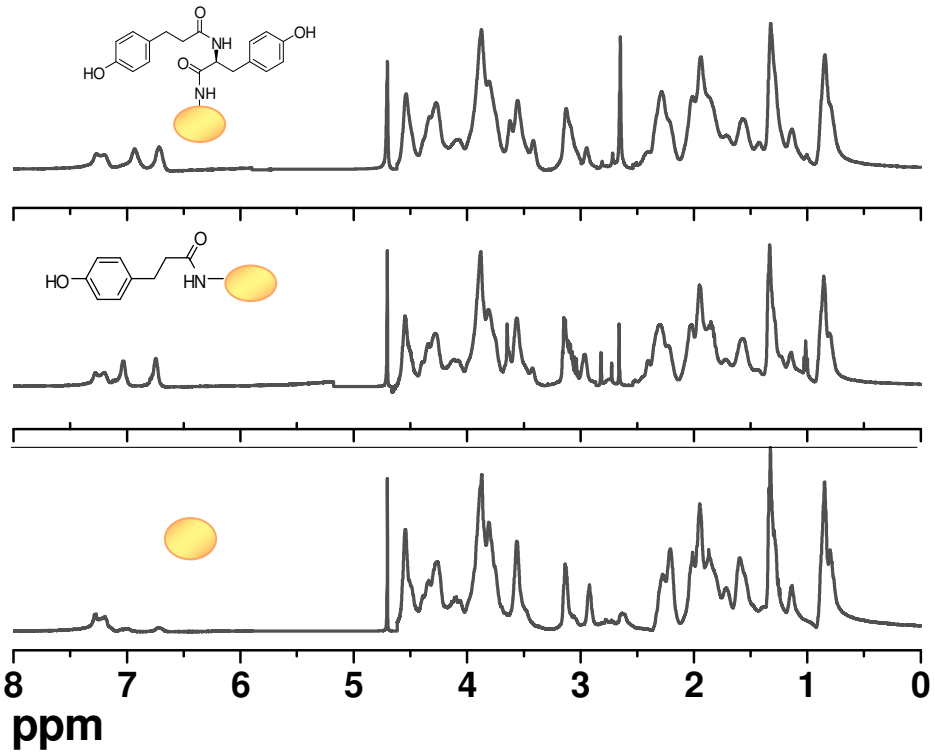

Figure 5.3. ^{1}H-NMR- spectra of gelatin (yellow circles) functionalized with DATT (top) and DAT (middle) compared to the pure gelatin (bottom) at 40 °C. The solvent consisted of 1 mL of D_2O

The ^{1}H-NMR comparison of the methods giving the total amount of introduced aromatic groups (NMR) and the percentage of reacted amino groups (TNBS assay) showed, that under the chosen reaction conditions only the amino functional groups were reactive. The reaction was performed in DMSO, which increases the pKa values of the hydroxyl functions on phenols,[150] serine, and threonine and reduced their reactivity towards carboxylic acids activated with EDC and reduced side-reactions with EDC, which permitted a systematic and controlled functionalization of gelatin on the amino groups.

5.3 Film formation

For characterization purposes, the aqueous solutions (5 wt.-%) of unfunctionalized gelatin, DAT-Gel, and DATT-Gel were dried at $T < T_c$ following the v_{long} procedure (see chapter 3) or the v_{short} procedure at $T > T_c$ giving films with thicknesses of 380 ± 30 µm, which are outlined in Scheme 5.2. Drying at $T < T_c$ (v_{long} procedure) allowed the association

and helicalization of chains given longer drying times, while drying at $T > T_c$ (v_{short} procedure) imparted higher chain mobility to the gelatin samples but for a shorter drying time, which inhibited helix formation and resulted in more amorphous films.

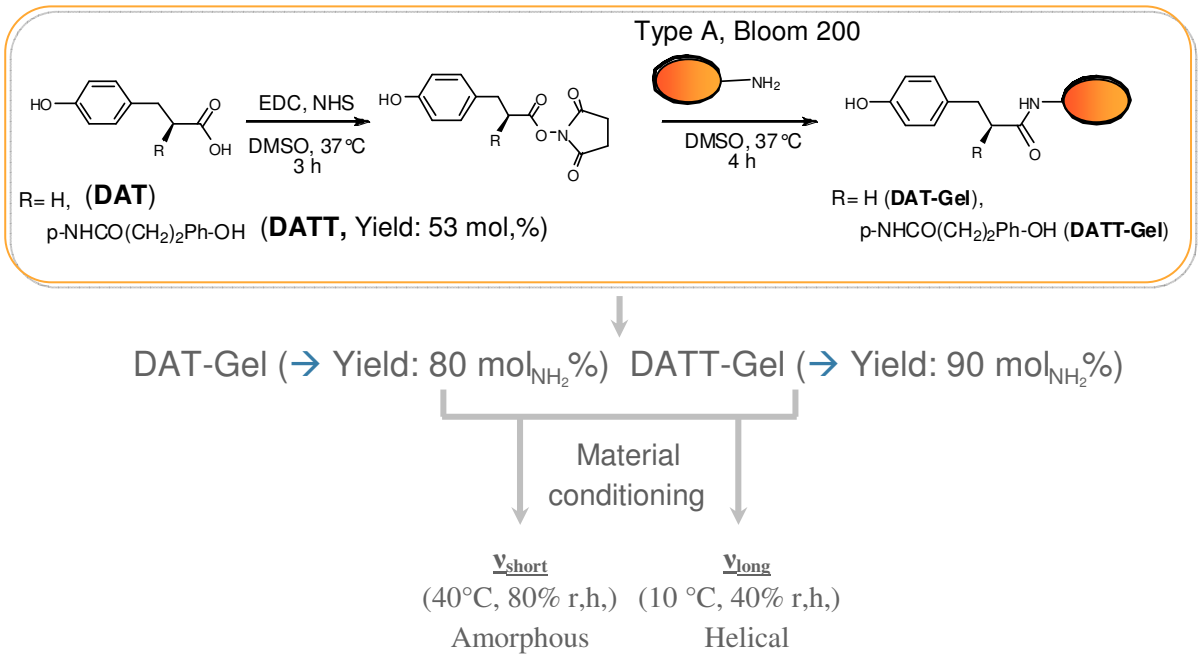

Figure 5.4. Schematic representation of synthetic route for polymer analogous reaction and material conditioning.

5.4 Material Characterization

5.4.1 Structural analysis

5.4.1.1 WAXS investigation on helical content

Following the treatments v_{long} and v_{short} for aqueous solutions of unmodified gelatin, DAT-Gel, and DATT-Gel, the chain organization in the dried samples was investigated by wide angle X-ray scattering (WAXS, Figure 5.5). The WAXS spectra for gelatin films (gelatin, DAT-Gel, and DATT-Gel) treated with v_{long} showed three peaks. In addition to the broad scattering peak around $2\theta = 21°$, which represents the average distance and distribution of the random coil chains (amorphous region), peaks at $2\theta = 7.5°$ (corresponding to the diameter of a triple-helix perpendicular to the chain direction) and at $2\theta = 32°$ (corresponding to the distance between prolines in a turn in the polyproline-II-helical single helices) were observed.

By dividing the integrated intensity of the peak at about 7.5° that accounts for the intermolecular lateral packing order inside the triple helical regions by the overall amorphous peak areas, it was possible to determine the degree of renaturation or relative amount of triple helices within the samples ($X_{c,t}$). Analogously, the single-helix peak (at about 32°) area in relation to the amorphous area permitted the determination of the single-helix ratio ($X_{c,s}$). This method monitored the changes in the scattering peak areas and therefore quantified the relative changes in the triple- and single helix contents of a samples ($X_{c,t}$ and $X_{c,s}$, Table 1). Qualitatively the WAXS curves indicated that the helicalization process was favored under the v_{long} drying process which was in agreement with the literature.[151, 152] The presence of one (DAT-Gel) or two (DATT-Gel) aromatic groups per lysine caused a reduction in $X_{c,t}$ following the v_{long} treatment. When changing the drying temperature to 40 °C and absolute humidity 40.83 $g \cdot m^{-3}$ (= 80% r.h.) (v_{short}), a shorter time was required for complete water evaporation than in v_{long} and the higher temperature ($T > T_c$) hindered helix nucleation. Consequently, the WAXS spectra of v_{short} gelatin showed only a small degree of single helices still present and a low amounts of triple helical regions ($X_{c,t}$ = 2.3 %) while for v_{short} DAT-Gel and DATT-Gel the helical contents was even more reduced.

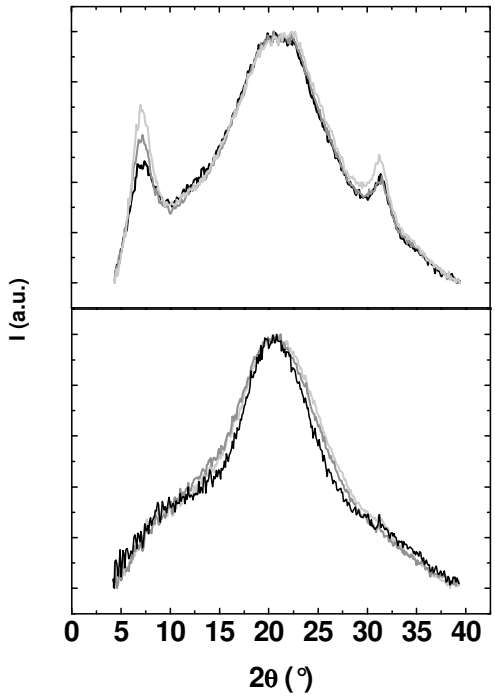

Figure 5.5. WAXS spectra of gelatin, DAT-Gel, and DATT-Gel v_{long} (top) or v_{short} (bottom) drying processes (—) gelatin, (—) DAT-Gel, (—) DATT-Gel.

Although longer chain mobilization time periods generally promote formation of triple helices,[153] the tendency for DAT-Gel and DATT-Gel to adopt typical collageneous features was reduced compared to pure gelatin by the introduction of the bulky aromatic groups. The formation and stabilization of the triple helices in collagen is strongly influenced by the amino acid side chains, where the presence of polar groups tends to stabilize the triple helix while aromatic amino acids destabilize it.[37, 154] On the other side, assembly of collagen fibrils in their biosynthesis is controlled by aromatic residues present at the non helical regions at both ends of a collagen molecule, known as telopeptides, which increase the kinetics of fibril self-association.[39] To identify whether the reduction in helical content observed in this study was a consequence of limited mobility of the chains due to the bulkiness of the introduced groups (kinetic effect), a kinetic drying study during v_{long} at different humidities was performed for the three materials (Figure 5.6). For v_{long} treated films, drying at different relative humidities altered the time points at which a constant low water content (resulting from water molecules tightly bound to the peptide chains) and chain fixation were reached. On the molecular level,

the X-ray patterns of the films showed in all cases the presence of a triple helical structure (2θ = 8°) and the single and triple helical contents increased with the drying time (i.e. with the humidity during the drying). The maximum relative content $X_{c,t}$ = 10.3% of triple-helical structure was determined for the gelatin dried with the longest drying process. For the functionalized gelatins DAT-Gel and DATT-Gel, the same trend was observed although $X_{c,t}$ was reduced. When comparing the WAXS spectra for three different humidities during the drying, which corresponded to the drying time periods, the single helical content increased first followed by an increase in triple helical contents only when the drying time was elongated. This can be explained by a two-step renaturation process into triple helices, where first an organization of chains into single helical polyproline-II helices took place followed by an association process that formed triple helices.[17, 155] A different interpretation of the helix formation kinetics also divided the process into multiple phases, which included the helix nucleation and helix growth.[59, 63] The helix nucleation process determines the number of triple helices and is temperature and concentration dependent. The helix growth process determines the length of helices and is temperature independent at $T < T_c$.. The results from this WAXS study indicated that the introduction of bulky aromatic groups introduced by DAT(T) interfered more with the triple helix formation than with single helical formation during the v_{long} treatments. Moreover, DAT-Gel and DATT-Gel showed lower $X_{c,t}$ values following v_{short} drying treatment compared with v_{short} gelatin, although the differences observed between the samples for each treatment were relatively minor.

Table 5.1 Evolution of relative single ($X_{c,s}$) and triple helix ($X_{c,t}$) content in the WAXS spectra for gelatin samples dried using v_{short} and v_{long} procedures as a function of time.

Sample ID	v_{long} treated samples								v_{short} treated samples
	1 day		2 days		3 days		10 days		
	$X_{c,t}$ [%]	$X_{c,s}$ [%]	$X_{c,t}$ [%]	$X_{c,s}$ [%]	$X_{c,t}$ [%]	$X_{c,s}$ [%]	$X_{c,t}$ [%]	$X_{c,s}$ [%]	$X_{c,t}$ [%]
Gel	9,9	1,8	8,0	2,1	9,6	3,0	10,3	2,7	2,3
DAT-Gel	7,3	1,0	7,5	1,5	7,3	2,3	7,7	1,7	0,9
DATT-Gel	6,2	1,8	5,6	1,8	7,5	1,4	8,2	2,2	0,8

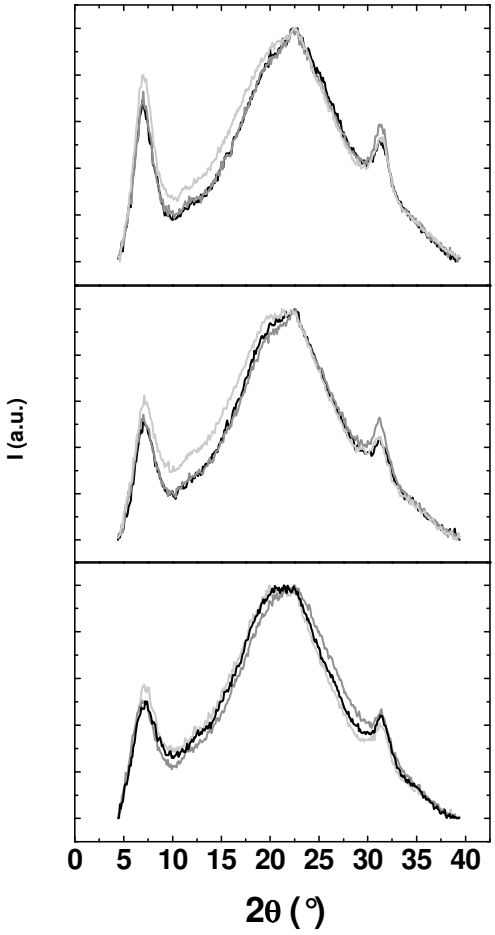

Figure 5.6. WAXS spectra of unmodified (top) and modified gelatins, DAT-Gel (middle) and DATT-Gel (bottom) after drying at 10 °C for 1 day (a.h.: 0.94 $g_{H2O} \cdot m^{-3}$; —), 3 days (a.h.: 4.73 $g_{H2O} \cdot m^{-3}$; —), and 10 days (a.h.: 7.60 $g_{H2O} \cdot m^{-3}$; —).

5.4.1.2 Thermodynamic investigation on helical content

The gelatin-based samples were characterized by TM-DSC to investigate whether the aromatic groups created a change in morphology within the gelatin-based materials. Figure 5.7 show the obtained curves for ν_{long} (a) and ν_{short} treated samples. The melting point (T_m), the enthalpy of melting (ΔH_m) were calculated during the first heating run, while the glass transition temperature (T_g), and the heat capacity change (Δc_p) value at the glass transition were calculated during the second heating run of polymer samples. Table 5.2 reports the measured values. The melting temperatures T_m correspond to the disaggregation of triple helices while the glass transition temperatures T_g correspond to chain mobility. Samples treated with ν_{long} showed a decrease of T_m from 142 °C to 126 °C when increasing the number

of aromatic groups, which indicated a lower stability of the helical structures or a reduction of helix content when increasing the number of aromatic groups. The T_g of gelatin after treatment with v_{long} (116 °C) decreased to 99 °C for DAT-Gel and 106 °C for DATT-Gel. This decrease in T_g following functionalization with bulky side groups can be explained by the decrease in barriers of rotation in the random coils due to the disruption in helical structures, i.e. the chain segments are on average more loosely packed. Furthermore, the mobility of chains in DAT-Gel and DATT-Gel was likely slightly higher than in gelatin as any residual water was not as tightly bound and because there are less interchain hydrogen bonds due to the introduced functional groups. The relative increase of T_g in DATT-Gel compared to that of DAT-Gel can be attributed to the fact that there were additional netpoints formed by aromatic clusters as predicted in modeling studies of this system.[127, 134] The predominantly amorphous gelatins obtained from v_{short} likewise showed a reduction of T_m (from 144 °C for gelatin to 123 °C for DAT-Gel and 127 °C for DATT-Gel) and T_g comparing gelatin and the functionalized gelatins. The presence of T_m in the DSC thermograms for the v_{short} samples was in agreement with the WAXS data, which indicated considerably smaller yet still visible amounts of helical content. The T_gs from v_{short} samples had the same tendency as observed above, where the values for unfunctionalized gelatin were higher than for DAT-Gel and DATT-Gel. The reduction of T_g in natural gelatin is potentially related to an increase in water bound to the gelatin backbone in case of amorphous samples leading to a stronger plasticization effect during TM-DSC measurements.[60, 65, 66, 156, 157] As no change in Δc_p was observed for this set of samples, the water content in the samples were similar, meaning that the presence of aromatic groups was not the only factor in determining chain mobility. The decrease in T_m for the functionalized systems demonstrated that the aromatic side groups destabilized helices, which indicated that thermodynamic disruptions were present in addition to the kinetic differences in v_{long} and v_{short}. These observations were

made under stable material conditions as the decomposition of gelatin, DAT-Gel, and DATT-Gel were observed at approximately 300 °C (Figure 5.8).

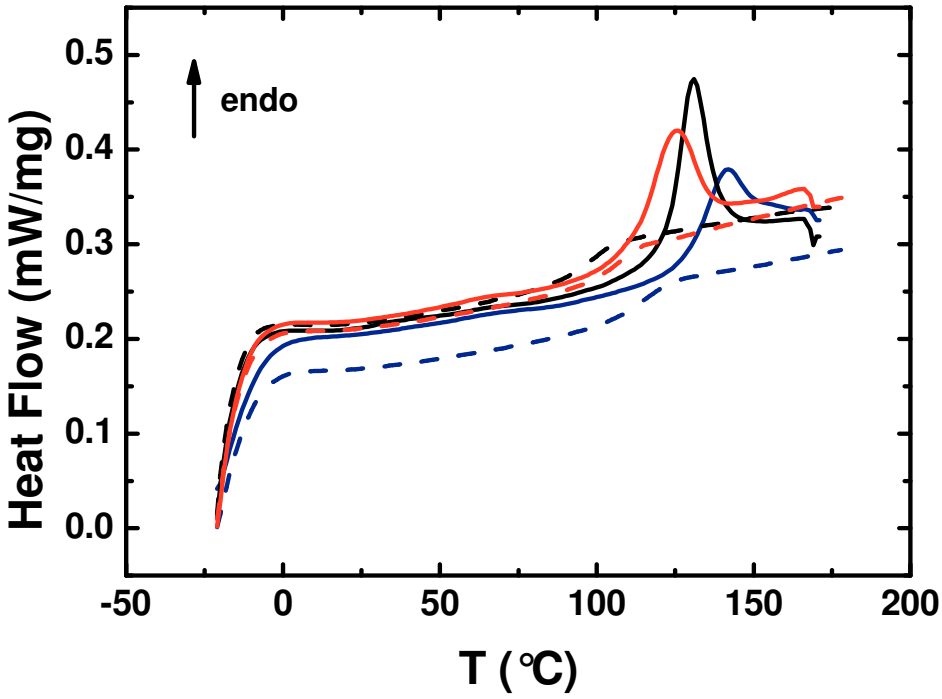

(a)

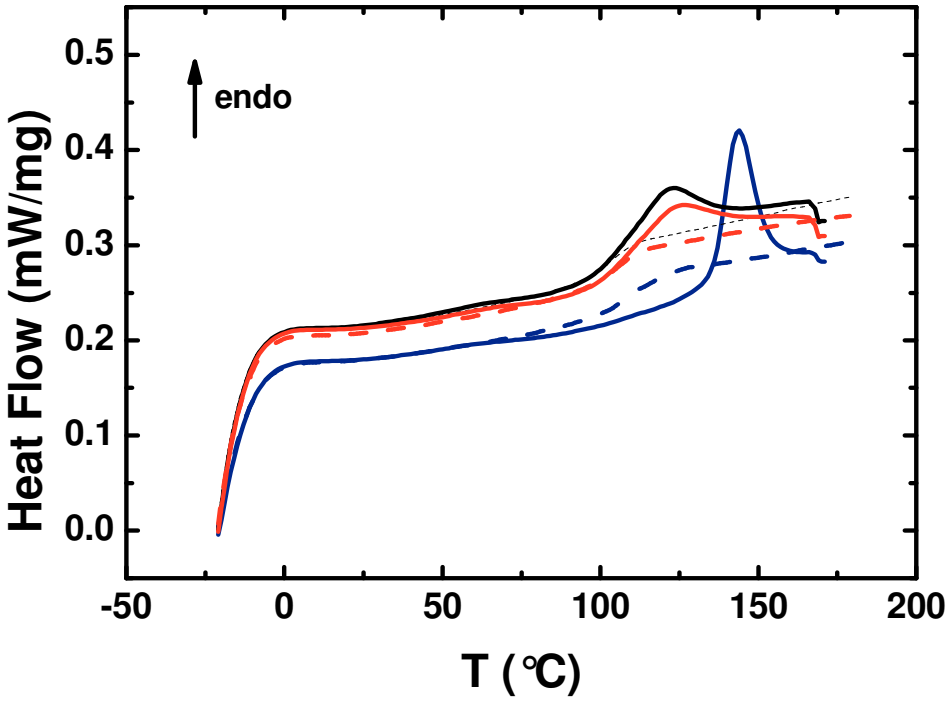

(b)

Figure 5.7. The first (–) and second (···) heating scans of TM-DSC thermograms of ν_{long} (a) and ν_{short} (b) gelatin films for Gel (—), DAT-Gel (—), and DATT-Gel (—)

.

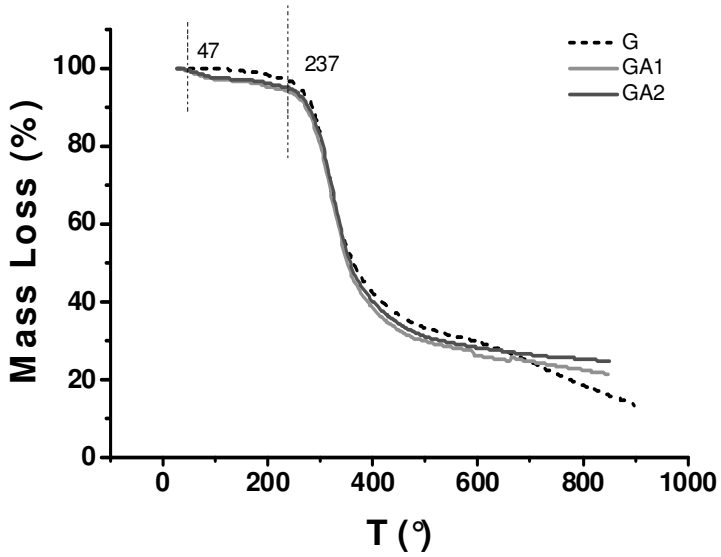

Figure 5.8. The Mass Loss (%) plotted against temperature for Gel (····), DAT-Gel (—), and DATT-Gel (—).

Table 5.2. Thermal transitions determined by TM-DSC of gelatin-based films. T_g: glass transition temperature;Δc_p = change of heat capacity at T_g; T_m: melting temperature, corresponding to the denaturation and ΔH_m: denaturation enthalpy.

Sample ID	v_{long} treatment				v_{short} treatment			
	T_m [°C] 1st run	ΔH_m [J·g^{-1}] 1st run	T_g [°C] 2nd run	Δc_p [J·(g·K)$^{-1}$] 2nd run	T_m [°C] 1st run	ΔH_m [J·g^{-1}] 1st run	T_g [°C] 2nd run	Δc_p [J·(g·K)$^{-1}$] 2nd run
Gel	142	18	116	0.35	144	22	110	0.35
DAT-Gel	131	26	99	0.33	123	17	103	0.35
DATT-Gel	126	19	106	0.29	127	14	105	0.36

5.4.2 Macroscopic properties

5.4.2.1 Swelling behavior of gelatin networks

The content of aromatic functional groups had a strong influence on the swelling properties of the pure and modified gelatin hydrogels (Table 5.4). A clear decrease in the degree of swelling at equilibrium (Q) with increasing number of aromatic moieties introduced per lysine modification was observed (Gelatin films treated with v_{long} showed a degree of swelling of 2080±65 Vol.-%, while the introduction of one aromatic moiety per lysine residue in DAT-Gel led to a decrease in volumetric swelling (1580 ± 440 Vol.-%) that was much more pronounced for DATT-Gel (300 ± 5 Vol.-%). For films from v_{short} a similar trend was observed, however, the absolute values were slightly higher (Q varying from 2805 ± 330 for

gelatin to 1730 ± 130 for DAT-Gel, and 265 ± 55 for DATT-Gel), which can be attributed in each case to the lower amounts of triple-helical domains which are also acting as crosslinks. In addition to the drying processes v_{short} and v_{long}, the differences observed in these swelling experiments highlight the major effects of the aromatic side groups in DAT-Gel and DATT-Gel with respect to the helical netpoints of gelatin for all of the samples.

Table 5.3. Density for dry gelatin Gel, DAT-Gel, and DATT-Gel and their volumetric swelling (Q) in water at 23 °C.

Sample ID	Density [g·cm-³]	v_{long} procedure Q [Vol. %]	v_{short} procedure Q [Vol. %]
Gel	1.28	2080 ± 65	2805 ± 330
DAT-Gel	1.27	1580 ± 440	1730 ± 130
DATT-Gel	1.25	300 ± 5	265 ± 55

Figure 5.9. Swelling behavior of aromatic functionalized gelatin. Supramolecular hydrogel (in front) and dry sample (back) for gelatin, DAT-Gel, and DATT-Gel, from left to right.

5.4.2.2 Rheological properties of gelatin networks

The hydrogels at the equilibrium degree of swelling described in the foregoing section were furthermore subjected to dynamic mechanical analysis. Figure 5.10a shows the change of the storage modulus G' and the loss modulus G'' as a function of temperature for gelatin treated by v_{long} and Figure 5.10b/c show the change of G' comparing the differently functionalized gelatins, which are summarized in Table 5.4. G' values for $T < T_c$ are reported to estimate the differences in storage modulus within this temperature range. The temperature associated to the dissolution of the elastic networks (T_c) was identified here as the crossover point between G' and G'' during the rheological measurements,[158] which were higher than values previously reported for bovine-hide gelatin and tuna-skin gelatin (T_c < 30 °C).[159] At T < 30 °C, the gelatin systems showed storage moduli G' with a pronounced plateau between

1 and 10 kPa and loss moduli G''(ω) that ranged from 10 Pa to 250 Pa as determined in frequency sweep measurements. The G' values for the different samples did not significantly differ at $T < T_c$; however, T_c was lower for the samples treated with ν_{long} than for the samples treated with ν_{short} for gelatin and DAT-Gel, while T_c was similar in both cases for DATT-Gel. The higher T_c values of DATT-Gel compared to DAT-Gel and gelatin in the ν_{long} samples might be related to the additional netpoints formed by the DATT groups, which were shown to destabilize the gelatin triple-helical network structures regardless of chain mobilization time.

Table 5.4 Storage modulus (G') and crossover temperature (T_c) based on rheological measurements on gelatin, DAT-Gel, and DATT-Gel hydrogels.

	ν_{long}		ν_{short}	
Sample ID	G' ($T < T_c$)	T_c	G' ($T < T_c$)	T_c
Gel	2.6 ± 1.6	35.5	2.6 ± 1.7	38.5
DAT-Gel	0.6 ± 0.3	33.0	2.5 ± 0.9	37.0
DATT-Gel	3.5 ± 1.6	37.5	2.9 ± 1.3	38.0

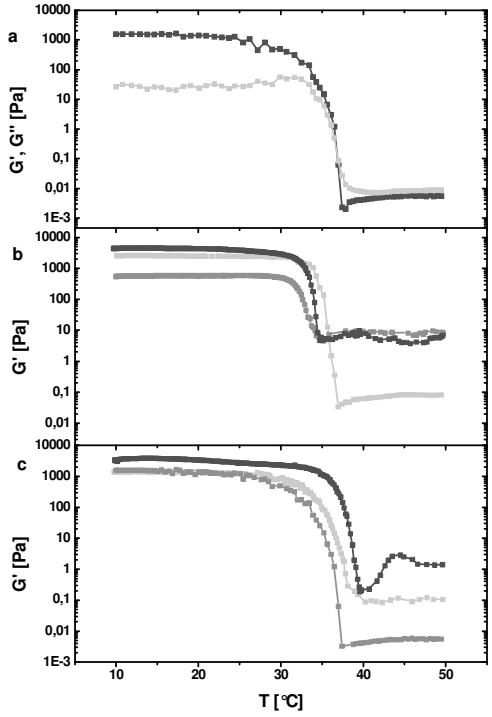

Figure 5.10. Dynamic rheological measurements of swollen gelatin hydrogels Gel, DAT-Gel, and DATT-Gel. Temperature dependence of the storage modulus G' (■) and the loss modulus G''(■) for natural gelatin (a). Temperature dependence of the storage modulus G' for cold dried (b), and warm dried gelatins (c) for gelatin (■), DAT-Gel (■), and DATT-Gel (■). Measurements were performed at constant stress 4 Pa and a frequency of 1 Hz, in a temperature range form 10 °C to 50 °C with a temperature ramp of 2.6 °C·min^{-1}.

5.4.2.3 Mechanical properties of gelatin networks

Data from tensile tests performed on materials with 25 wt.-% water content[69] are shown in Table 5.5. The 25 wt.-% water content was selected for handling purposes as samples with lower water contents were too brittle and could not be characterized by tensile testing. All materials exhibited E = 2 – 2.5 GPa under these conditions, which were similar values to previously reported for porcine gelatins.[67]

Gelatin films treated with v_{long}, which possessed a higher relative triple helix content than the samples produced with v_{short}, showed elastic mechanical behavior with 25 wt.-% water content (Figure 5.11). Gelatin films (v_{short}) and DAT(T)-Gel films, which possessed a low triple-helical content, showed a brittle behavior of the material and reduced tensile strength σ_{max}, elongation at break ε_b, and Young's modulus E. These results were in agreement with previously observed mechanical properties for materials with differing chain mobilization times.[69, 66, 65] However, the mechanical properties of the functionalized gelatins with 25 wt.-% water content were not drastically affected by the different drying procedures, with greater differences being observed for the DAT-Gel samples than for the DATT-Gel samples. Overall, for materials containing 25 wt.-% water content, the elastic behavior as indicated by E did not show any clear correlation with the samples' respective renaturation degrees $X_{c,s}$ or $X_{c,t}$. This can be understood by the fact that the Young modulus is determined at very small deformations where crosslinks like triple helical regions often do not have major influence on the material response. Larger deformations, however, as described e.g. by σ_{max} and ε_b, the effect of crosslinks can be more pronounced (Table 5.5).

Table 5.5. Mechanical properties of cold and warm dried gelatin films containing 25 wt.-% water. E: Young's modulus; σ_{max}: ultimate tensile strength; ε_b: elongation at break.

	v_{long} treatment			v_{short} treatment		
Sample ID	E [GPa]	σ_{max} [MPa]	ε_b [%]	E [GPa]	σ_{max} [MPa]	ε_b [%]
Gel	2.38 ± 0.17	75 ± 11	14 ± 2.6	2.26 ± 0.27	69 ± 18	6 ± 1.2
DAT-Gel	2.05 ± 0.47	69 ± 6	12 ± 1.4	2.03 ± 0.24	51 ± 27	3 ± 0.8
DATT-Gel	2.05 ± 0.44	41 ± 12	2 ± 0.4	2.08 ± 0.46	39 ± 10	3 ± 0.9

In addition, the mechanical properties of the hydrogels at equilibrium swelling were determined as these conditions were similar to those present for implanted bone regenerative devices (Table 5.6). The change of mechanical properties according to the number of aromatic modifier groups and helical content of samples at equilibrium swelling was remarkable. For example, tensile tests performed in the swollen state showed a drastic increase in E and ε_b for samples which before the equilibrium swelling experiment were originally obtained via the v_{short} procedure compared to the respective v_{long} samples (Figure 5.11). The difference in elastic behavior of the swollen samples can be correlated with their renaturation degree of triple helices $X_{c,t}$, where the v_{short} samples containing $X_{c,t}$ = ~1 - 2% showed higher E values than the v_{long} samples containing $X_{c,t}$ = 8 – 10%. However, the trend observed here did not corroborate with a previous report relating elasticity and $X_{c,t}$ in 5 wt.-% gelatin films,[17] where the elastic moduli of gelatins start to increase from zero (within the limits of accuracy of the reported data) at triple helical contents higher than $X_{c,t}$ = 7% (tested between 24 – 28 °C). Rather, the data reported here showed that the swollen films containing $X_{c,t}$ < 7% (v_{short}) possessed much higher E values than the films containing $X_{c,t}$ > 7% (v_{long}). A possible explanation for this is that the v_{long} samples, which possessed $X_{c,t}$ = 8 – 10%, agree with Djabourov's conclusions since the amount of triple helical contents was sufficient to dictate the physical interactions at equilibrium swelling. Indeed, the previous models also showed that E = 150 kPa for gelatin solutions (5 wt.-%) with $X_{c,t}$ = 15%, and the maximum E value obtained for the v_{short} treated samples was 10 kPa for gelatin ($X_{c,t}$ = 10.3%), which are similar to the v_{long} treated samples. Since the swollen v_{short} samples were stronger and more elastic, yet possessed only $X_{c,t}$ = 0.8 – 2.3%, their mechanical properties were obviously ruled by other interactions, including those based on the aromatic functional groups for DAT- and DATT-functionalized gelatins. The general increase in maximum tensile strength σ_{max}, elongation at break ε_b, and E for v_{short} samples can be explained by the swelling mechanism of gelatin, which causes the fibrils to align, expands the matrix, endows greater chain mobility, and

ultimately strengthens the network.[160, 161] This also explains why the swollen unfunctionalized gelatin, which possessed no additional net points, also showed greater *E* values following treatment with v_{short} than following treatment with v_{long}, even though v_{long} produced gelatin with higher $X_{c,t}$.

The *E* values increased for the v_{short} treated gelatins with increasing contents of aromatic modifier groups because of the formation of additional net points as determined in molecular modeling studies.[127, 134] Overall, the differences between the v_{short} and v_{long} treated materials in the swollen state demonstrated how chemical functionalization combined with drying procedures may be used to achieve controlled properties of gelatin-based materials intended for bone regeneration applications.

Table 5.6. Mechanical properties polymer samples at equilibrium swelling measured by tensile test in aqueous environment at $T = 23$ °C. E: Young's modulus; σ_{max}: ultimate tensile strength; ε_b: elongation at break.

	v_{long} treatment			v_{short} treatment		
Sample ID	E [kPa]	ε_b [%]	σ_{max} [kPa]	E [kPa]	ε_b [%]	σ_{max} [kPa]
Gel	10.4 ± 2.5	8.8 ± 1.3	1.9 ± 0.2	173 ± 59	15 ± 6	30 ± 10
DAT-Gel	4.5 ± 0.5	21.2 ± 12	1.5 ± 0.6	190 ± 30	57 ± 23	60 ± 20
DATT-Gel	8.6 ± 4.0	11 ± 8	2.1 ± 1.1	598 ± 92	80 ± 20	70 ± 40

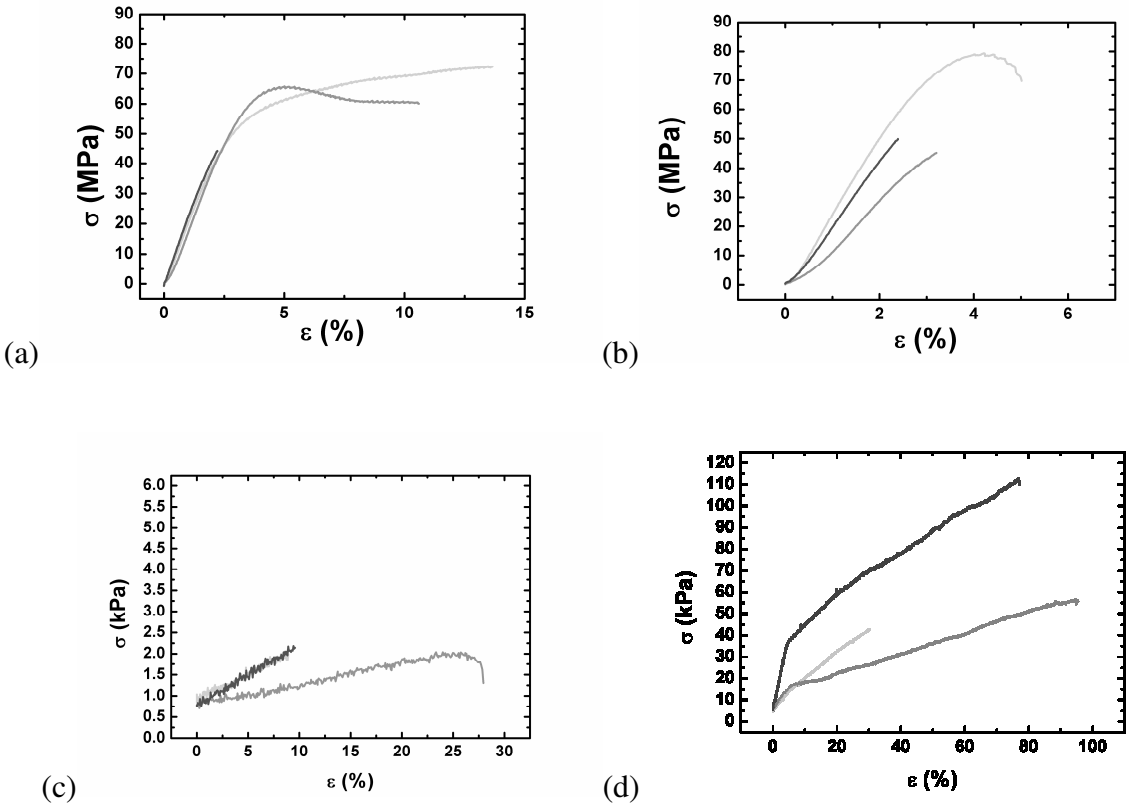

Figure 5.11. σ-ε diagrams from tensile test of gelatin samples with 25 wt.-% water content (a, b) and hydrogels at equilibrium swelling (c, d) obtained by v_{long} (a, c) and v_{short} (b, d) drying process. (—) Gel, (—) DAT-Gel, and (—) DATT-Gel.

5.4.3 Comparison of models and experimental results

While in the foregoing chapters the results of simulation and experimental work were mostly presented separately, here a summarizing joined discussion shall be provided. The simulations started prior to the lab work. Insofar a first set of comparisons with experimental data concerned the validation of the applied model construction and equilibration strategy by comparison with already then available experimental data for pure, i,e. unmodified gelatin. Here considering the variability of experimentally available gelatin sources an acceptable fit between measured and simulated density values was found as well as a reasonable coincidence between simulated and measured WAXS data. The models showed only one broad peak as expected for completely amorphous situations and the observed difference in

the peak position could be explained by the action of small amounts of local triple helical regions present in most “real” gelatins due to partial renaturation. The 25 wt.-% water containing models also showed the amorphous WAXS peak in the expected region.

After this proof that the model construction and equilibration procedure can lead to reasonable models these models were utilized for predictions of relevant properties for the modified (DAT-Gel and DATT-Gel) models vs. the unmodified gelatin case. Key properties calculated concerned the formation of aromatic clusters in the models, solubility parameters (as measures of the degree of hydrophilicity) and mechanical properties.

Regarding the formation of aromatic clusters the models actually predicted an increasing number of specific π-π interactions and hydrogen bonds of gelatins functionalized with increasing numbers of tyrosine-derived phenol moieties. This for the most relevant example of the models containing 25 wt.-% water led to the creation of relatively stable physical crosslinks (per model on average zero for Gel_25, 1 for Gel_DAT_25 and 6 for Gel_DATT_25). These crosslink densities permitted a link to the experimentally observable key property of equilibrium degree of swelling Q in water using the Flory-Rehner model (Table 4.4). The main result was a reduction of Q by a factor 6 for DATT-Gel with respect to pure amorphous gelatin (zero crosslink density). In experimental measurements performed on gelatin films the DATT-Gel also showed a strong reduction of Q by a factor of 7 (to 300) in comparison to the respective amorphous unfunctionalized but partly renaturated gelatin reference materials (Q = 2800%). In this case the formation of aromatic crosslinking clusters which could be proven by the MD can explain the observed trend. The higher absolute values for the predicted swelling degree from the models, in comparison with experiments, can most likely be related to the absence of a small amount of triple helical domains in the models that in the real systems contribute as additional net-points to the stability of the network.

The calculated Young’s moduli for the models did not show any significant change with the degree of functionalization. The same trend is observed also experimentally, just that the

absolute E-values are by a factor of 3 lower than for the models, which can be explained by the “perfectly” amorphous nature of the models, while real gelatin samples of course contain heterogeneities on longer length scales reducing the macroscopic E-values. The models permit to discuss some structural background with this regard. It was e.g. found that the degree of functionalization had no significant impact on the chain segment mobility or the local spatial arrangement of individual chain segments as indicated by the calculated free volume distributions. Here it should be mentioned that the E-modulus refers to small deformations, where the formed physical crosslinks do not contribute (at least not in the given case of low hydration state).

Modeling calculation also showed a decrease of the solubility parameter (square root of the cohesive energy density of a model) with an increasing concentration of introduced aromatic modifier groups being related with a more hydrophobic character which is experimentally visible by the observed dramatic reduction of equilibrium swelling capacity. This reduction hydrophilicity could be associated with the formation of (hydrophobic) aromatic clusters observed in the models.

6 Hydroxyapatite composites

In the following, the formation of composite films from pure gelatin, desaminotyrosine (DAT) functionalized gelatin (DAT-Gel) (bearing one aromatic ring per free amino group of gelatin), and desaminotyrosyl tyrosine (DATT) functionalized gelatin (DATT-Gel) (bearing two aromatic rings per free amino group of gelatin) with two types of hydroxyapatite in two different weight ratios are described. The material properties thereby should on the one hand be ruled by the physical crosslinking of the matrix by π-π interactions of the aromatic groups and, potentially, formation of triple helical regions, and furthermore by the matrix-HAp interactions. The films were characterized by IR spectroscopy, SEM/TEM, water uptake and degree of swelling, tensile tests, and rheology to describe the molecular structure of the composites and the effect on the macroscopic properties. Especially the water uptake and swelling, mechanical properties, and the thermal transitions of the composites compared to the pure matrix were of interest. Most of the experiments in this section have been performed by Axel Löbus in his diploma thesis.[162] I supervised the work in the lab, helped with the design and setting up of the experiments as well with the analysis of the data. The joined paper submitted to *Acta Biomaterialia* is under revision at the moment.[163]

6.1 Composite formation

The hydroxyapatite particles used for the formation of composites were synthesized and characterized at the University of Jena (group Frank A. Müller). Details of the particles can be found in the appendix.

The particles (HAp Type 1 or Type 2) were mixed (20 or 50 wt.-%) with pure gelatin, DAT-Gel, and DATT-Gel under stirring and ultrasonic sound before casting to give the composites as films. Gelatin composite mixture in the process of casting gave stable suspensions, while in the composites based on DAT-Gel and DATT-Gel immediate precipitation occurred. TGA of the dried composite films confirmed the composition of the samples as set during the synthesis. Determination of the relative content of single- or triple helices in the composites was not possible due to the much higher intensity of the HAp peaks.

The morphology of the dry composite films was investigated with scanning electron microscopy (representative picture: see Figure 6.1). Interestingly, HAp Type 1 gave larger agglomerates in the matrix while for HAp Type 2 no such agglomeration was observed.

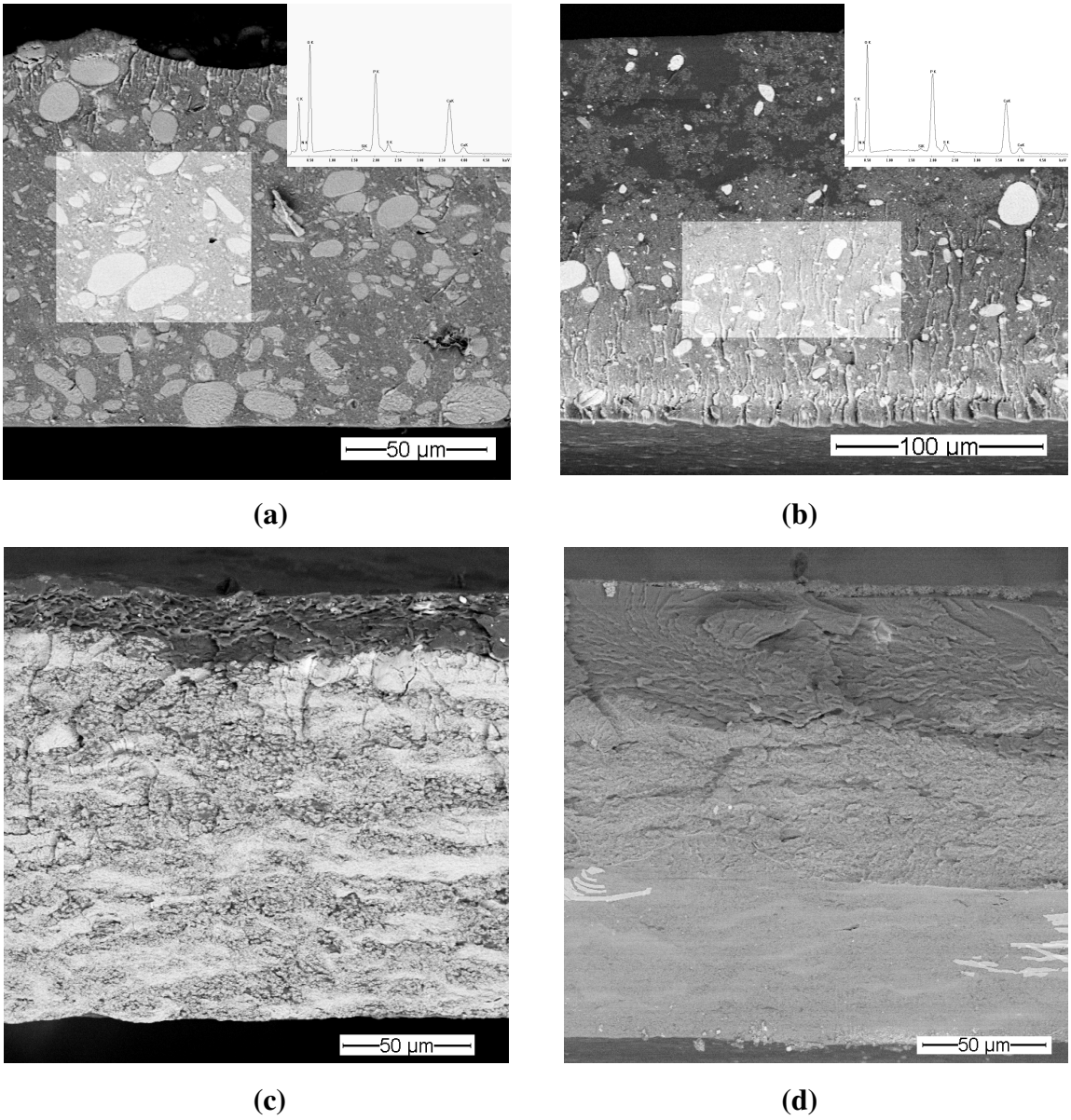

(a) **(b)**

(c) **(d)**

Figure 6.1. Cross-sections of DAT-Gel-composites with different amounts of HAp Type1 (a-50wt%; b-20wt%) and HAp Type2 (c-50wt%; d-20wt%).

6.2 IR spectroscopy of the composites

The chemical compositions of the composite materials were investigated by IR spectroscopy in order to identify characteristic bands for HAp and gelatins used. The IR spectra of DAT-Gel, DATT-Gel, the HAp Type 1 and 2, and their composites are displayed in Figure 6.2. Bands representative for the matrix included amides I at ~1650 cm^{-1}, amides II at ~1540 cm^{-1}, and amides III at ~1240 cm^{-1}, corresponding to C=O stretch, N-H in plane bend and C-H stretch, and C-N and N-H stretch in plane. Furthermore, carboxyl bands ascribed to amino acids in the gelatin backbone appear between 1300 cm^{-1} and 1450 cm^{-1}. Bands

correlated to the hydroxyapatites were observed in the fingerprint region (~630 cm^{-1} for OH ions, and 960 and 1030-1090 cm^{-1} for PO_4^{3-} ions). In Figure 6.3, the most obvious shifts of IR bands in the composites compared to the free matrices are highlighted. In DAT-Gel composites at 2800 cm^{-1} to 3000 cm^{-1} either strong shifts of up to 15 cm^{-1} or new bands occurred. For DATT-Gel composites, these shifts were similarly observed, yet the shifts of amino- and carboxyl peaks were much more pronounced. The type and amount of HAp influenced the intensity of the chemical shifts, whereby HAp Type1 had a stronger influence than HAp Type 2. Interestingly, in DAT-Gel composites, the most obvious shifts were in the region of 2800 to 3000 cm^{-1}, while for DATT-Gel composites, shifts of band between 1200 and 1700 cm^{-1} were more pronounced. In gelatin composites, no shifts of IR bands compared to the pure matrix were observed.

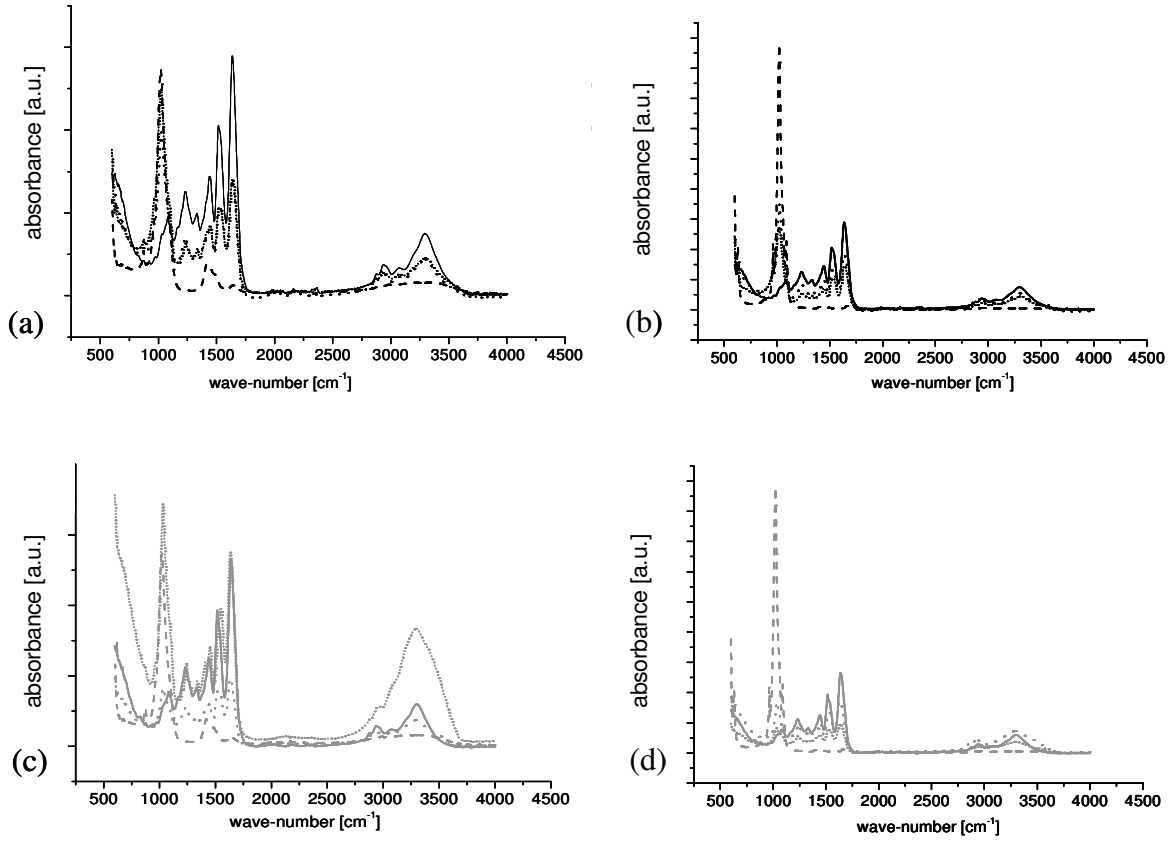

Figure 6.2. IR spectra of matrices, HAp, and composites. a) DAT/HAp Type 1, b) DAT/HAp Type 2, c) DATT/HAp Type 1, d) DAT/HAp Type 2. Black: DAT composites, grey: DATT composites. — matrix (pure), --- HAp (pure), · · · 20 wt.-% HAp, ··· 50 wt.-% HAp.

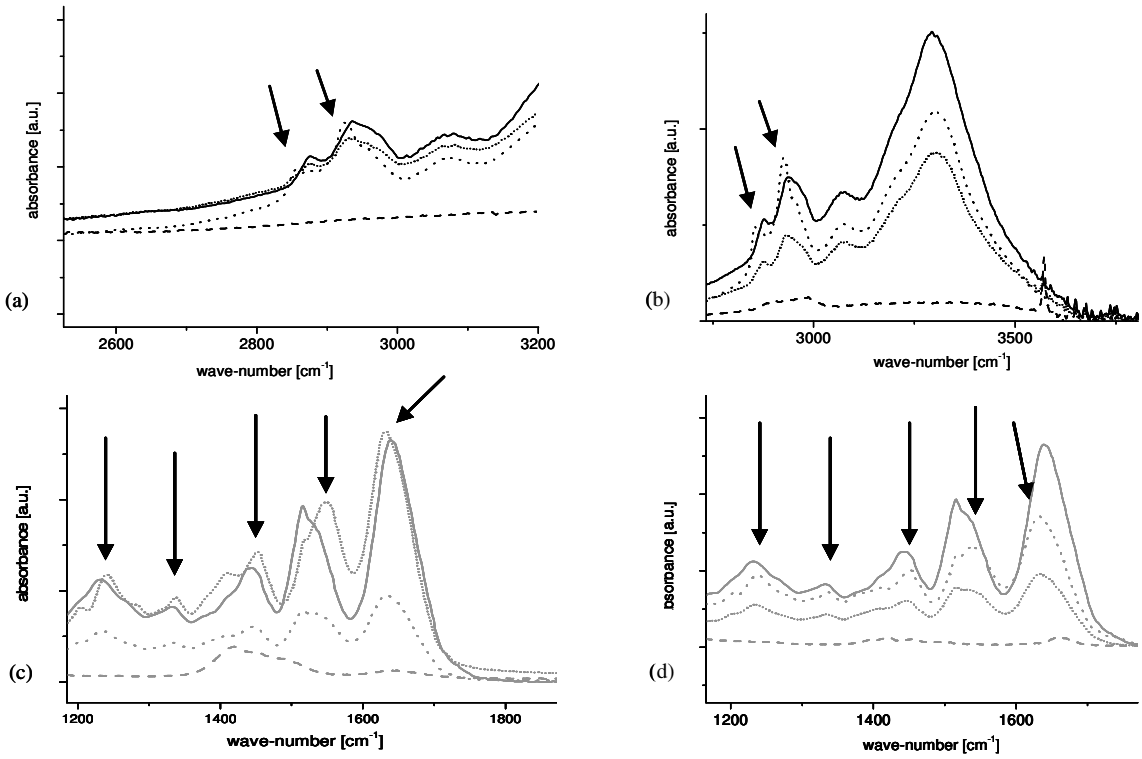

Figure 6.3. Shifts of bands in the IR spectra of the composites compared to the free matrices. a) DAT/HAp Type 1, b) DAT/HAp Type 2, c) DATT/HAp Type 1, d) DAT/HAp Type 2. Black: DAT composites, grey: DATT composites. — matrix (pure), --- HAp (pure), • • • 20 wt.-% HAp, ••• 50 wt.-% HAp.

6.3 Water uptake and swelling

The water-uptake H and the degree of swelling Q at 25 and 37 °C of the pure matrices and the different composites are summarized in Table 2. HAp tended to reduce water-uptake and swelling. Further analysis of the data verified the anticipated decrease of water-uptake and swelling when incorporating higher amounts of HAp. Moreover, DAT-Gel composites remained stable at 37 °C, confirming the effect of HAp on the thermal stabilization of DAT-Gel. HAp Type1 incorporation resulted in significantly less water-uptake and swelling than the introduction of HAp Type2 into DAT-Gel. This was especially significant for DAT-Gel composites at 37 °C. Such a behavior could not be monitored for the related composites since DATT-Gel is stable at 37 °C. The obtained data indicated that DATT-Gel composites have roughly the same water uptake and degree of swelling at 25 and 37 °C, respectively. On the

contrary, at higher temperature DAT-Gel composites showed much higher water-uptake and swelling. The elevated level of water-uptake of DAT-Gel / HAp Type 2 composites compared to DAT-Gel / HAp Type 1 composites could be due to a higher free volume present in the HAp Type 2 composites, a higher elasticity in these composites, or due to a different attraction to water of the two types of HAp.

Table 6.1. Water Uptake and swelling of the matrices and composites. n.r.: Sample dissolved under these conditions

Material		H (25 °C)	Q (25 °C)	H (37 °C)	Q (37 °C)
Matrix	Filler	[wt.-%]	[Vol.-%]	[wt.-%]	[Vol.-%]
Gel	-	2340±380	2740±500	n.r.	n.r.
DAT-Gel	-	400±45	600±60*	n.r.	n.r.
DATT-Gel	-	425±45	600±60	435±85	615±100
DAT-Gel	20 wt.-% Type 1	290±15	515±50	785±65	1230±90
DAT-Gel	50 wt.-% Type 1	180±10	410±20	410±70	800±115
DAT-Gel	20 wt.-% Type 2	285±35	555±50	1070±240	1815±380
DAT-Gel	50 wt.-% Type 2	200±40	475±75	650±85	1300±155
DATT-Gel	20 wt.-% Type 1	145±10	300±15	180±30	350±45
DATT-Gel	50 wt.-% Type 1	130±25	270±20	120±30	265±40
DATT-Gel	20 wt.-% Type 2	140±5	290±10	300±30	505±45
DATT-Gel	50 wt.-% Type 2	100±5	240±10	110±25	255±35

6.4 Mechanical characterization

Tensile tests were performed on samples equilibrated in water, i.e. on composite hydrogels along with non-functionalized gelatin as reference material (Table 6.2). The DATT-Gel composites were too brittle to be measured in tensile tests, therefore, in the following only gelatin and DAT-Gel based materials are discussed.

Tensile tests revealed significant alteration of mechanical performance of the composites with the introduction of HAp. Young's modulus (E) and the maximum tensile strength σ_{max} increased with increasing amount of filler in the composites, while no significant changes for the elongation at break (ε_b) were observed. The trend was generally more pronounced for HAp Type 2 than for Type 1, and the changes were different for the two matrices, e.g. the effect of 20 wt.-% filler in DAT-Gel was similar to the effect of 50 wt.-% filler in gelatin.

Table 6.2. Values obtained from mechanical testing together with calculated standard deviation. [a]: from tensile tests. [b]: from rheological measurements.

Matrix	Gelatin		DAT-Gel				
Filler	0 wt.-%	50 wt.-%	0 wt.-%	20 wt.-%	20 wt.-%	50 wt.-%	50 wt.-%
E [kPa][a]	215±60	570±180	340±55	620±85	415±60	1760±260	1860±280
σ_{max} [kPa][a]	70±30	230±40	100±20	100±50	210±70	1070±170	430±140
ε_b [%][a]	16±4	21±6	20±9	15±3	22±9	27±3	17±5
T_{Gel} [°C][b]	37	38-42	37	42-45	42-47	>85	>85

For non-functionalized gelatin, HAp created significant mechanical stiffness and strength without inducing brittleness. However, mechanical performance of DAT-Gel in terms of stiffness and strength exceeded that of native gelatin. Although mechanical properties for the two types of HAp composite materials are in a similar range, DAT-Gel containing HAp Type1 reached a mechanical strength of up to 1 MPa when 50 wt% of HAp was incorporated in the composite. As could be expected, the amount of HAp in the composites had a stronger effect on the mechanical properties than the type of HAp.

Rheological measurements were performed in order to investigate the thermal stability of the composites equilibrated in water. Here the elastic modulus (G'), viscous modulus (G") and complex viscosity (η^*) in dependence of the temperature were recorded. The temperature at which the elastic and the viscous moduli intersect is defined as Elastic-Viscous-Transition-Temperature T_{Gel}, above which the material starts to behave more like a liquid rather than like a solid material. In order to determine T_{Gel}, the sample was gradually heated as depicted in Figure 6.4 showing a typical course of G' and G" for gelatin, for DAT-Gel and for DAT-Gel composites with different HAp ratios.

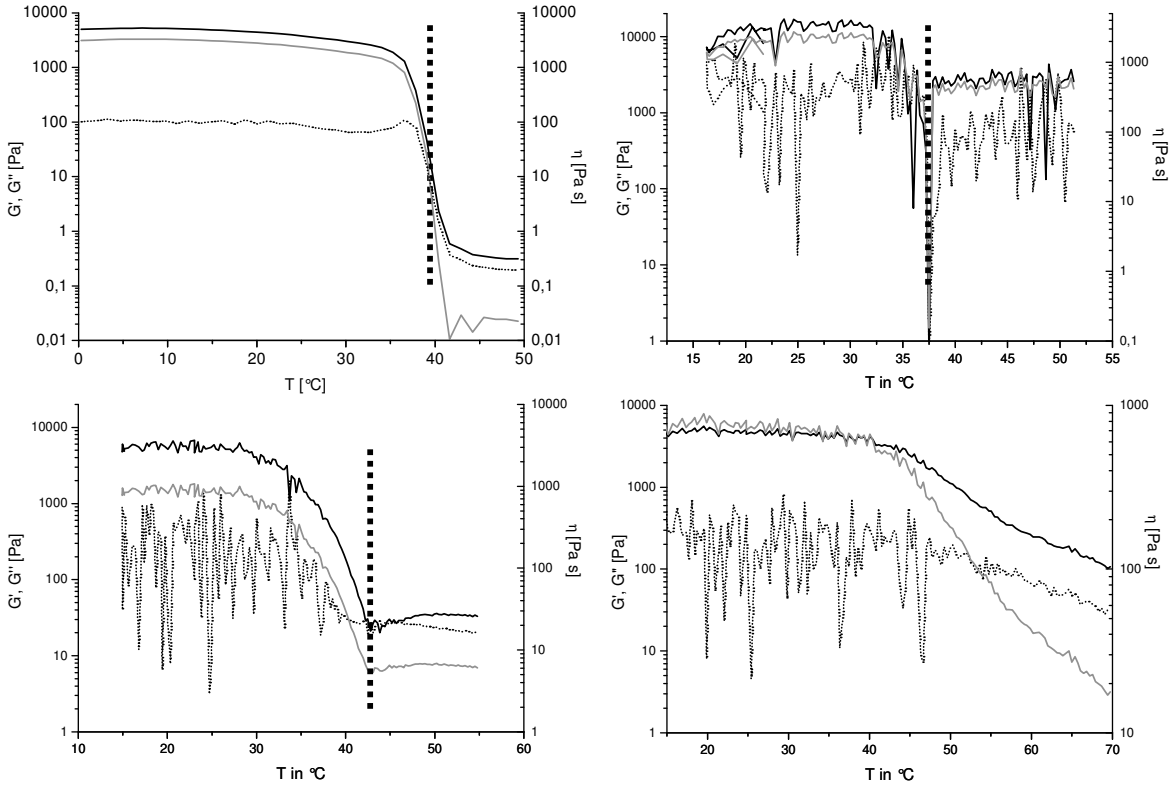

Figure 6.4. Representative course of temperature dependant G' (black line), G" (black dotted line), and η (grey line) for pure gelatin (a) and DAT-Gel (b) and DAT-Gel composites containing 20 wt% HAp (c) and 50 wt.-% HAp Type 1 (d). T_{gel} is labeled with the vertical dashed line.

It can be noted that the crossover of G' and G" increased significantly with increasing amounts of HAp. No influence originating from the type of HAp could be observed.

6.5 Discussion

The precipitation during the mixing of HAp with DAT-Gel or DATT-Gel solutions during the formation of the composite films was likely due to an interaction between the matrix materials and the filler. As no precipitation occurred with pure gelatin, this phenomenon can be associated with the aromatic functionalization of the materials. Specific interactions between matrix and filler are supported by the shifts of the IR bands in the composites compared to the pure matrices. The shifts observed in DATT-Gel composites are either related to Ca^{2+} -COO^- chelation ($RCOO^-$),[164] ascribed by the shift of COO^- at ~1340 cm^{-1} or to PO_4^{3-} and NH_3^+ ionic interaction, identified as band shifts of phosphate and amino groups.[165] The shift attributed to

asymmetric stretching of COO^- at 1650 cm^{-1} indicates weakening of the C=O bond in the peptide chain, which was caused by the formation of new bonding interactions between Ca^{2+} and C=O bonds. The shift in the phosphate band for DATT-Gel composites indicated polar interaction with NH_3^+ as well as hydrogen bonding and therefore participation in the interfacial interactions. These alterations of the IR pattern could also be observed with DAT-Gel composites, yet at a less pronounced level of intensity. In FTIR, bands corresponding to aromatic rings or phenolic OH groups were not observed; therefore this method did not help in directly identifying interactions between surface HAp ions and the aromatic rings or phenolic OH groups of functionalized gelatins. However, the shifts reported above were stronger for matrices with increased aromatic content. This can on the one hand be because of direct interactions between the incorporated phenols and the filler, or because the reaction of DAT and DATT with free amino groups reduced the electrostatic interaction between free carboxylic and amino groups on the gelatin, so that more carboxylates can engage in binding to Ca^{2+}. It is possible that a slightly different water content also resulted in shifts of some IR bands, however, as there were no differences observed in the IR spectra of pure gelatin and its composites, it is more likely that the IR band shifts indicate direct interactions of matrix and filler.

Incorporation of HAp resulted in reduced degree of swelling and water-uptake of the polymer-networks. However, the amount of HAp and therefore presumingly the Ca^{2+} ion concentration was crucial. This suggests that HAp strengthens the polymer-network by inducing higher stiffness to the overall network. Water-uptake into a matrix takes place first by filling the free volume of the material and by tight binding of water molecules to functional groups of the polymer, which does not necessarily result in swelling. Further uptake of water is then an equilibrium process between the elasticity of the polymer-network and osmotic pressure of entering water. The less water that penetrates in this third step into the matrix, the stiffer is the network. Since polymer networks with HAp exhibit considerably

less swelling than polymer networks without HAp, the HAp crystals seem to strengthen the system by physical crosslinking of polymer strands through labile Ca^{2+}-ions on the surface. Composites of functionalized gelatin immersed in water retained their shape and integrity with incorporation of HAp. This is not the case for the DAT-Gel matrix alone. Samples lost integrity at 37 °C within 24h because of a higher mobility polymer-strand when Ca^{2+} crosslinks were missing. Additionally, the water-uptake and swelling tests demonstrated the different influence of HAp Type1 and Type2 in DAT-Gel, particularly for samples with 50 wt.-% HAp content. The generally lower uptake of water of DATT-Gel composites compared to DAT-Gel composites can be explained by the increase of the hydrophobicity of the matrix.

The increase in E modulus and σ_{max} of samples with 50 wt.-% HAp incorporated can also be explained by physical interaction between labile ions of HAp and free reactive sites of the DAT-Gel, most likely π-electrons provided by the aromatic groups. The proposed interfacial interaction can be described as a physical crosslinking of different strands of gelatins via Ca^{2+} ions provided by HAp. This interaction is reported in literature and suggests a stabilization of the DAT-Gel system.[166, 167]

The additional crosslinks also increased the thermal stability of the swollen systems. Thermal stability under shear stress was raised up to 85 °C with incorporation of HAp into the system. DAT-Gel without HAp dissolves at around 40 °C. This effect is a strong testimony of effective physical crosslinking of gelatin strands by HAp. The reduced mobility of the polymer-strands is to be considered as key feature for thermal stability. This in turn leads to the observed results, which states that stronger networks exhibit better thermal resistance. Altogether, the potential interactions in the composites are summarized in Figure 6.5.

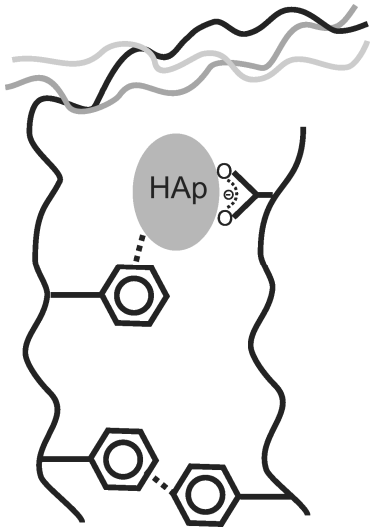

Figure 6.5. Overview of the potential interactions stabilizing the composites. Association of protein chains into collagen-like triple helices is the reason for gelation of unmodified gelatin gels below T_{Gel}. Aromatic substituents have been shown on the one hand to decrease the triple helix formation but on the other hand to generate new crosslinks by π-π interactions. In the composites, chelation of Ca^{2+} ions on the surface of the HAp fillers, and interactions between the aromatic rings and the Ca^{2+} ions form additional physical netpoints contributing to the mechanical properties of the composites.

Altogether, the type of filler did not have a major effect on the composite macroscopic properties when comparing composites with equal amount of filler. A possible explanation can be seen in Figure 1, where agglomerates of the HAp Type 1 are visible. If these large agglomerates would consist only of HAp, not such a strong effect on the macroscopic properties of the composites would be expected, contrary to what was observed. More likely is that the agglomerates consisted of HAp particles connected by polymer chains, so that the strong interaction between matrix and filler were simultaneously responsible for the increase in Young's modulus and maximum tensile strength as well as for the agglomeration. The larger size of the agglomerates compared to the putatively homogeneously distributed HAp Type 2 particles is then compensated by the better interaction with the matrix. The reason for the agglomeration of HAp Type 1 might be the higher specific surface area and lower crystallinity of this material.

7 Conclusions and Outlook

Growth and repair of human tissues follow different biological paths, so that in most cases even under ideal conditions scarring occurs as a consequence of repair of damaged tissues. In some cases, damage of tissues results in critical, i.e. non self-healing, defects, so that clinical intervention is necessary to restore a level of tissue function. Regenerative medicine aims to support the biological regeneration while preventing scarring. One approach in this context is material induced autoregeneration, where a biomaterial temporarily substitutes the extracellular matrix (ECM) at a defect site, and is subsequently replaced by functional neotissue. Generally the use of biopolymers from the ECM as basis for such biomaterials is highly desirable but challenging due to difficulties in tailoring and controlling the material properties.

In this study, a knowledge-based approach was used to investigate the systematic variation of material properties of gelatin by introducing groups engaging in specific physical interactions using a combination of modeling studies and synthetic methods.

Gelatin was selected as non-immunogenic and degradable derivative of the ECM component collagen, and control of material properties was achieved by incorporation of aromatic residues derived from tyrosine, desaminotyrosine (DAT) and desaminotyrosyl tyrosine (DATT), that led to the reduction of the residual helical conformation and to the formation of physical net-points by π–π interactions and hydrogen bonds.

Molecular models of (functionalized) gelatins as amorphous bulk materials were successfully developed and validated with experimental data. Atomistic molecular modeling could be utilized to obtain an improved insight into structural features of gelatin and gelatins functionalized with aromatic moieties as amorphous bulk materials. Using NPT-MD simulations, well-equilibrated bulk models of amorphous gelatin could be prepared and the influence of supramolecular aggregation of the introduced aromatic groups on the structural features and bulk properties of the respective materials could be investigated. It could be proven from the models that the applied functionalization of gelatin side chains with aromatic moieties leads to a self-assembling process by formation of aromatic clusters. This process is based on specific, non-covalent interactions between the π-electron systems of the involved aromatic units and by hydrogen bonds from and to the phenolic OH-groups.

The models predicted an increasing number of specific π–π interactions and hydrogen bonds of gelatins functionalized with increasing numbers of tyrosine-derived phenol moieties.

This for the most relevant example of the models containing 25 wt.-% water led to the creation of relatively stable physical crosslinks (per model on average zero for Gel_25, 1 for Gel_DAT_25 and 6 for Gel_DATT_25). These crosslink densities permitted a link to the experimentally observable key property of equilibrium degree of swelling Q in water using the Flory-Rehner model (Table 4.4). The main result was a reduction of Q by a factor 6 for DATT-Gel with respect to pure amorphous gelatin (zero crosslink density). The calculated Young's moduli for the models did not show any significant change with the degree of functionalization. The same trend is observed also experimentally, just that the absolute E-values are by a factor of 3 lower than for the models, which can be explained by the "perfectly" amorphous nature of the models, while real gelatin samples of course contain heterogeneities on longer length scales reducing the macroscopic E-values. The models permit to discuss some structural background with this regard. It was e.g. found that the degree of functionalization had no significant impact on the chain segment mobility or the

local spatial arrangement of individual chain segments as indicated by the calculated free volume distributions. Here it should be mentioned that the E-modulus refers to small deformations, where the formed physical crosslinks do not contribute (at least not in the given case of low crosslink densities). Modeling calculation also showed a decrease of the solubility parameter (square root of the cohesive energy density of a model) with an increasing concentration of introduced aromatic modifier groups being related with a more hydrophobic character which is experimentally visible by the observed dramatic reduction of equilibrium swelling capacity. This reduction of hydrophilicity could be associated with the formation of (hydrophobic) aromatic clusters observed in the models.

The materials were synthesized as planned, and a chemoselective functionalization of free amino groups could be proven. Chemical (functionalization with tyrosine derived moieties) and physical (drying conditions) methods were successfully employed to tailor the helical content of the gelatin-based materials. Shorter drying times at elevated temperatures (ν_{short} drying procedure) created amorphous systems with lower helical contents (1 – 2%) when compared to samples dried at longer times at lower temperatures (ν_{long} drying procedure) (8 – 10%) as measured by WAXS. In addition, the functionalization of gelatin with DAT and DATT resulted in materials with lower tendencies to form helices when compared with pure gelatin. The reduction in the degree of renaturation was confirmed by TM-DSC analysis, which showed a reduction of helix stability in terms of reduced T_m. The degree of helicity furthermore had only little influence on the mechanical performance of the materials at 25 wt.-% water content (E = 2.0 – 2.4 GPa), while at equilibrium swelling the amount of aromatic interactions showed to be a key factor (e.g. Q = 2100 vol.-% for ν_{long} treated gelatin, 1600 vol.-% for ν_{long} treated DAT-Gel, and 300 vol.-% for ν_{long} treated DATT-Gel). The modification of the molecular architecture with aromatic moieties resulted in materials with reduced water uptake, increased gel-strength, and increased elasticity at equilibrium swelling.

The experimental measurements could be correlated to the molecular models in order of magnitude of the respective property and trend of changes. This on the one hand indicates a sufficient quality of the models and on the other hand shows the predictive potential of the chosen computer aided modeling approach. There were several examples of excellent agreement observed when comparing the modeling predictions and the experimental data for gelatin, DAT-Gel, and DATT-Gel, including the density measurements and the structural organization of the gelatins. Already in the present case, the relatively low concentration of the introduced groups led to a dramatic reduction of swelling capacity that could be qualitatively correlated to the amount of aromatic cluster observed in the models using the Flory-Rehner equation. The limited variation observed on some other bulk properties e.g. elastic moduli and fractional free volume distribution suggest that just modifying the 3 mol-% of lysine groups on native gelatin will not result in more dramatic changes of macroscopic properties in the dry state.

The processing of synthetic samples was an important factor in using the predictive power of the models. Because the models were based on perfectly amorphous systems, the v_{short} treated samples were more comparable to the models than the v_{long} treated samples. The synthesized samples showed lower mechanical properties (E = 2.26±0.27 GPa for gelatin; 2.03±0.24 GPa for DAT-Gel; and 2.08±0.46 GPa for DATT-Gel) at 25 wt.-% water content than the predicted values using a static method of analysis (E = 6.7±0.4 GPa for gelatin; 6.4±0.3 GPa for DAT-Gel; and 6.6±0.1 GPa for DATT-Gel). This difference may have been due to the defects that are invariably present in synthesized materials but absent in the ideal structures used in the modeling studies. The drastic change in swelling degree (Q) for the functionalized gelatins could only be partly explained using the atomistic modeling studies. Importantly, the triple helical contents also greatly influenced the swelling capacities of the materials (e.g. Q for v_{short} treated and v_{long} treated gelatin) but were absent in the models. In addition, the influence of water content on the material mechanics with different processing

histories was a surprising result for the synthetic studies. Because the models were based on purely amorphous, ideal structures, this correlation was not made.

The formation of composites from gelatin functionalized with increasing numbers of tyrosine derived phenolic groups with hydroxyapatites gave materials with much reduced degrees of swelling. Shifts in the bands in IR spectra indicated direct interactions between matrix and filler, however, as these interactions were dependent on the type of matrix, the aromatic groups introduced in DAT-Gel and DATT-Gel seem to have directly contributed to the interaction. Young's moduli and maximum tensile strengths of the composites increased with the amount of HAp but were not dependent on the type of HAp. The increasing mechanical strength was not accompanied by increased brittleness of the materials. Even at equilibrium swelling the hydrogel composites reached Young's moduli up to 2 MPa, which is much higher than typically observed in hydrogels and is close to cancellous bone (3.5 MPa). Furthermore, the thermal stability of the network was increased to above 85 °C. These observations can be explained by additional physical crosslinking of the networks by interactions between the matrix and Ca^{2+} ions of the filler. Interestingly, these types of interactions have been observed for biomineralized composites but not for composites formed by mixing HAp particles and dissolved polymer matrices.

The pure matrices have shown Young's moduli in the dry state in the low GPa range. In a potential application as bone fillers or coatings of implants, this should result in good protection against abrasion. This should be all the more true for the composites, since a similar increase in mechanical properties was observed in the equilibrium swollen state. Theoretically, after being implanted in the dry state, the low swelling of the investigated materials would then result in an adjustment of the materials to the mechanical properties needed in the biological environment without disintegrating immediately. These composites would therefore be an interesting field of study as bone fillers and implant coatings. Additionally, the results from the synthesized materials prove that material properties that are

determined by physical crosslinks are quite promising for the possible applicability of this natural biopolymer as induced autoregeneration matrices, cell seeding hydrogels, or drug release system.

7.1 Future Directions

7.1.1 Increase number of aromatic functional groups in the models

Future modeling studies could be used to predict the effects of even higher degrees of functionalization e.g., on alternative attachment points or by utilizing modifiers with more than two aromatic units

7.1.2 Knowledge-Based Approach towards Hydrolytic Degradation

Furthermore, as has been already demonstrated for synthetic polymer systems, where the architecture of the network has a strong influence on the degradation behaviour,[13] the developed models can help to predict the degradation behavior of the physical gelatin networks.[168] In this way, modeling studies can help to direct the experimental work towards the development of new materials with desired properties.

7.1.3 Degradation studies molecular modeling Simulate body fluids (SBF)

As the experimental level the study of degradation behavior of the obtained hydrogels is of high importance for its possible application in tissue regeneration, an implanted gelatin hydrogel should show a controlled degradation behavior in order to assure adequate mechanical properties over the time of the neo-tissue formation. On that line, the variation of the macroscopic properties over time of the materials in contact with buffer solution or simulated body fluids shall be studied.

7.1.4 Complete biological characterization studies form in-vitro to in-vivo and reduction endotoxins content

The risk of infection caused by the implantation of medical devices has to be minimized, and the hydrogels have to be non toxic with contacting tissue, cells, and body fluids (Council Directive 93/42/EEC). *In vitro* toxicity testing to measure cytotoxicity, cytocompatibility, cell adhesion, genotoxicity, and hemocompatibility will then be addressed. Eluate and direct cell test[169, 170] and endotoxin contamination shall be investigated .

8 Materials and methods

This chapter provides information about the simulation details and experimental methods employed in this work. Detailed information of the generation of molecular models, the theoretical background of analytical methods, as well as the synthetic procedures and characterization of materials are presented. More detailed description of the basic of molecular modeling techniques used in this work is given in Appendix A.

8.1 Details for molecular dynamic simulation (MD)

8.1.1 Selected model systems

All simulations were performed using the Amorphous cell and Discover interfaces from Accelrys Software Inc., with the Material Studio Modeling Environment, Release 4.3s.[144] The CFF91 force field[171] was selected as a second generation force field that reasonably reproduces condensed-phase properties and is more accurate than CVFF force field for most proteins.

The amino acid (aa) sequence of the gelatin molecule selected for this study is a 276 aa portion of a human collagen type I (GenBankTM accession No. NP_000079). The DAT and DATT carboxylic acid groups were attached to the amino groups on lysine residues of the selected chain as amides to resemble the synthetic bond formation (see Table 4.1). The initial

gelatin structure (G) was built in a helical conformation using the Discovery Studio software.[140] The dihedral angles φ and ψ were set to -65° and 170°, respectively, corresponding to the mean values of a typical collagen chain.[143]

8.1.2 Bulk models

The (functionalized) gelatin chains were used as topological templates to be packed into amorphous bulk models with 0.8 and of 25 wt.-% of water content using the Amorphous Cell module of Material Studio software (Figure 8.1). The Amorphous Cell code makes use of the Theodorou and Suter chain-generation approach,[117] based on a modified interdependent rotational isomeric state (RIS) model (cf. A.1.5). The final density for the gelatin models with water content of 0.8-wt. % and 25-wt. % were set to the theoretical values of 1.36 g·cm-³ and 1.23 g·cm-³, respectively.[172] Details on the basic techniques for the packing and equilibration of the cells are described in A.1.5.[118]

8.1.3 General Equilibration procedure and data production

In summary, all initial packing models were subjected to an extensive equilibration consisting of several steps. A first relaxation procedure was performed using cycles of energy minimization iterations followed by a 5 ps molecular dynamics at constant volume (NVT-MD) with down-scaled torsional terms and nonbonding interactions. During these cycles, the mentioned force-field parameters are then gradually increased until they reach their normal values. Details for the scaling factor applied to the different terms can be found in Table 8.1

Table 8.1. Scaling of torsional terms and nonbonding interaction parameters of the forcefiels during first equilibration process.

	Scaling factors	
Cycle	Torsional term	Non-bonding interactions
1	0.001	0.001
2	0.01	0.001
3	1	0.001
4	1	0.01
5	1	1

Afterwards, 300 ps NVT-MD simulations and simulated annealing (in each case 20 ps NVT-MD at 750, 600, 450 and 100 ps at 303 K) were performed. The cells were then subjected to a set of NPT-MD simulations (p = 1 bar, T = 303 K) with increasing time step (0.3 fs, 0.4 fs, and 0.5 fs) using a combination of a Berendsen thermostat[173] and an Andersen barostat,[174] to permit the system to finally release the stresses due to the fixed box dimension. Finally, a 5 ns NPT-MD simulation, with a time step of 1 fs was run for data collection. For all simulation setups, a "non bond cutoff" of 15 Å was utilized, not evaluating any Lennard-Jones term for atom pairs which are further apart from each other than this value. All data presented in this work were obtained as an average over the values computed for three independent models built for each gelatin type. For each model, the value is calculated as the average over a large number of snapshots extracted from the trajectories of the data collection run.

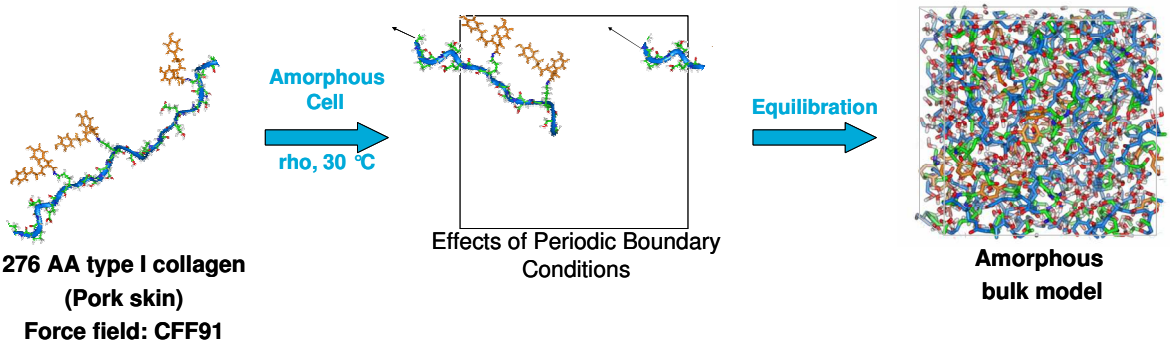

Figure 8.1. Generation of the atomistic models

8.2 Analysis methodology of modeled systems

8.2.1 X-ray scattering

The X-ray scattering intensity I(Q) of the amorphous models is calculated from the projections of each of the interatomic vectors, r_{jk}, on the respective scattering vector, Q via the following equation: [175]

$$I(Q) = \sum_i \sum_j f_i(Q) f_j(Q) \exp(i r_{ik} Q) \qquad \text{(eq. 8.1)}$$

With

$$Q = \frac{2\sin\theta}{\lambda} \qquad \text{(eq. 8.2)}$$

θ = scattering angle, λ = wave length of the X-ray radiation

8.2.2 Determination of free fractional volume (FFV)

The free fractional volume accessible for water molecules was determined by overlaying a grid with a grid spacing of 0.5 Å over the cubic packing cells of interest. Then, a hard sphere with a radius of 1.1 Å or 1.4 Å, resembling a hydrogen and a water molecule, respectively was placed on each grid point and checked if an overlap with any gelatin atom occurred. The result of each particle insertion is a classification of the respective grid point as "occupied" or "free". If the grid point is considered "free", not occupied by gelatin atoms, than the surrounding lattice cube of 0.5 Å side length belongs to the accessible free volume of the model. Subsequently, the connectivity of the free grid point is checked and connected free grid points are collected into groups, which represent the individual holes. The linear dimensions of the final holes are here expressed as the radius of a sphere of equal volume. For the examination of the free accessible volume all the water molecules were removed and the atoms of gelatin are represented by hard spheres with radii derived from the Van der Waals radii of respective atoms.

8.2.3 Determination of mean square displacement (MSD)

The self diffusion of gelatin chains in gels with 0.8 and 25 wt.-% water content was evaluated parting term of the mean squared displacement of the atoms of the respective gelatin backbone, during the 2 ns NPT-MD data production simulations with snapshots taken every 1 ps.

$$s(t) = \left\langle \left| r(t) - r(t_0) \right|^2 \right\rangle \qquad \text{(eq. 8.3)}$$

The angular brackets denote an average over all backbone atoms and all time origins within the dynamic trajectory. r is the respective position vector of an atom.

8.2.4 Determination of cohesive energy density (CED)

The cohesive energy density is a parameter derived from the heat of vaporization and thus it can be considered a numerical value of the van der Waals and electrostatic forces holding the molecules of a system together: the higher the CED (and δ) the higher the physical interaction between the modified gelatin chain segments.

$$CED = \frac{\Delta H_{vap} - RT}{V_m} \qquad \text{(eq. 8.4)}$$

$$\delta = \sqrt{CED} = \left[\frac{\Delta H_{vap} - RT}{V_m} \right]^{\frac{1}{2}} \qquad \text{(eq. 8.5)}$$

where ΔH_{vap} is the heat of vaporization, R is the gas constant, T is the absolute temperature, and V_m is the molar volume. During the NPT-MD simulation performed as data production phase, ΔH_{vap} is computed as follows:

$$\Delta H_{vap} = \left\langle E_{cell} - \sum_{i=1}^{n} E_i \right\rangle_P + RT \qquad \text{(eq. 8.6)}$$

where E_{cell} is the total energy of the periodic unit cell and E_i is the energy of the individual n molecules packed into this cell after removal of periodic boundary conditions. The difference between E_{cell} and the sum of the E_i components was averaged over all the recorded frames at pressure P constant.[176]

8.2.5 Determination of elastic constants by static structure deformation

The calculated elastic constants of the gelatin models were obtained utilizing a constant-strain minimization method (static method)[135] applied to the equilibrated system. After an

initial energy minimization, a very small strain (within the elastic limits, ± 0.1 %) was applied to the system in the intended direction allowing the unit cell dimensions and angles to vary, and the energy of the structure is minimized under constant stress. The first derivatives of the potential energy with respect to all relevant strains can provide the relevant elements of the internal stress tensor σ, while the stiffness matrix C is calculated from the second derivative of the potential energy (U) with respect to strain (ε) as follow:

$$C_{ij} = \frac{1}{V}\frac{\vartheta^2 U}{\vartheta\varepsilon_i \vartheta\varepsilon_j} = \frac{\vartheta\sigma_i}{\vartheta\varepsilon_j} = \frac{\sigma_{i+} - \sigma_{i-}}{2\varepsilon_j} \qquad \text{(eq. 8.7)}$$

Where ε_i and ε_j are the components i and j of the strain tensor, σi+ and σi- are the components associated with the stress tensor under tension and compression, respectively.

In the limit of zero strain and for isotropic materials the stiffness matrix can be reduced to a 6x6 second rank tensor with only two independent coefficients λ and μ (Lamé constants). These coefficient permits to obtain the elastic properties of the material, like Young's modulus E, bulk modulus K, and shear modulus G:

$$E = \mu\left(\frac{3\lambda+\mu}{\lambda+\mu}\right), \quad K = \lambda + \frac{2}{3}\mu, \quad G = \mu \qquad \text{(eq. 8.8)}$$

8.2.6 Cluster formation

Aromatic interactions were calculated from the spatial distance of centroid atoms, defined for every aromatic ring, along the trajectory when the geometric distance between any two of them is below 7.5 Å. Of course also larger clusters could be identified (cf. e.g. Figure 4.12).

8.2.7 Hydrogen bonds

Interactions involving the phenolic group were calculated along the trajectory using the following criteria, $1 < d_{D\text{-}H\text{-}A} < 2.5$ Å, $\sphericalangle_{D\text{-}H\text{-}A} > 90.0°$). D=donor, A = acceptor, d = distance, $\sphericalangle$ = donor-hydrogen-acceptor angle.

8.2.8 Degree of swelling

Generally, the equilibrium degree of swelling ($Q = 1/\nu_s$, with ν_s being the volume fraction of polymer at swelling equilibrium) of a polymer network is used to estimate the density of crosslinks (μ/V), the density of elastic network chains (an elastic network chain connects two crosslinks with each other) (ν/V), and the molecular weight between two crosslinks (M_c). Here, the density of elastic network chains (ν/V) was used and was calculated according to the number of cluster (μ) found in the models and the average functionality of the network crosslinks (Φ) using the formula:

$$\frac{\upsilon}{V} = \frac{\mu \cdot \phi}{2 \cdot V \cdot 10^{-21} \cdot N_A} \qquad \text{(eq. 8.9)}$$

The obtained values were utilized to approximate the degree of equilibrium swelling $Q = 1/\nu_s$ using the Flory-Rehner equation:[148]

$$\frac{\upsilon}{V} = \frac{\left[\ln(1-\upsilon_s) + \upsilon_s + \chi_1 \cdot \upsilon_s^2\right]}{V_1\left[\upsilon_s^{1/3} - \frac{2\upsilon_s}{\phi}\right]} \qquad \text{(eq. 8.10)}$$

with $\chi_1 = 0.49$ being the Flory polymer-solvent interaction parameter for isoelectric gelatin and V_1 being the molar volume of the solvent (V_1=18 mL/mol for water).

8.3 Experimental details

Gelatin type A, β-mercaptoethanol, desaminotyrosine (DAT), N-hydroxysuccinimide (NHS), 1-ethyl-3-(3-dimethyl-aminopropyl) carbodiimide (EDC), 2,4,6-trinitro-benzensulfonic acid (TNBS), and N,N-Diisopropylethylamine (DIPEA) were purchased from Sigma Aldrich (Munich, Germany). Dimethyl sulfoxide DMSO, *N*-Methyl-2-pyrrolidone (NMP), Trifluoroacetic acid (TFA), and ethyl acetate (EtOAc) were purchased from Merck (Darmstadt, Germany). IRIS Biotech GmbH (Marktredwitz, Germany) was the provider of DCM, L-Tyrosine *tert*-butyl ester (H-L-Tyr-OtBu), and Triisopropylsilane (TIPS). All

reagents and solvents were of analytical grade and used without further purification. Details to the hydroxyapatite particles are given in Appendix B.

8.3.1 Synthesis of Desaminotyrosyl-tyrosine

Desaminotyrosine (12.6 g, 76 mmol, 1.2 eq) was activated by reaction with EDC·HCl (17.4 g, 91 mmol, 1.4 eq), and DIPEA (37 mL, 215 mmol, 3.4 eq) in NMP (80 mL). While the reaction mixture was chilled in a ice bath at -5 °C for ten minutes. H-L-Tyr-OtBu (15 g, 63 mmol, 1 eq), dissolved in NMP (30 mL) was added and the reaction mixture stirred for 1h in an ice bath and for 17 h at room temperature. The reaction mixture was poured into 1 L water, which was extracted with ethyl acetate. The combined organic phases were then washed with 0.1 M aq. HCl, 0.1 M aq. $NaHCO_3$ solution, and conc. NaCl solution. The organic phases were dried over magnesium sulfate, filtered, and the solvent removed by evaporation under reduced pressure to give the protected Desaminotyrosyl-tyrosine *tert*-butyl ester as a white powder (14.35 g, Yield: 69 %).

Found: *m/z*(ESI) m/z: 386.19 ($M+H^+$), m.p.: 140.3 °C; ^{1}H NMR (500 MHz,; DMSO-d6; Me_4Si) δ = 9.18, 9.10 (2H, s, OH), 8.09 (1H, d, NH), 6.95 (4H, ad, Ph), 6.63 (4H, ad, Ph), 4.27 (1H, m, $C_\alpha H$), 2.79 (1H, m, $C_\beta H$), 2.73 (1H, m, $C_\beta H$), 2.63 (2H, m, $C_\beta H$), 2.31 (2H, t, $C_\gamma H$), 2.33 (9H, s, CH_3), 1.32 (s, 9H) ppm; ^{13}C NMR (125 MHz,; DMSO-d6; Me_4Si) δ = 171.41 (C=O amide), 170.81 (C=O ester), 155.34 (C aromatic ether), 153.45 (C aromatic phenol, *d*), 131.77, 131.17, 129.92, 128.92, 123.43, 114.89(C aromatic), 80.31, 77.58 (C(CH3)3), 53.96 (Cα), *39.43 (DMSO)*, 37.04, 36.44, 30.17 (C aliphatic), 28.42, 27.42 (C tBu) ppm. IR (reflection) υ_{max}/cm^{-1} 3342.85 (O-H phenol), 2978.22 (C-H stretch alkane), 2956.97 (C-H stretch aliphatic), 1712.13 (C=O stretch in ester), 1645.3 (N-H bend primary amide), 1613.51(N-H bend primary amide), 1600.01 (N-H bend primary amide), 1514.17 (C-N stretch amide), 1367.61 (C-O-C stretch ester), 1151.54 (C-O stretch ester)).

Deprotected desaminotyrosyl-tyrosine was obtained by reaction of Desaminotyrosyl-tyrosine *tert*-butyl ester (9 g, 23 mmol) with TFA (76 mL) in DCM (153 mL) at 0 °C (1h) first and 12 h at room temperature. The solvents were evaporated under reduced pressure, the residue redissolved in 0.1 M HCl and extracted with ethyl acetate. The organic phase was washed with conc. NaCl solution, dried over magnesium sulfate, filtered, and the solvent removed by evaporation under reduced pressure to yield crude DATT, which was purified using column chromatography to yield pure DATT (7.1 g, 93%).

Found: *m/z* (ESI) *330.13* ($M+H^+$), m.p. 161.2; ^{1}H NMR (500 MHz,; DMSO-d6; Me_4Si) δ_H 12.57 (1H, s, COOH), 9.18 (2H, s, OH), 8.06 (1H, d, NH), 6.96 (4H, 2d, Ph), 6.63 (4H, d, Ph), 4.34 (1H, m, $C_\alpha H$), 2.89 (1H, m, $C_\beta H$), 2.72 (1H, m, $C_\beta H$), 2.61 (2H, t, $C_\beta H$), 2.3 (2H, t, $C_\gamma H$) ppm; ^{13}C NMR (125 MHz,; DMSO-d6; Me_4Si) δ = 173.2 (t, COOH), 171.5 (t, CONH), 155.8, 155.4 (t, COH), 131.1 (t, CPh), 130, 128.2 (t, CPh), 127.7 (t, CPh), 59 (t, C_α), 37.1 (t, C_β), 36.11 (t, C_β) 30.2 (t, C_γ) ppm. IR (reflection) υ_{max}/cm^{-1} 3247.3 (OH-phenol), 2957-2919.4 (C-H stretch aliphatic), 1718.7- 1707 (C=O stretch in carboxylic acid), 1651.1 (N-C primary amide), 1613.51 (N-H bend primary amide), 1600.01 (N-H bend primary amide), 1514.17 (C-N stretch amide), 1549.6 (COO^- stretch carboxylate), 1333.3 (COOH stretch carboxylate), 682 (COOH stretch).

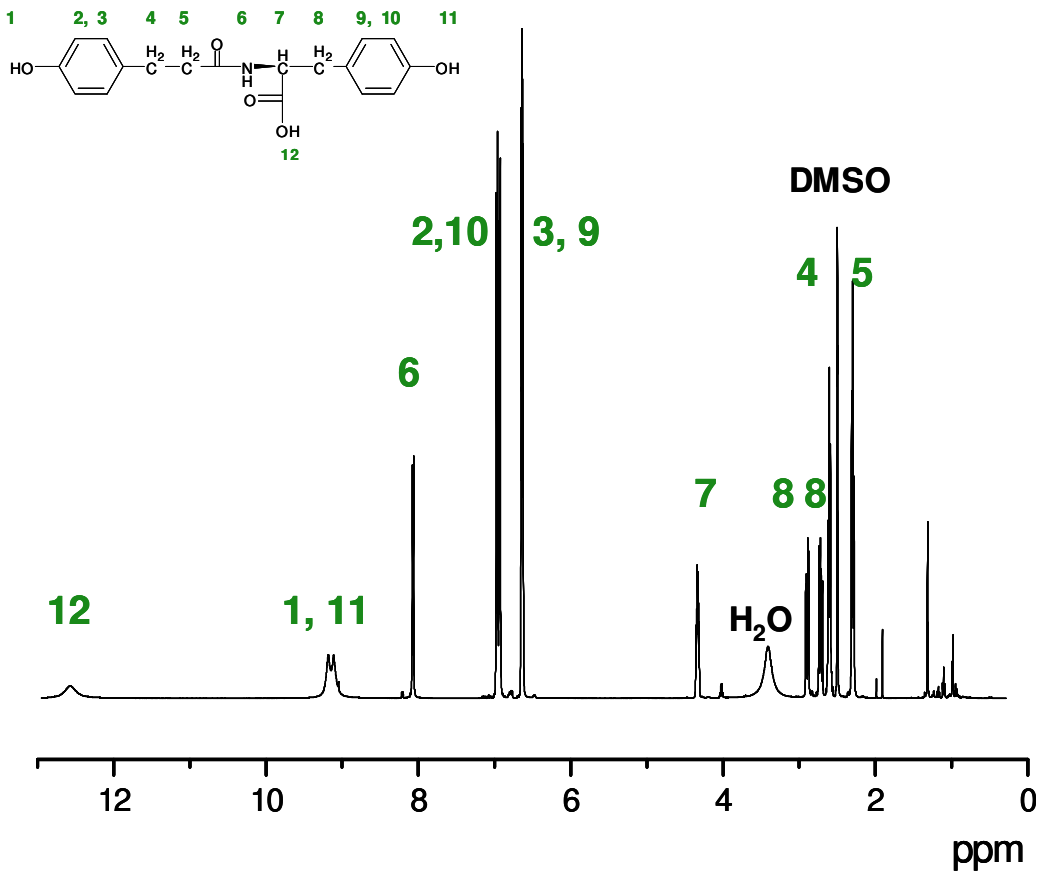

Figure 8.2 NMR spectra of DATT.

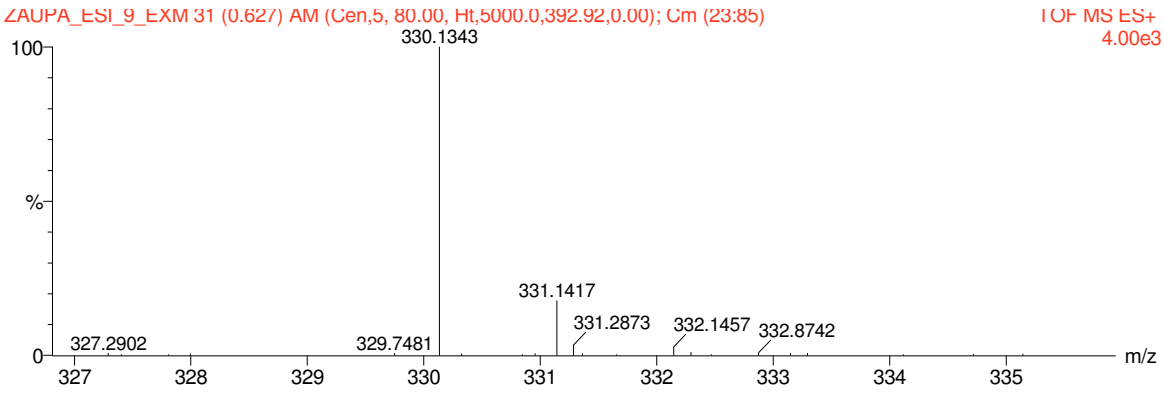

Figure 8.3. ESI-MS spectra of DATT.

8.3.2 Functionalization of gelatin

Functionalized gelatins were obtained by specific reaction of the carboxylic acid groups of either DAT or DATT with the free amino groups of gelatin. DAT or DATT (29 mmol) were activated by reaction with EDC (32 mmol) and NHS (43 mmol) in 110 mL of DMSO at 37 °C. After 3 h, β-Mercaptoethanol (43 mmol) was added to quench the unreacted EDC and further stirred for 30 min. A gelatin solution (15 g in 150 mL DMSO) was added and the

mixture stirred at 37 °C for 5 h. The functionalized products (DAT-Gel and DATT-Gel respectively) were then precipitated in ethanol, filtered, washed with ethanol and acetone, and dried under vacuum. The degree of substitution (90 mol.-%) was determined by ^{1}H NMR spectroscopy (area of the aromatic peaks (δ 6.5 – 7.5) compared to the methyl groups of the apolar amino acid residues Leucine, Valine, and Isoleucine (δ 0.6 – 0.9)) and the TNBS colorimetric assay described by Bubnis et al.[149]

8.3.3 Preparation of films and conditions of hydration

Films were prepared by casting a 5 wt.-% aq. gelatin solution into polystyrene Petri dishes. Drying conditions (temperature and absolute humidity (a.h.)) were varied using a climatic chamber KBT (Binder, Tuttlingen, Germany) to obtain films named v_{long} and v_{short}. v_{long} films were dried at 10 °C and 2.81 g·m^{-3} a.h. until constant weight was achieved, which was obtained following 2 days of drying time, while v_{short} were evaporated at 40 °C and 40.83 g·m^{-3} a.h. until constant weight was achieved, which was obtained within hours. Drying at 10 °C was performed at different a.h. of 0.92 g·m^{-3}, 4.69 g·m^{-3}, and 7.50 g·m^{-3} that corresponded to films dried after 1 day, 3 days, and 10 days, respectively. Shortly after drying, the films were cut into dogbone shaped samples for tensile tests. The samples were later statically hydrated in a KBT climatic chamber at 24.41 g·m^{-3} a.h. and 30 °C for 1 week to obtain films with 25 wt.-% water content.[65]

8.3.4 Temperature modulated differential scanning calorimetry (TM-DSC)

A Phönix DSC 204 F1 (Netzsch, Selb, Germany) apparatus was used to measure the melting point (T_m), enthalpy of melting (ΔH_m) during the first heating run, the glass transition temperature (T_g), and the heat capacity change (ΔC_p) at the glass transition during the second heating run of polymer samples. The gelatin samples were hermetically sealed in a pan to prevent any loss of moisture during TM-DSC measurements. Two consecutive heating runs

from -20 to 150 °C in the first heating run and up to 250 °C in the second heating run were performed with a modulated heating rate with a period of 60 s, amplitude of 0.5 °C, and an underlying heating rate of 5 °C·min^{-1}. Between heating runs, the samples were rapidly cooled (10 °C·min^{-1}).

8.3.5 Wide-angle X-ray scattering investigation (WAXS)

Measurements were performed on a Bruker D8 Discover (Bruker AXS, Karlsruhe, Germany). The X-ray generator was operated at a voltage of 40 kV and a current of 40 mA. A copper anode and a graphite monochromator produced Cu Kα-radiation with a wavelength $\lambda = 0.154$ nm. WAXS images were collected from gelatin films (thickness of about 0.3 mm, exposure times of 120 s per frame) in transmission geometry with a collimator-opening of 0.8 mm at a sample-to-detector distance of 15 cm. Samples were oscillated perpendicular to the primary beam direction ±1 mm in order to average over a large region of the sample. Integration of the two-dimensional scattering data gave the intensity as a function of the scattering angle 2θ. A beam stop was placed immediately after the sample to avoid air scattering. Two procedures were tested for the extraction of the individual peak areas. A peak-fitting program (TOPAS, from Bruker) inserted peaks at the desired positions and fit them to the total scattering curve, and then the peak areas were calculated. A second method consisted of cutting the helix-peaks from the curve and fit the residual data points with a spline function (leading in the pure amorphous scattering), after subtraction from the total scattering, the helix-peaks were obtained and the areas were calculated by integration.

8.3.6 Mechanical tests

Young's modulus E, maximum tensile strength σ_{max}, and elongation at break ε_b were measured using standard test specimen (ISO 527-2/1BB) punched from dried gelatin films for a minimum of five samples (sample thickness = 380 ± 30 µm) using a Zwick Z005 (Zwick

GmbH, Ulm, Germany), where the averages of the results from these samples are reported with standard deviation Dry samples were statically hydrated in a climatic chamber KBT (Binder) at 24.41 $g \cdot m^{-3}$ a.h. and 30 °C for 1 week to obtain films with 25 wt.-% water content.[65]

For hydrogel measurements, the punched samples were swollen and the dimensions of hydrogels were measured with a micrometer screw gauge. A slow extension rate of 0.033 mm·s-1 was adopted in order to consider the elongation regime as isothermal. The tensile tests were performed at 25 °C for dry sample and samples swollen at 23 °C. Tensile properties were determined from stress-strain ($\sigma = f(\varepsilon)$) diagrams.

8.3.7 Degree of swelling

The degree of swelling Q of gelatin films in water at 23 °C was calculated by:[177]

$$Q = 1 + \rho_g \cdot \left(\frac{m_{sw}}{m_d \rho_{H_2O}} - \frac{1}{\rho_{H_2O}} \right) \qquad \text{(eq. 8.11)}$$

where m_{sw} is the weight of the sample in the swollen state, m_d is the weight of the dry extracted sample, ρ_{H2O} (1 $g \cdot cm^{-1}$) and ρ_g are the specific densities of the water and of gelatin, respectively. ρ_g was determined using a Ultrapycnometer 1000 (Quantachrome GmbH & Col. KG, Germany) on gelatin powders dried for 48 h under vacuum.

8.3.8 Rheology

Oscillatory experiments were performed with a plate-plate rheoviscosimeter (Thermo Electron, Karlsruhe, Germany) with a Peltier-element of 20 mm diameter. All dynamic measurements were performed in the linear viscosity region measured at 23 °C with a frequency of 1 Hz and constant stress of 5 Pa. A solvent trap was used to prevent evaporation of solvent. The viscoelastic properties of the associative networks were determined by measuring changes in the storage modulus G’ and loss modulus G’’ as a function of

temperature by oscillatory shear stress at different temperatures ranging from 20 to 60 °C with a heating rate of 2.6 °C·min^{-1}. The error for the T_c determination was ± 1 – 2 °C.

8.3.9 Chemical characterization

^{1}H and ^{13}C NMR spectroscopy were recorded on a Bruker Advance DRX500 Spectrometer at 40 °C (gelatins) and 25°C (DATT). Samples were dissolved in D_2O (gelatins) or DMSO-d_6 (DATT). FT-IR was carried out on Perkin-Elmer, System2000. UV/Vis-Spektroscopy was performed on a Uvicon 931. Mass Spectrometry measurements were obtained from Institute of Organic Chemistry and Structural Analytics (*Prof. E. Kleinpeter,* University of Potsdam, DE) using the 2 GC/MS- System SSQ 710 from Finnigan using GC-TOF und ESI / APCI-Q-TOFmicro (Time of Flight Massenspectrometer).

8.3.10 Thermo-gravimetric analysis (TGA)

To prove the inorganic content within composites a thermogravimetric was performed. Measurements were conducted on a thermo microbalance (Netsch GmbH, TG 209C) under Nitrogen atmosphere within a temperature range of 25°C – 850°C at a heating rate of 10 K · min^{-1}.

8.3.11 Transmission-electron- and scanning-electron-microscopy

A Transmission-Electron- and Scanning-Electron-Microscope (Zeiss, Supra 40VP Gemini) were applied to visualize HAp-particle-size and cross-sections of composite hydrogels respectively. TEM samples were prepared by depositing the powder of interest on platinum-nets and applying an acceleration voltage of 80 kV. SEM samples were carbon coated and an acceleration voltage of 10 kV was applied yielding EDX spectra at a penetration depth of around 2 µm. These measurements were conducted towards identifying the Ca/P ratio of HAp Type1 and HAp Type2 incorporated in the composites.

8.3.12 Composite hydrogels

Composite hydrogels were prepared in a mixing process of HAp Type1 or HAp Type2 as inorganic filler and gelatin, DAT-Gel or DATT-Gel as matrix at a weight ratio 1:4 and 1:1. In order to gain homogeneous composite hydrogels, a solution of 20 wt.-% and 50 wt.-% of HAp-powder with respect to gelatin, DAT-Gel or DATT-Gel was dispersed in distilled water under constant magnetic stirring and ultrasonic excitation (25 W, continuous mode; Bandelin Sonopuls HA2070) in order to de-agglomerate the HAp particles, and subsequently combined to a 3 wt.-% aqueous solution of gelatin, DAT-Gel or DATT-Gel prepared at 70 °C. The obtained mixtures were promptly cast into Petri dishes and allowed to dry at ambient conditions.

A Appendix A: Theoretical Aspects of Atomistic Simulations

This chapter provides information about the theoretical background of molecular modeling calculations. These informations are essential for the definition of the condition of the simulations, which are described in the chapter 4. The basic of the forcefield method is described in section A.1 followed by an extended description of the forcefield used in this work. The theoretical background and its implementation for the generation of detailed atomistic models for amorphous polymer are described in section A.1.5. Then, the approaches to molecular energy minimization and description of the molecular dynamics (MD) simulation are introduced.

A.1 Theoretical aspect of atomistic simulation of gelatin

A.1.1 Forcefield method

Molecular modeling and simulation is the process of first building a mathematical model that mimicking complex biological systems (such as proteins, nucleic acids and lipid bilayers) is then used to conduct computer experiments, i.e. simulations, in order to describe, explain, investigate, and predict the behavior of that specific situation.

In forcefield based methods the molecules are considered as collections of distinct atoms, of a given diameter, d_i, and mass, m_i. that interact with each other, with these interactions being described by means of molecular mechanical forcefields.

A forcefield is a combination of an analytical function of the atomic coordinates, which describes the potential energy of a given configuration of atoms and a set of parameters describing the characteristic of the different atomic types and charges and their interaction. This combination of energy expression and set of parameters permits to calculate structure and dynamic properties of the given model-system making use of the expression of the classical mechanics.

The bonded interactions between atoms, concerning mainly bond length, bond angles, and dihedral angles are described by mechanical springs and other mechanical analogues, with the force constants of the springs related to experimental or *ab-initio* calculations of the strength and equilibrium parameters for bond length-, bond-angles-, and dihedral-angle deformation. The non-bond interactions for pairs of atoms belonging to different molecules or belonging to the same molecule but separated by more then three bonds, are e.g. described using Lennard-Jones and Coulomb potential.

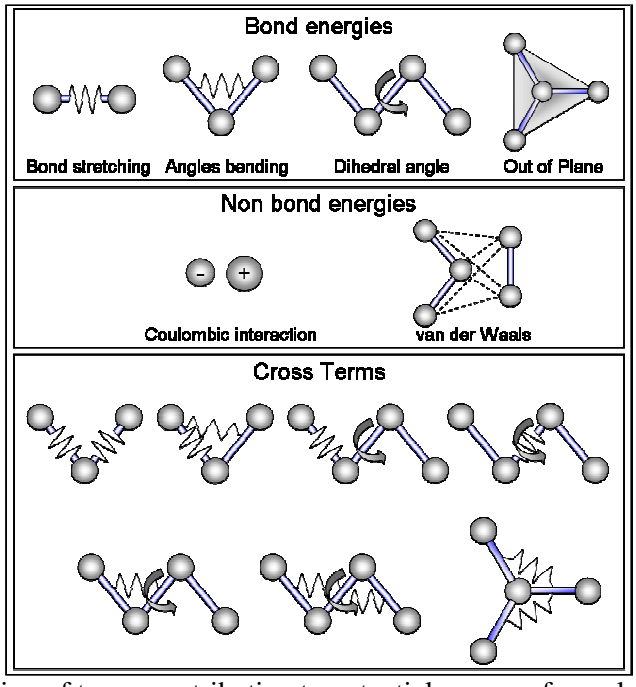

Figure A.1. Representation of terms contributing to potential energy of a molecular system.

The potential energy of a system of atoms can be calculated using the following general equation:

$$E_{Potential} = E_{valence} + E_{crossterm} + E_{nonbond} \quad \text{((eq. A.1)}$$

$E_{valence,}$ valence or bonded energy term, can be split according the relative contributions:

$$E_{valence} = E_{bond} + E_{angles} + E_{torsion} + E_{oop} \quad \text{((eq. A.2)}$$

The E_{bond} is the stretching contribution, E_{angle} the valence angle bending contribution, $E_{torsion}$ the contribution for the dihedral angles torsion, and the E_{oop} refers to the inversion or out of plane interactions.

$E_{crossterm}$ includes the contributions to the total energy arising from the distortions to bond and angles caused by nearby atoms. This term is implemented in modern force fields, so called second generation forcefields, and confers them higher accuracy. Cross terms usually includes the following terms: stretch- stretch, stretch-bend- stretch, bend-bend, torsion- stretch, torsion-bend-bend, bend-torsion-bend, stretch-torsion- stretch.

$E_{nonbond}$ is the energy of interactions between nonbonded atoms and accounts for the van der Waals contribution, E_{vdW}, and an electrostatic term, $E_{Coulomb}$. These interaction arise form the electrostatic distribution in the system. The van der Waals contribution account for the non polar attraction of electron clouds due to induced dipoles at medium distance, while it is zero at high distances and highly repulsive for short distances. The electrostatic interaction take into account the contribution of ionic interactions, hydrogen bond, and dipole-dipole interactions and is usually described by the Coulomb's law.

$$E_{nonbond} = E_{vdW} + E_{Coulomb} \quad \text{(eq. A.3)}$$

Furthermore the force field comprise a specific set of parameters to describe the physical characteristics of each atom type and bonding pattern that occurs in the regularly simulated systems. These characteristics include atomic mass, radii and charge for individual atoms, as

well as the deformation of individual bond length, bond angles, and dihedral angles for pairs, triplets, and quadruplets of bonded atoms.

Different types of force field have been developed for molecular modeling studies, depending on the respective molecular systems and the specific properties which have to be investigated. The selection of the specific forcefield is then of extreme importance for the correct description of the system of interest.

A.1.2 Second generation forcefields

Consistence Force Fields (CFF) are a class of the second generation forcefields, based on existing experimental data and *ab initio* quantum mechanical calculations, that allow the calculation of molecular properties such as conformations, vibrational frequencies and thermodynamic functions with an higher accuracy respect to first generation forcefields like AMBER, CHARMM, CVFF, and GROMACS.[171, 178] All the force fields belonging to this class have the same functional form to describe atom interactions but differs in their parametization. The potential energy is calculated making use of the following equation, where the represented term are schematically represented in (Figure A.1):

$$E = \sum_{b}\left[K_b^2(b-b_0)^2 + K_b^3(b-b_0)^3 + K_b^4(b-b_0)^4\right] \quad \text{(eq. A.4)}$$

$$+\sum_{\theta}\left[K_\theta^2(\theta-\theta_0)^2 + K_\theta^3(\theta-\theta_0)^3 + K_\theta^4(\theta-\theta_0)^4\right] \quad \text{(eq. A.5)}$$

$$+\sum_{\phi}\left[K_\phi^1(1-\cos\phi) + K_\phi^2(1-\cos 2\phi) + K_\phi^3(1-\cos 3\phi)\right] \quad \text{(eq. A.6)}$$

$$+\sum_{\chi} K_\chi \chi^2 \quad \text{(eq. A.7)}$$

$$+\sum_{b}\sum_{b'} K_{bb'}(b-b_0)(b'-b_0') + \sum_{\theta}\sum_{\theta'} K_{\theta\theta'}(\theta-\theta_0)(\theta'-\theta_0') \quad \text{(eq. A.8)}$$

$$+\sum_{b}\sum_{\theta} K_{b\theta}(b-b_0)(\theta-\theta_0) \quad \text{(eq. A.9)}$$

$$+\sum_{\phi}\sum_{b}(b-b_0)\times\left[K_{\phi b}^1\cos\phi + K_{\phi b}^2\cos 2\phi + K_{\phi b}^3\cos 3\phi\right] \quad \text{(eq. A.10)}$$

$$+\sum_{\phi}\sum_{b'}(b'-b_0')\times\left[K_{\phi b'}^1\cos\phi + K_{\phi b'}^2\cos 2\phi + K_{\phi b'}^3\cos 3\phi\right] \quad \text{(eq. A.11)}$$

$$+\sum_{\phi}\sum_{\theta}(\theta-\theta_0)\times\left[K_{\phi\theta}^1\cos\phi + K_{\phi\theta}^2\cos 2\phi + K_{\phi\theta}^3\cos 3\phi\right] \quad \text{(eq. A.12)}$$

$$+\sum_{\phi}\sum_{\theta}\sum_{\theta'} K_{\phi\theta\theta'}(\theta-\theta_0)(\theta'-\theta_0')\cos\phi \quad \text{(eq. A.13)}$$

$$+\sum_{i>j}\varepsilon_{ij}\left[2\left(\frac{\sigma_{ij}}{r_{ij}}\right)^9 - 3\left(\frac{\sigma_{ij}}{r_{ij}}\right)^6\right] + \sum_{i>j}\frac{q_i q_j}{r_{ij}} \quad \text{(eq. A.14)}$$

where b represent the bonds, θ and Φ the angles and torsional angles between three and four atoms respectively, and χ refers to the out of plane angles. q represent atomics partial charges, r_{ij} is the distance between pairs of atoms and σ_{ij} and ε_{ij} are the Lennard-Jones 9-6 parameters. All parameters were determined by previous quantum mechanical calculations.

The first four terms of equation above describe the bond energy in terms of:

Bond stretching and angle bending are described as quadratic function above (eq.A.4-A5).

- The conformational angle deformations are described as three-term Fourier expansion(eq. A.6).

- For the out of plane deformation energy is defined according to the Wilson definition[179] as an harmonic term(eq. A.7).
- All the cross terms between internal coordinates up to the third order: bond-bond, angle-angle, bond-angle, bond-torsion 1 (between a torsion angle and the central bond in the torsion), bond-torsion 2 (between a torsion angle and a side bond in the torsion), angle-torsion, and angle-angle-torsion, are included in (eq. A.8-A.13).
- The non-bonding interactions are considered in term of van der Waals interactions, described as a Lennard-Jones 9-6 potential using an inverse 9^{th} power term for repulsion and 6^{th} for attraction and the Coulomb term to describe the electrostatic interactions (eq. A.14).

The introduction of anharmonic and cross terms was found to improve significantly the accuracy and transferability of the CFF force field. In this study, the CFF version parameterized and tested on amides and peptides, the so called CFF91 force field[171] was applied to all macromolecular models developed.

A.1.3 Molecular mechanic (MM) and molecular dynamic (MD)

While forcefields permit to describe and represent the potential energy surface of a system, minimization and molecular mechanics (MM) in general permit to explore the potential energy surface of a system in order to refine the molecule configuration in order remove unrealistic stresses, non-bonded atomic overlaps, severe bond-length and bond angle distortions, and obtain more stable conformations based on the hypothesis that the lower the energy the more stable is the respective system.

The main strategy involve the determination of the potential energy of the system with respect to the atoms coordinates by application of the respective forcefield function and modify the geometry of the models in a systematic way as to reduce the potential energy of the system. A minimization algorithm has to estimate both the direction and distance of a

given starting point from the next minimum. The vector of the first derivatives of the energy function with respect to the Cartesian coordinates defines a good guess for the initial direction of search. Moving then form the starting point *a* on a certain way along the negative direction of the gradient $-\nabla E$ should bring closer to that minimum (Figure A.6a).

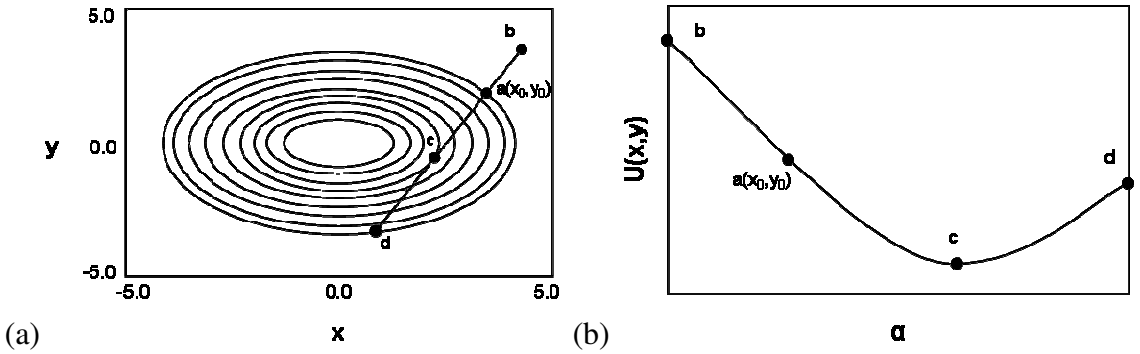

Figure A.2. Example of an elliptic energy surface $E(x, y) = x^2 + 3y^2$ with isoenergy lines and overlaid line search direction b-d (a). Sketch of the system energy along a line search past as function of the line parameter α (b).

In general a necessary but not sufficient criterion for the presence of a minimum (saddle point), is that all first derivatives of a function $E(x_1, x_2,\ldots, x_n)$ are zero. The gradient vector is always oriented perpendicular to the isoenergy line passing through the calculation point a. Many minimizer make use of a straight line (eq.15), "line search", defined by the above mentioned gradient, to come closer to the minimum.

$$\begin{pmatrix} x_1 \\ x_2 \\ . \\ . \\ x_n \end{pmatrix} = \begin{pmatrix} x_{10} + \alpha \dfrac{\partial E}{\partial x_1} \\ x_{20} + \alpha \dfrac{\partial E}{\partial x2} \\ . \\ . \\ x_{n10} + \alpha \dfrac{\partial E}{\partial x_n} \\ \end{pmatrix} \qquad \text{(eq. A.15)}$$

The energy E is then calculated along this line as a function of α (Figure A.6b) and the point *c* is selected as the new starting point. Each line search in a minimization algorithm constitutes on iteration step.

There are several methods that can be used to perform a minimization on a molecular system The most common numerical algorithms for minimization purposes are: *Steepest descent (SD)*, *Conjugate gradient (CG)*, and *Newton-Raphson (NR)*

The *SD methods* evaluates the first derivative of the energy and move the atoms in the downhill direction of the potential energy surface. Although it is fast and robust, SD is limited by the fact that each direction is chosen using only information regarding the present sampling point but disregarding the knowledge of previous search directions. This means that in many cases a large number of iterations are needed and it is not guaranteed to converge in a finite number of steps. It is used mainly during initial minimization stages when the structure is far from the minimum configuration.

The *CG methods,* with three different variants: Polak-Ribiere, Fletcher-Reeves and Powell are iterative and makes use of the previous history of minimization steps as well as the current gradient to determine the next step thus allowing a better convergence than the steepest descents method.

The more sophisticated *NR methods* make use also of the second energy derivative via the calculation of the Hessian matrix, a 3N x 3N matrix, and although it is highly accurate in the search of minimum energy state, it was shown to be less numerically stable for molecular systems involving thousands of atoms. In this study only a combination of the first two method was then utilized.

It has to be reminded that in these minimization procedure only the potential energy is evaluated, while the kinetic energy is not included, so that the most stable conformation found by these algorithms corresponds to a structure at 0 K, and usually only a local minimum of the energy surface is reached.

Molecular dynamic (MD) simulations involve integration of the Newtonian equation of motion for each atom in an ensemble, in order to generate information on the variation in the position, velocity, and acceleration of each particle as a function of time and temperature.

Considered a system with N interacting atoms with mass m_i, the instantaneous force acting on an atom, $\vec{F}_i$ can be computed from the potential energy as the negative value of the gradient:

$$\vec{F}_i(t) = -\frac{\partial U(\vec{r}_1, \vec{r}_2, ..., \vec{r}_i, ..., \vec{r}_N)}{\partial \vec{r}_i(t)} \qquad \text{(eq. A.16)}$$

Where $\vec{r}_i$ are the coordinate of the atom. These parameters can be used to determine the velocity (v_i) or change of position (r_i) of an atom in the structure with time can by solving the Newton's equations of motion:

$$\vec{F}_i(t) = m_i \cdot \vec{a}_i = m_i \cdot \frac{d^2\vec{r}_i(t)}{dt^2} \qquad \text{(eq. A.17)}$$

Newton's equation of motion can only be solved (integrated) numerically These calculation are performed through time integration algorithms based on finite difference methods. There time is decomposed in a sequence of much smaller time periods in which the force is supposed to remain constant, the displacement and change in velocities that take place due to these forces are calculated by the combination of (eq. A16) and (eq. A17) applied to the current conformation. The process is repeated as long as it is necessary.

If we know the positions and some of their time derivatives, it is possible to calculate this quantities at the time t + Δt. MD-simulations are often applied to rather large systems (many thousand atoms). Therefore the cpu- and memory time is often very high and specific algorithm have been developed meeting the following conditions:

- Fast with ideally only one calculation of the potential energy E per time step.
- Low demand in physical memory
- Possibility of relatively large time steps Δt

- Acceptable level of energy conservation

In this work the velocity Verlet scheme[180] has been applied that has been proven to be an effective and reliable method for the integration of the equations of motion (eq. A.16-17).

The velocity Verlet algorithm is obtained by a Taylor expansion of the position of particle *i* at t_{n-1} and t_{n+1}, and is a second order integration scheme. In this scheme, the position vector $\vec{r}$ and velocity vector $\vec{v}$ are obtained as:

$$\vec{r}(t+\Delta t) = \vec{r}(t) + \vec{v}(t)\Delta t + \vec{a}(t)\frac{\Delta t^2}{2}$$

$$\vec{v}(t+\Delta t) = \vec{v}(t) + (\vec{a}(t) + \vec{a}(t+\Delta t))\frac{\Delta t}{2} \qquad \text{(eq. A.18)}$$

$$a(t+\Delta t) = \frac{\vec{F}(t+\Delta t)}{m}$$

The accuracy of results depend mostly on the value of the time step Δt. In general, it is chosen to be able to represent the highest frequencies, namely the vibrations of hydrogens $10^{-14}\cdot sec^{-1}$, therefore the time step should not be larger then 10^{-15}, one femtosecond (fs). Higher timesteps, although permitting a more efficient utilization of the cpu-time, on the other hand would trigger numerical instabilities and unacceptable inaccuracy in the respective integration process.

During a simulation the velocities can be measured and controlled via the well know relation between the kinetics and thermal energies of a multi particle system.

$$\mathrm{E}_{\mathrm{kin}} = \sum_{\mathrm{i}=1}^{\mathrm{N}} \frac{1}{2} m_i \cdot \vec{v}_i^{\,2} = \frac{(3\mathrm{N} - 6)}{2} k_B T \qquad \text{(eq. A.19)}$$

Where (3N - 6) are the degree of freedom for a N particle system, taking into consideration that the center of mass of the system does not move during the dynamic, k_B is the Boltzmann constant, T is the temperature of the system and E_{kin} is the kinetic energy.

Depending on which macroscopic observables are held constant, different ensembles can be defined for the calculation. After the initial velocities of the particles are drawn via a

Metropolis Montecarlo procedure, basically from the appropriate Maxwell-Boltzmann distribution of velocities of particles at a given temperature T, the system is simply evolved according to Newton's law of motion. This corresponds to the microcanonic *NV E* ensemble and is most frequently used because it is the most reliable simulation scheme. This means that the trajectory sampled is the one of an isolated system, no exchange of heat or work. Real experiments, especially in biological sciences, are performed in thermal equilibrium (T), i.e., in the canonical ensemble (NVT), and/or mechanical (PV) equilibrium, i.e. isobaric ensembles (NPH or NPT). In this work then the canonical *NVT* ensemble for studying equilibration processes at constant temperature T and volume V and the isothermal-isobaric *NPT* ensemble to investigate system properties at atmospheric pressure were used.

A.1.4 Control of state variable during molecular dynamics

In this work the behavior of the system was studied at a specific temperature and pressure, so the number of atoms N, the temperature T and pressure P, were kept constant during the MD simulation and both NVT and NPT ensemble were used . In these cases an additional thermostat and barostat has to be added to the system to permit the control of temperature and pressure and avoid cumulative numerical error.

A.1.4.1 The control of Temperature

The initial temperature of the system, determined by the distribution of atom velocities according to the Maxwell-Boltzmann relationship (eq. A.19), changes during the dynamic simulation. This variation occur due to the transformation of potential energy into kinetic energy and vice versa, in particular when typically energy-minimized starting structure of a model changes to the respective thermal equilibrium structure. The velocities need then to be scaled appropriately in each simulation step, by the application of a thermostat that should permit to produce a correct statistical ensemble where the occurrence of certain configuration obeys the laws of statistical mechanics. A variety of techniques have been developed: *direct*

velocity scaling, *Berendsen method*, *Nosé and Nosé-Hoover temperature coupling*, and *Andersen method*.

In *velocity scaling* method is an easy and rapid method where the velocities of the atoms are drastically modified by multiplying them by a factor $\lambda = \sqrt{T_0 / T(t)}$ for each step or when is needed, where T(t) is the current temperature calculated by (eq. A.19) and T_0 is the desired temperature:

$$v_{new} = \lambda \cdot v_{old} \qquad \text{(eq. A.20)}$$

The main problem of this approach is that it does not allow fluctuation in the temperature which are present in the canonical ensemble and is then mainly suitable for the early steps of equilibration.

After equilibration a more gentle approach of coupling the system to a heat bath can be applied as in the *Berendsen* method.[173] In this case the velocities are multiplied by a factor λ that connect the time step used Δt, the instantaneous and target temperature T_o and T(t), and the characteristic relaxation time τ that permit to adjust strength of the coupling:

$$\lambda = \left[1 + \frac{\Delta t}{\tau} \left(\frac{T_0 - T(t)}{T(t)} \right) \right]^{1/2} \qquad \text{(eq. A.21)}$$

If $\tau \to \infty$ the thermostat is inactive and the run is sampling a microcanonical ensemble, while for $\tau = \Delta t$ the Berendsen is nothing more then a simple velocity scaling. in this simulation a value of $\tau = 0.1$ was used, as typical reasonable choice for condensed phase systems.

In the *Nosé-Hoover* thermostat[181] the heat bath is an integral part of the system and so the by addition of an artificial variable $\tilde{s}$ with mass Q and velocity $\dot{\tilde{s}}$ that introduce a new degree of freedom. The equations of motion are then solved for this extended system. This

integration of the bath permit a better control of the temperature of the system once the equilibrium is reached.

In the *Andersen* thermostat[174] the coupling to a heat bath is represented by the stochastic impulsive forces of fictitious particle in the heat bath that act occasionally on randomly selected particle of the system.

A.1.4.2 The control of pressure

The pressure is a thermodynamic variable that can define the state of the system, and is defined as the force per unit area. Standard atmospheric pressure is 1.013 bar. In *Discover*[144] pressure is expressed in GPa, a positive pressure implies a compressive force pushing the system inward.

In isothermal-isobaric ensemble, NPT-simulations, in addition to a thermostat, a barostat is needed to control the pressure. This ensemble is used when the correct density of the system is of great significance for the simulation. It can be applied only under PBC condition, where the adjustment of the pressure is done by regulating the volume of the unit cell.

The pressure of the atomistic system can be calculated using the viral theorem. In the most isotropic case:

$$pV = Nk_BT + \frac{2}{3}\langle W \rangle \qquad \text{(eq. A.22)}$$

With $W = \frac{1}{2}\sum_{i=1}^{N} \vec{r}_i * \vec{F}_i$

Where r_i are the position of the particles and F_i the forces acting on the atoms.

Pressure control is often performed exploiting the Berendsen method[173] of coupling the simulated system to a pressure bath. Then at each simulation step, the edge-lengths of the cell containing the system and the x, y, z coordinate of each original atom are scaled by the following factor:

$$\mu = \left(1 + \frac{\Delta t}{\tau} \cdot \gamma \cdot [\, p(t) - p_0 \,] \right) \qquad \text{(eq. A.23)}$$

Where γ and τ are respectively the compressibility of the systems and the relaxation time constants and determine the strength of the coupling between the model and the pressure bath. If available a measured value for γ can be used otherwise the compressibility of liquid water ($5 \cdot 10^{-5}$ bar) is applicable. In this method only cell size and atom position are modified but not the shape of the simulation box.

The Andersen control method[174] involves changing the volume of the cell but keeping its shape fixed by allowing the cell to change isotropically. This volume is considered as a dynamic variable in the system with a defined mass and potential, derived form the external pressure.

If the atomistic system shall be subjected to external stresses, then a method like *Parinello-Rahman* technique is needed. This method which will be not explained further in this script is based on the Lagrangian mechanics thus permitting simultaneous change of volume and shape of a basic cell.

Finally it should be mentioned that the application of cut off distances for log ranging pair interactions may lead to systematic errors in pressure calculation. Therefore, an additional so called *van der Waals tail correction cutoff* is applied in NPT simulations.

A.1.5 Packing models for amorphous cell

The construction of amorphous packing models were obtained under PBC by the Amorphous Cell package of Material Studio, Accelrys Software Inc. that make use of an algorithm based on a technique developed by Theodorou and Suter,[117] a well known procedure for polymers, which considers the rotational isomeric states (RIS model, Flory Huggins theory) for the description of the distribution of backbone conformational angles.

The aim of this technique is the generation of bulk disordered systems containing polymer chains in realistic equilibrium conformations.

The Theodoru-Suter chain-generation method can be explained as follows:

1. The number of polymer molecules and possibly required solvent molecules is chosen, together with the target temperature, density (with a possible ramp from a lower initial value in case of ring-containing polymers), cell type (e.g. cubic, rectangular) and number of desired configurations.
2. The algorithm then attempt to create a chain which shows a distribution of conformation angles and a global chain geometry representative for the simulated material at expense of a realistic homogeneity of the packing of chain segments. It starts by randomly inserting the first three backbone atoms (together with their pendant atoms) of the first constituent molecule listed in the Amorphous Cell construction setup in the defined cell.
3. The chain is grown by adding stepwise one backbone atom (with relative bond and pendant atoms) after the other according to the requirements of the RIS (Rotational Isomeric States) theory: for every new added bond *i*, a possible rotational state has to be assigned by computing a conditional probability:

$$q'_{i-1,i}\left(\phi',\phi\right)=\frac{q_{i-1,i}\left(\phi',\phi\right)\exp\left(\frac{-\Delta E_i}{RT}\right)}{\sum_i q_{i-1,i}\left(\phi',\phi\right)\exp\left(\frac{-\Delta E_i}{RT}\right)} \qquad \text{(eq. A.24)}$$

where R is the universal gas constant, T is the absolute temperature, ΔEi is the increase of non-bonding interaction energy caused by the addition of the backbone atom i+1 with pendant atoms of the backbone atom i, $q_{i-1,i}(\Phi',\Phi)$ is the conditional probability of finding the i^{th} backbone bond in the conformation state Φ considering that the conformation state of the $(i-1)^{th}$ backbone bond is Φ'. In a theoretical point of view, $q_{i-1,i}(\Phi',\Phi)$ can be defined as the ratio between the bond pair (i-1, i)

probability, $p_{i-1,i}(\Phi',\Phi)$, and the bond (i-1) probability, $p_{i-1}(\Phi')$, related to their respective conformation state:[182]

$$q'_{i-1,i}(\phi',\phi) = \frac{p_{i-1,i}(\phi',\phi)}{p_{i-1}(\phi')} \qquad \text{(eq. A.25)}$$

The criterion applied to select the rotational state of the next backbone bond implies the normalization of $q_{i-1,i}$ (Φ',Φ) followed by a Metropolis selection procedure: a number *M* between 0 and 1 is randomly generated and compared with $q_{i-1,i}$ (Φ',Φ); the new rotational state is accepted only if

$$M \leq q'_{i-1,i}(\phi',\phi) \qquad \text{(eq. A.26)}$$

After a certain number of algorithm steps, it is possible that the growing polymer chain leaves the original cell, re-entering as a ghost chain from the opposite side of the box thanks to PBC.

All the generated conformations were checked in order to avoid catenations of the ring structures and spearing of chains. After building the initial strain of the models have to be removed using relaxation procedures involving a initial down scaling of force field parameter related to non-bond interactions and torsional angles to increase mobility of polymer chain and a stepwise restore of initial force field parameter, followed by molecular annealing molecular dynamics.

A.1.6 Non bonded interaction and periodic boundary conditions (PBC)

The number of atoms considered in the atomistic simulations ($< 10^4$) is extremely low in comparison with the one at the macroscopic scale ($\sim 10^{23}$). Obviously, it will not be possible to take into account such a high number of degrees of freedom, for computational time grounds.

So as to simulate an infinite system, the so-called periodic boundary conditions (PBC) are used. The basic idea is to put the system in a cubic lattice, which is reproduce in the three

dimensions in an infinite manner, by mathematical conditions (Figure A.3). in this manner the original box is surrounded by replica of itself. During simulation, when a molecule moves in the original box, its periodic image in every other box moves in the exactly same way in terms of direction and velocity. According to this principle when a particle leaves the original box, one of its images enters through the opposite face of the cube. The number of atoms in the box remains in this way constant. The use of a periodic lattice permit to avoid surface discontinuity effects the interaction between the initial system and its nearest images is calculated. Its important to notice that one atom in the original box, is in principle interacting with several copies or images of the rest of the atoms and itself in the replicated boxes. This fact would eventually lead to an infinite number of non-bonded interactions to be considered in MM and MD calculation. At the same time, considering the interaction of an atoms with several copies of another atoms or itself would results in artificial periodicity that are not present in the "real" polymer system. For that reason, the *minimum-image condition* is applied, where only the interaction of particles located closer to half of the cubic lattice size are computed (Figure A.4). This maximal distance of interaction is called the cut-off distance $r_{cut\text{-}off}$ and as will be better explained in the next section, it permits to limit the number of pair-interactions calculated and therefore to increase the speed of the dynamics.

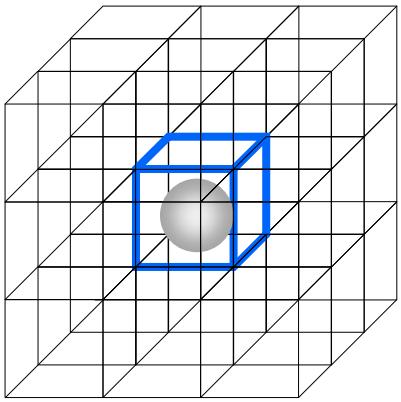

Figure A.3. Example of simulation box with a solute particle replicated along the three dimensions according to periodic boundary conditions in order to better represent a bulk environment.

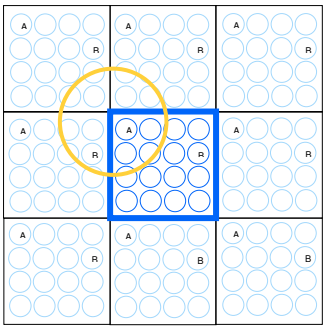

Figure A.4 Minimum image model showing that each real molecule interacts with at most one image of each real molecule.

A.1.7 Treatment of non-bonded interactions

The evaluation of non-boned interactions, e.g., the electrostatic and van der Waals interactions are the most computationally intensive because they need to be performed for almost all atom pairs in the respective system (last two terms in eq. A.14). Considering a system of N atoms, the corresponding numbers of non-bonded interactions increases proportional to the square in number of atoms (N_2).[183] A popular choice to limit these interactions is to utilize a cutoff scheme, such that the interactions are calculated only for the atoms residing within a certain defined distance (r_c) from each other, assuming that the overall contribution of far away atoms is small (referred to Figure A.4).

For all simulation setups, a "non bond cutoff" of 15 Å was utilized, not evaluating any Lennard-Jones term for atom pairs which are further apart from each other than this value.

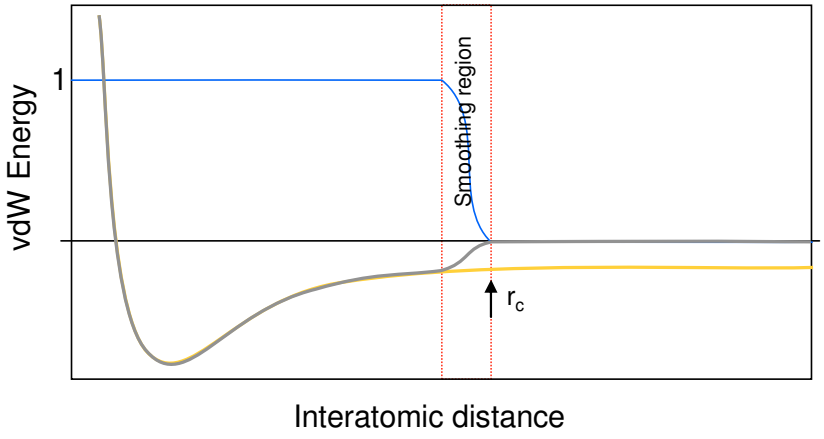

Figure A.5. Example of Lennard-Jones potential (orange curve) and smoothing function (blue curve) applied to a switch cutoff criterion (gray line). Beyond the cutoff distance, r_c, the potential is zero.

These approaches are commonly applied to van der Waals interactions which are usually computed using a Lennard-Jones 9-6 potential (first term of eq. A.14). The potential energy term decay rapidly as the inverse 6^{th} power of the distance between pair of atoms, hence it is often sufficient to compute it only for atoms within a certain cutoff distance. Basically there are three categories of cutoff techniques: *truncation*, *switch*, and *shift*, respect to the smoothness used to reduce the energy function. To avoid numerical problems caused by a sudden shut down of the potential, the switch methods has to be preferred where a step function is used and the Lennard-Jones potential is fully considered until the beginning of a smoothing region, then partially reduced (defined over a distance of 1.5 Å in this work), while the van der Waals interactions are not calculated after the smoothing region (Figure A.5). The behavior in the smoothing region is defined by an appropriate spline function.

If electrostatic interactions are important in the simulated model system, it's needed to consider that the Coulomb potential for large atoms pairs decays just with r_{ij}^{-1} (instead of r_{ij}^{-6} for van der Waals. Then the cut off distances need to be much larger than in the case of van der Waals interaction. In Material Studio the cutoff can be applied to two different elements: *atom-based* cutoffs, the cut off distance is considered between all pairs of atom, in the *group-based* cutoff the exclusion principle is based on electrically neutral groups. This second approach permit partially to overcome this problem in the case the simulated system is overall neutral, it does not contain explicit charges but only partial charges. The molecule is here divided in subunits of neutral charge (so called *charge groups*) and a *switching* atom, generally in the geometrical center of the group, is defined for each group. Then, the cutoff is referred to the distance between all pairs of switching atoms. If the distance between the switching atoms is smaller then the defined cutoff, all the atoms within these two groups are used for the calculation of the non-bond interactions. Otherwise no non-bond interactions are considered between these two groups. This techniques avoids the splitting of individual

dipoles which converts the general Coulomb interactions between partial charges in pure dipole-dipole interaction. Then the following theoretical consideration based on the central multipole expansion can be applied. It considers the electrostatic potential of a charge group as a summation of various electric moments.[183]

$$\phi(r) = \frac{1}{4\pi\varepsilon}\left(\frac{q}{r} + \frac{\mu\cos\theta}{r^2} + \frac{\Theta\left(3\cos^2\theta - 1\right)}{r^3} + \ldots\right) \qquad \text{(eq. A.27)}$$

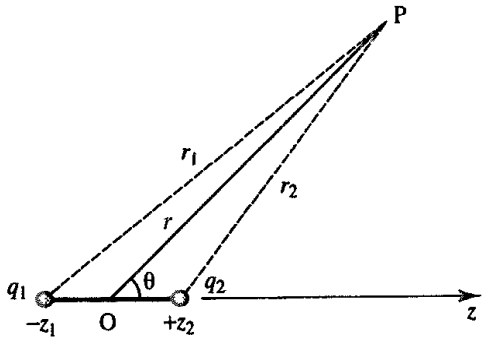

Figure A.6. Electrostatic potential calculated in the point P due to two point charges (q_1 and q_2).

where q is the overall electrical charge, μ is the total dipole moment, Θ is the quadrupole moment, ε is the dielectric constant, and all the geometrical parameters are shown in Figure A.6. Every charge group is electronically neutral, thus q is zero, and the quadrupole contribution is not considered: it remains the dipole contribution. This means that the interactions between charged groups are interactions between dipole moments, which are known to be proportional to r_{ij}^{-3}, showing steeper energy decay than direct charge-charge interactions (proportional to r_{ij}^{-1}). This results in an increased accuracy of the model.

B Appendix B

B.1 HAp particles

The synthesis of HAp particles was performed at r.t. or +100 °C in a wet-precipitation procedure by mixing Calcium nitrate tetra-hydrate and Diammonium hydrogen phosphate, followed by adjusting the pH with aqueous ammonia solution. The two types were denoted as Type 1 (r.t.) and Type 2 (100 °C), respectively. HAp Type 1 had a lower crystallinity and crystal size but higher specific surface area, higher Ca/P ratio, and higher carbonate content than HAp Type 2. The two HAp types however had the same aspect ratio of about 2.5. Using the two types of HAp particles, composites with fillers with different properties could be compared. A summary of the HAp particle properties is given in Table 1.

Table 1: Summary of the obtained properties of Carbonated HA powders. AR: aspect ratio, X_s: Crystal size, X_c Degree of crystallinity, SSA: Specific Surface Area, Ca/P: Calcium/Phosphor ratio.

	AR	X_s [nm]	X_c [%]	SSA [m^2/g]	Ca/P	CO_3^{2-} [wt%]
HA Type1	~2.5	~16	<5	162	1.77	2
HA Type2	~2.5	~31	48	52	1.62	1.1

References

1. Annual report of the U.S. Organ procurement and transplantation network and the scientific registry of transplant recipients: Transplant data 1999-2008. U.S. Department of health and human services, health resources and services administration, healthcare systems bureau, division of transplantation, Rockville, MD. (2009).
2. Shevchenko, R.V., James, S.L., James, S.E. A review of tissue-engineered skin bioconstructs available for skin reconstruction. *Journal of The Royal Society Interface* **7**, 229-258 (2009).
3. Hutmacher, D.W. Scaffolds in tissue engineering bone and cartilage. *Biomaterials* **21**, 2529-2543 (2000).
4. Langer, R. Biomaterials in drug delivery and tissue engineering: One laboratory's experience. *Accounts of Chemical Research* **33**, 94-101 (1999).
5. Middleton, J.C., Tipton, A.J. Synthetic biodegradable polymers as orthopedic devices. *Biomaterials* **21**, 2335-2346 (2000).
6. Shastri, V.P., Lendlein, A. Materials in regenerative medicine. *Advanced Materials* **21**, 3231-3234 (2009).
7. Shastri, V.P., Lendlein, A. Engineering materials for regenerative medicine. *MRS Bulletin* **35**, 571-575 (2010).
8. Ratner, B.D., Bryant, S.J. Biomaterials: Where we have been and where we are going. *Annual Review of Biomedical Engineering* **6**, 41-75 (2004).
9. Lendlein, A., Zotzmann, J., Feng, Y.K., Alteheld, A., Kelch, S. Controlling the switching temperature of biodegradable, amorphous, shape-memory poly(rac-lactide)urethane networks by incorporation of different comonomers. *Biomacromolecules* **10**, 975-982 (2009).
10. Lendlein, A., Colussi, M., Neuenschwander, P., Suter, U.W. Hydrolytic degradation of phase-segregated multiblock copoly(ester urethane)s containing weak links. *Macromolecular Chemistry and Physics* **202**, 2702-2711 (2001).
11. Lendlein, A., Neuenschwander, P., Suter, U.W. Tissue-compatible multiblock copolymers for medical applications, controllable in degradation rate and mechanical properties. *Macromolecular Chemistry and Physics* **199**, 2785-2796 (1998).
12. Valappil, S.P., Misra, S.K., Boccaccini, A.R., Roy, I. Biomedical applications of polyhydroxyalkanoates, an overview of animal testing and in vivo responses. *Expert Review of Medical Devices* **3**, 853-868 (2006).
13. Neffe, A.T., Tronci, G., Alteheld, A., Lendlein, A. Controlled change of mechanical properties during hydrolytic degradation of polyester urethane networks. *Macromolecular Chemistry and Physics* **211**, 182-194 (2010).

14. Hong, H.D., Park, S., Jimenez, R.H.F., Rinehart, D., Tamm, L.K. Role of aromatic side chains in the folding and thermodynamic stability of integral membrane proteins. *Journal of the American Chemical Society* **129**, 8320-8327 (2007).
15. Burley, S.K., Petsko, G.A. Aromatic-aromatic interaction - a mechanism of protein-structure stabilization. *Science* **229**, 23-28 (1985).
16. Park, S., Radmer, R.J., Klein, T.E., Pande, V.S. A new set of molecular mechanics parameters for hydroxyproline and its use in molecular dynamics simulations of collagen-like peptides. *Journal of Computational Chemistry* **26**, 1612-1616 (2005).
17. Djabourov, M. Architecture of gelatin gels. *Contemporary Physics* **29**, 273-297 (1988).
18. Lutolf, M.P., Hubbell, J.A. Synthetic biomaterials as instructive extracellular microenvironments for morphogenesis in tissue engineering. *Nature Biotechnology* **23**, 47-55 (2005).
19. Bonzani, I.C., George, J.H., Stevens, M.M. Novel materials for bone and cartilage regeneration. *Current Opinion in Chemical Biology* **10**, 568-575 (2006).
20. Rickert, D., Lendlein, A., Peters, I., Moses, M.A., Franke, R.P. Biocompatibility testing of novel multifunctional polymeric biomaterials for tissue engineering applications in head and neck surgery: An overview. *European Archives of Oto-Rhino-Laryngology* **263**, 215-222 (2006).
21. Augst, A.D., Kong, H.J., Mooney, D.J. Alginate hydrogels as biomaterials. *Macromolecular Bioscience* **6**, 623-633 (2006).
22. Darr, A., Calabro, A. Synthesis and characterization of tyramine-based hyaluronan hydrogels. *Journal of Materials Science: Materials in Medicine* **20**, 33-44 (2009).
23. Gillette, B.M., Jensen, J.A., Wang, M., Tchao, J., Sia, S.K. Dynamic hydrogels: Switching of 3d microenvironments using two-component naturally derived extracellular matrices. *Advanced Materials* **9999**, NA (2009).
24. Aamer, K.A., Sardinha, H., Bhatia, S.R., Tew, G.N. Rheological studies of plla-peo-plla triblock copolymer hydrogels. *Biomaterials* **25**, 1087-1093 (2004).
25. Elisseeff, J., Mcintosh, W., Anseth, K., Riley, S., Ragan, P., Langer, R. Photoencapsulation of chondrocytes in poly(ethylene oxide)-based semi-interpenetrating networks. *Journal of Biomedical Materials Research* **51**, 164-171 (2000).
26. Slaughter, B.V., Khurshid, S.S., Fisher, O.Z., Khademhosseini, A., Peppas, N.A. Hydrogels in regenerative medicine. *Advanced Materials* **21**, 3307-3329 (2009).
27. Peppas, N.A., Hilt, J.Z., Khademhosseini, A., Langer, R. Hydrogels in biology and medicine: From molecular principles to bionanotechnology. *Advanced Materials* **18**, 1345-1360 (2006).
28. Temenoff, J.S., Mikos, A.G. Review: Tissue engineering for regeneration of articular cartilage. *Biomaterials* **21**, 431-440 (2000).
29. Von Der Mark, K., Park, J., Bauer, S., Schmuki, P. Nanoscale engineering of biomimetic surfaces: Cues from the extracellular matrix. *Cell and Tissue Research* **339**, 131-153 (2010).
30. Bruckner-Tuderman, L., Von Der Mark, K., Pihlajaniemi, T., Unsicker, K. Cell interactions with the extracellular matrix. *Cell and Tissue Research* **339**, 1-5 (2010).
31. Shoulders, M.D., Raines, R.T. Collagen structure and stability. *Annual Review of Biochemistry* **78**, 929-958 (2009).
32. Speakman, P. Proposed mechanism for the biological assembly of collagen triple helix. *Nature* **229**, 241-243 (1971).
33. Ramachandran, G.X., Chandrasekharan, R. Interchain hydrogen bonds via bound water molecules in the collagen triple helix. *Biopolymers* **6**, 1649-1658 (1968).

34. Prockop, J.D. Collagens: Molecular biology, diseases, and potentials for therapy. *Annual Review of Biochemistry* **64**, 403-434 (1995).
35. Persikov, A.V., Ramshaw, J.A.M., Kirkpatrick, A., Brodsky, B. Electrostatic interactions involving lysine make major contributions to collagen triple-helix stability. *Biochemistry* **44**, 1414-1422 (2005).
36. Sundar, R.S., Vijayaraj, R., Parthasarathi, R., Subramanian, V., Ramasami, T. A molecular dynamics analysis of ion pairs formed by lysine in collagen: Implication for collagen function and stability. *Journal of Molecular Structure - THEOCHEM* **851**, 299-312 (2008).
37. Kuivaniemi, H., Tromp, G., Prockop, D.J. Mutations in collagen genes: Causes of rare and some common diseases in humans. *The FASEB Journal* **5**, 2052-2060 (1991).
38. Brodsky, B., Baum, J. Structural biology: Modelling collagen diseases. *Nature* **453**, 998-999 (2008).
39. Kar, K., Ibrar, S., Nanda, V., Getz, T.M., Kunapuli, S.P., Brodsky, B. Aromatic interactions promote self-association of collagen triple-helical peptides to higher-order structures. *Biochemistry* **48**, 7959-7968 (2009).
40. Midwood, K.S., Williams, L.V., Schwarzbauer, J.E. Tissue repair and the dynamics of the extracellular matrix. *The International Journal of Biochemistry & Cell Biology* **36**, 1031-1037 (2004).
41. Guthold, M., Liu, W., Sparks, E., Jawerth, L., Peng, L., Falvo, M., Superfine, R., Hantgan, R., Lord, S. A comparison of the mechanical and structural properties of fibrin fibers with other protein fibers. *Cell Biochemistry and Biophysics* **49**, 165-181 (2007).
42. Vesely, I. Heart valve tissue engineering. *Circulation Research* **97**, 743-755 (2005).
43. Schmidt, C.E., Baier, J.M. Acellular vascular tissues: Natural biomaterials for tissue repair and tissue engineering. *Biomaterials* **21**, 2215-2231 (2000).
44. Zioupos, P., Currey, J.D., Hamer, A.J. The role of collagen in the declining mechanical properties of aging human cortical bone. *Journal of Biomedical Materials Research* **45**, 108-116 (1999).
45. Chvapil, M., Holuša, R. Experimental experiences with the collagen sponge as hemostaticum and tampon. *Journal of Biomedical Materials Research* **2**, 245-264 (1968).
46. Lennox, F.G. Shrinkage of collagen. *Biochimica et Biophysica Acta* **3**, 170-187 (1949).
47. Lynn, A.K., Yannas, I.V., Bonfield, W. Antigenicity and immunogenicity of collagen. *Journal of Biomedical Materials Research Part B-Applied Biomaterials* **71B**, 343-354 (2004).
48. Jayakrishnan, A., Jameela, S.R. Glutaraldehyde as a fixative in bioprostheses and drug delivery matrices. *Biomaterials* **17**, 471-484 (1996).
49. Damink, L.H.H.O., Dijkstra, P.J., Vanluyn, M.J.A., Vanwachem, P.B., Nieuwenhuis, P., Feijen, J. Glutaraldehyde as a cross-linking agent for collagen-based biomaterials. *Journal of Materials Science-Materials in Medicine* **6**, 460-472 (1995).
50. Hey, K.B., Lachs, C.M., Raxworthy, M.J., Wood, E.J. Crosslinked fibrous collagen for use as a dermal implant: Control of the cytotoxic effects of glutaraldehyde and dimethylsuberimidate. *Biotechnology and applied Biochemistry* **12**, 85-93 (1990).
51. Olde Damink, L.H.H., Dijkstra, P.J., Van Luyn, M.J.A., Van Wachem, P.B., Nieuwenhuis, P., Feijen, J. Cross-linking of dermal sheep collagen using a water-soluble carbodiimide. *Biomaterials* **17**, 765-773 (1996).
52. Yannas, I.V., Tobolsky, A.V. Cross-linking of gelatin by dehydration. *Nature* **215**, 509-510 (1967).

53. Petite, H., Rault, I., Huc, A., Menasche, P., Herbage, D. Use of the acyl azide method for cross-linking collagen-rich tissues such as pericardium. *Journal of Biomedical Materials Research* **24**, 179-187 (1990).
54. Kato, Y.P., Silver, F.H. Formation of continuous collagen fibres: Evaluation of biocompatibilily and mechanical properties. *Biomaterials* **11**, 169-175 (1990).
55. Djagny, K.B., Wang, Z., Xu, S. Gelatin: A valuable protein for food and pharmaceutical industries: Review. *Critical Reviews in Food Science and Nutrition* **41**, 481 - 492 (2001).
56. Vaca Chavez, F., Hellstrand, E., Halle, B. Hydrogen exchange and hydration dynamics in gelatin gels. *The Journal of Physical Chemistry B* **110**, 21551-21559 (2006).
57. Benguigui, L., Busnel, J.-P., Durand, D. Study of junction zones in gelatin gels through selective enzymatic digestion. *Polymer* **32**, 2680-2685 (1991).
58. Guo, L., Colby, R.H., Lusignan, C.P., Whitesides, T.H. Kinetics of triple helix formation in semidilute gelatin solutions. *Macromolecules* **36**, 9999-10008 (2003).
59. Normand, V., Muller, S., Ravey, J.C., Parker, A. Gelation kinetics of gelatin: A master curve and network modeling. *Macromolecules* **33**, 1063-1071 (2000).
60. Gornall, J.L., Terentjev, E.M. Helix-coil transition of gelatin: Helical morphology and stability. *Soft Matter* **4**, 544-549 (2008).
61. Guo, L., Colby, R.H., Lusignan, C.P., Howe, A.M. Physical gelation of gelatin studied with rheo-optics. *Macromolecules* **36**, 10009-10020 (2003).
62. Gornall, J.L., Terentjev, E.M. Helix-coil transition of gelatin: Helical morphology and stability. *Soft Matter* **4**, 544 (2008).
63. Guo, L., Colby, R.H., Lusignan, C.P., Whitesides, T.H. *Macromolecules* **36**, 9999 (2003).
64. Benguigui, L., Busnel, J.-P., Durand, D. Study of junction zones in gelatin gels through selective enzymatic digestion. *Polymer* **32**, 2680 (1991).
65. Yakimets, I., Wellner, N., Smith, A.C., Wilson, R.H., Farhat, I., Mitchell, J. Mechanical properties with respect to water content of gelatin films in glassy state. *Polymer* **46**, 12577-12585 (2005).
66. Dai, C.-A., Liu, M.-W. The effect of crystallinity and aging enthalpy on the mechanical properties of gelatin films. *Materials Science and Engineering: A* **423**, 121-127 (2006).
67. Chiou, B.-S., Avena-Bustillos, R.J., Bechtel, P.J., Jafri, H., Narayan, R., Imam, S.H., Glenn, G.M., Orts, W.J. Cold water fish gelatin films: Effects of cross-linking on thermal, mechanical, barrier, and biodegradation properties. *European Polymer Journal* **44**, 3748 (2008).
68. Choy, Y.B., Cheng, F., Choi, H., Kim, K. Monodisperse gelatin microspheres as a drug delivery vehicle: Release profile and effect of crosslinking density. *Macromolecular Bioscience* **8**, 758-765 (2008).
69. Yakimets, I., Paes, S.S., Wellner, N., Smith, A.C., Wilson, R.H., Mitchell, J.R. Effect of water content on the structural reorganization and elastic properties of biopolymer films: a comparative study. *Biomacromolecules* **8**, 1710-1722 (2007).
70. Dreesmann, L., Ahlers, M., Schlosshauer, B. The pro-angiogenic characteristics of a cross-linked gelatin matrix. *Biomaterials* **28**, 5536-5543 (2007).
71. Liu, X., Smith, L.A., Hu, J., Ma, P.X. Biomimetic nanofibrous gelatin/apatite composite scaffolds for bone tissue engineering. *Biomaterials* **30**, 2252-2258 (2009).
72. Draye, J.-P., Delaey, B., Voorde, A.V.D., Bulcke, A.V.D., Reu, B.D., Schacht, E. In vitro and in vivo biocompatibility of dextran dialdehyde cross-linked gelatin hydrogel films. *Biomaterials* **19**, 1677-1687 (1998).

73. Digenis, G.A., Gold, T.B., Shah, V.P. Cross-linking of gelatin capsules and its relevance to their in-vitro in-vivo performance. *Journal of Pharmaceutical Sciences* **83**, 915-921 (1994).
74. M. J. Zohuriaan-Mehr, A.P., H. Salimi and M. Kurdtabar Protein- and homo poly(amino acid)-based hydrogels with super-swelling properties. *Polymer Advanced Technology* **20**, 655-671 (2009).
75. Kuijpers, A.J., Engbers, G.H.M., Feijen, J., De Smedt, S.C., Meyvis, T.K.L., Demeester, J., Krijgsveld, J., Zaat, S.A.J., Dankert, J. Characterization of the network structure of carbodiimide cross-linked gelatin gels. *Macromolecules* **32**, 3325-3333 (1999).
76. Marois, Y., Chakfé, N., Deng, X., Marois, M., How, T., King, M.W., Guidoin, R. Carbodiimide cross-linked gelatin: A new coating for porous polyester arterial prostheses. *Biomaterials* **16**, 1131-1139 (1995).
77. Fuchsbauer, H.-L., Gerber, U., Engelmann, J., Seeger, T., Sinks, C., Hecht, T. Influence of gelatin matrices cross-linked with transglutaminase on the properties of an enclosed bioactive material using [beta]-galactosidase as model system. *Biomaterials* **17**, 1481-1488 (1996).
78. Crescenzi, V., Francescangeli, A., Taglienti, A. New gelatin-based hydrogels via enzymatic networking. *Biomacromolecules* **3**, 1384-1391 (2002).
79. Chiou, B.-S., Avena-Bustillos, R.J., Bechtel, P.J., Jafri, H., Narayan, R., Imam, S.H., Glenn, G.M., Orts, W.J. Cold water fish gelatin films: Effects of cross-linking on thermal, mechanical, barrier, and biodegradation properties. *European Polymer Journal* **44**, 3748-3753 (2008).
80. Bigi, A., Cojazzi, G., Panzavolta, S., Rubini, K., Roveri, N. Mechanical and thermal properties of gelatin films at different degrees of glutaraldehyde crosslinking. *Biomaterials* **22**, 763-768 (2001).
81. Bigi, A., Bracci, B., Cojazzi, G., Panzavolta, S., Roveri, N. Drawn gelatin films with improved mechanical properties. *Biomaterials* **19**, 2335-2340 (1998).
82. Bigi, A., Cojazzi, G., Panzavolta, S., Roveri, N., Rubini, K. Stabilization of gelatin films by crosslinking with genipin. *Biomaterials* **23**, 4827-4832 (2002).
83. S. Dawlee, A. Sugandhi, Biji Balakrishnan, Labarre, D., Jayakrishnan, A. Oxidized chondroitin sulfate-cross-linked gelatin matrixes: A new class of hydrogels. *Biomacromolecules* **6**, 2040-2048 (2005).
84. Fan, H., Tao, H., Wu, Y., Hu, Y., Yan, Y., Luo, Z. Tgf-β3 immobilized plga-gelatin/chondroitin sulfate/hyaluronic acid hybrid scaffold for cartilage regeneration. *Journal of Biomedical Materials Research Part A* **95A**, 982–992 (2010).
85. Tronci, G., Neffe, A.T., Pierce, B.F., Lendlein, A. An entropy-elastic gelatin-based hydrogel system. *Journal of Materials Chemistry* **20**, 8875-8884 (2010).
86. Bertoldo, M., Bronco, S., Gragnoli, T., Ciardelli, F. Modification of gelatin by reaction with 1,6-diisocyanatohexane *Macromolecular Bioscience* **7**, 328-338 (2007).
87. Gattas-Asfura, K.M., Weisman, E., Andreopoulos, F.M., Micic, M., Muller, B., Sirpal, S., Pham, S.M., Leblanc, R.M. Nitrocinnamate-functionalized gelatin: Synthesis and smart hydrogel formation via photo-cross-linking. *Biomacromolecules* **6**, 1503-1509 (2005).
88. Hennink, W.E., Nostrum, C.F.V. Novel crosslinking methods to design hydrogels. *Advanced Drug Delivery Reviews* **54**, 13-36 (2002).
89. Sun, C.X., Mee, M.A.J.V.D., Goossens, J.G.P., Duin, M.V. Thermoreversible cross-linking of maleated ethylene/propylene copolymers using hydrogen-bonding and ionic interactions. *Macromolecules* **39**, 3441-3449 (2006).
90. Lehn, J.M. Supramolecular chemistry. *Science* **260**, 1762-1763 (1993).

91. Zayed, J.M., Nouvel, N., Rauwald, U., Scherman, O.A. Chemical complexity-supramolecular self-assembly of synthetic and biological building blocks in water. *Chemical Society Reviews* **39**, 2806-2816 (2010).
92. Sijbesma, R.P., Beijer, F.H., Brunsveld, L., Folmer, B.J.B., Hirschberg, J.H.K.K., Lange, R.F.M., Lowe, J.K.L., Meijer, E.W. Reversible polymers formed from self-complementary monomers using quadruple hydrogen bonding. *Science* **278**, 1601-1604 (1997).
93. Cordier, P., Tournilhac, F., Soulié-Ziakovic, C., Leibler, L. Self-healing and thermoreversible rubber from supramolecular assembly. *Nature* **451**, 977-980 (2008).
94. Holmes, T.C., De Lacalle, S., Su, X., Liu, G., Rich, A., Zhang, S. Extensive neurite outgrowth and active synapse formation on self-assembling peptide scaffolds. *Proceedings of the National Academy of Sciences of the United States of America* **97**, 6728-6733 (2000).
95. Dankers, P.Y.W., Harmsen, M.C., Brouwer, L.A., Luyn, M.J.A.V., Meijer, E.W. A modular and supramolecular approach to bioactive scaffolds for tissue engineering. *Nature Materials* **4**, 568-574 (2005).
96. Dillon, P.F., Root-Bernstein, R.S., Lieder, C.M. Molecular shielding of electric field complex dissociation. *Biophysical Journal* **90**, 1432-1438 (2006).
97. Matyjaszewski, K., Beers, K.L., Kern, A., Gaynor, S.G. Hydrogels by atom transfer radical polymerization. I. Poly(n-vinylpyrrolidinone-g-styrene) via the macromonomer method. *Journal of Polymer Science Part A: Polymer Chemistry* **36**, 823-830 (1998).
98. Mahler, A., Reches, M., Rechter, M., Cohen, S., Gazit, E. Rigid, self-assembled hydrogel composed of a modified aromatic dipeptide. *Advanced Materials* **18**, 1365-1370 (2006).
99. Madbouly, S.A., Lendlein, A. Shape-memory polymer composites. *Shape-Memory Polymers* **226**, 41-95 (2010).
100. Fu, S.-Y., Feng, X.-Q., Lauke, B., Mai, Y.-W. Effects of particle size, particle/matrix interface adhesion and particle loading on mechanical properties of particulate-polymer composites. *Composites Part B: Engineering* **39**, 933-961 (2008).
101. Alexandre, M., Dubois, P. Polymer-layered silicate nanocomposites: Preparation, properties and uses of a new class of materials. *Materials Science and Engineering: R: Reports* **28**, 1-63 (2000).
102. Lau, K.-T., Gu, C., Hui, D. A critical review on nanotube and nanotube/nanoclay related polymer composite materials. *Composites Part B: Engineering* **37**, 425-436 (2006).
103. Padilla, S., Izquierdo-Barba, I., Vallet-Regí, M. High specific surface area in nanometric carbonated hydroxyapatite. *Chemistry of Materials* **20**, 5942-5944 (2008).
104. Kilian, O., Wenisch, S., Karnati, S., Baumgart-Vogt, E., Hild, A., Fuhrmann, R., Jonuleit, T., Dingeldein, E., Schnettler, R., Franke, R.-P. Observations on the microvasculature of bone defects filled with biodegradable nanoparticulate hydroxyapatite. *Biomaterials* **29**, 3429-3437 (2008).
105. Thein-Han, W.W., Shah, J., Misra, R.D.K. Superior in vitro biological response and mechanical properties of an implantable nanostructured biomaterial: Nanohydroxyapatite-silicone rubber composite. *Acta Biomaterialia* **5**, 2668-2679 (2009).
106. Thein-Han, W.W., Misra, R.D.K. Biomimetic chitosan-nanohydroxyapatite composite scaffolds for bone tissue engineering. *Acta Biomaterialia* **5**, 1182-1197 (2009).
107. Cimerman, M., Cör, A., Čveh, M., Kristan, A., Pižvem, J., Tonin, M. Microstructural analysis of implant-bone interface of hydroxyapatite-coated and uncoated schanz screws. *Journal of Materials Science: Materials in Medicine* **16**, 627-634 (2005).

108. Davies, J.E. Bone bonding at natural and biomaterial surfaces. *Biomaterials* **28**, 5058-5067 (2007).
109. Hayakawa, T., Mochizuki, C., Hara, H., Fukushima, T., Yang, F., Shen, H., Wang, S., Sato, M. Influence of apatite crystallinity in porous plga/apatite composite scaffold on cortical bone response. *Journal of Hard Tissue Biology* **18**, 7-12 (2009).
110. Chuenjitkuntaworn, B., Inrung, W., Damrongsri, D., Mekaapiruk, K., Supaphol, P., Pavasant, P. Polycaprolactone/hydroxyapatite composite scaffolds: Preparation, characterization, and in vitro and in vivo biological responses of human primary bone cells. *Journal of Biomedical Materials Research Part A* **94A**, 241-251.
111. Castell, P., Wouters, M., De with, G., Fischer, H., Huijs, F., Vol. 92 2341-2350 (Wiley Subscription Services, Inc., A Wiley Company, 2004).
112. Samuel, J., Raccurt, O., Poncelet, O., Auger, A., Ling, W.-L., Cherns, P., Grunwald, D., Tillement, O. Surface characterizations of fluorescent-functionalized silica nanoparticles: From the macroscale to the nanoscale. *Journal of Nanoparticle Research* **12**, 2255-2265 (2005).
113. Thio, Y.S., Argon, A.S., Cohen, R.E. Role of interfacial adhesion strength on toughening polypropylene with rigid particles. *Polymer* **45**, 3139-3147 (2004).
114. Tlatlik, H., Simon, P., Kawska, A., Zahn, D., Kniep, R. Biomimetic fluorapatite-gelatine nanocomposites: Pre-structuring of gelatine matrices by ion impregnation and its effect on form development. *Angewandte Chemie-International Edition* **45**, 1905-1910 (2006).
115. Zahn, D., Hochrein, O., Kawska, A., Brickmann, J., Kniep, R. Towards an atomistic understanding of apatite–collagen biomaterials: Linking molecular simulation studies of complex-, crystal- and composite-formation to experimental findings. *Journal of Materials Science* **42**, 8966-8973 (2007).
116. Zhang, L., Lin, J. Hierarchically ordered nanocomposites self-assembled from linear-alternating block copolymer/nanoparticle mixture. *Macromolecules* **42**, 1410-1414 (2009).
117. Theodorou, D.N., Suter, U.W. Detailed molecular structure of a vinyl polymer glass. *Macromolecules* **18**, 1467-1478 (1985).
118. Hofmann, D., Fritz, L., Ulbrich, J., Schepers, C., Böhning, M. Detailed-atomistic molecular modeling of small molecule diffusion and solution processes in polymeric membrane materials. *Macromolecular Theory and Simulations* **9**, 293-327 (2000).
119. Zhou, J., Nicholson, T.M., Davies, G.R., Ward, I.M. Towards first-principles modelling of the mechanical properties of oriented poly(ethylene terephthalate). *Computational and Theoretical Polymer Science* **10**, 43-51 (2000).
120. Raaska, T., Niemela, S., Sundholm, F. Atom-based modeling of elastic-constants in amorphous polystyrene. *Macromolecules* **27**, 5751-5757 (1994).
121. Stultz, C.M. The folding mechanism of collagen-like model peptides explored through detailed molecular simulations. *Protein Science* **15**, 2166-2177 (2006).
122. Vaidyanathan, J., Vaidyanathan, T.K., Yadav, P., Linaras, C.E. Collagen-ligand interaction in dentinal adhesion: Computer visualization and analysis. *Biomaterials* **22**, 2911-2920 (2001).
123. Madhan, B., Thanikaivelan, P., Subramanian, V., Rao, J.R., Nair, B.U., Ramasami, T. Molecular mechanics and dynamics studies on the interaction of gallic acid with collagen-like peptides. *Chemical Physics Letters* **346**, 334-340 (2001).
124. Liu, X., Smith, L.A., Hu, J., Ma, P.X. Biomimetic nanofibrous gelatin/apatite composite scaffolds for bone tissue engineering. *Biomaterials* **30**, 2252-2258 (2009).
125. Bigi, A., Panzavolta, S., Rubini, K. Relationship between triple-helix content and mechanical properties of gelatin films. *Biomaterials* **25**, 5675-5680 (2004).

126. Feng, Y.K., Behl, M., Kelch, S., Lendlein, A. Biodegradable multiblock copolymers based on oligodepsipeptides with shape-memory properties. *Macromolecular Bioscience* **9**, 45-54 (2009).
127. Neffe, A.T., Zaupa, A., Pierce, B.F., Hofmann, D., Lendlein, A. Knowledge-based tailoring of gelatin-based materials by functionalization with tyrosine-derived groups. *Macromolecular Rapid Communications* **31**, 1534-1539 (2010).
128. Chen, X., Jia, Y., Sun, S., Feng, L., An, L. Performance inhomogeneity of gelatin during gelation process. *Polymer* **50**, 6186-6191 (2009).
129. Sheihet, L., Piotrowska, K., Dubin, R.A., Kohn, J., Devore, D. Effect of tyrosine-derived triblock copolymer compositions on nanosphere self-assembly and drug delivery. *Biomacromolecules* **8**, 998-1003 (2007).
130. Tangpasuthadol, V., Pendharkar, S.M., Kohn, J. Hydrolytic degradation of tyrosine-derived polycarbonates, a class of new biomaterials. Part i: Study of model compounds. *Biomaterials* **21**, 2371-2378 (2000).
131. Nahmany, M., Melman, A. Chemoselectivity in reactions of esterification. *Organic & Biomolecular Chemistry* **2**, 1563-1572 (2004).
132. Entrialgo-Castano, M., Lendlein, A., Hofmann, D. Molecular modeling investigations of dry and two water-swollen states of biodegradable polymers. *Advanced Engineering Materials* **8**, 434-439 (2006).
133. Hofmann, D., Heuchel, M., Yampolskii, Y., Khotimskii, V., Shantarovich, V. Free volume distributions in ultrahigh and lower free volume polymers: Comparison between molecular modeling and positron lifetime studies. *Macromolecules* **35**, 2129-2140 (2002).
134. Zaupa, A., Neffe, A.T., Pierce, B.F., Lendlein, A., Hofmann, D. A molecular dynamic analysis of gelatin as an amorphous material: Prediction of mechanical properties of gelatin systems. *The International Journal of Artificial Organs* **34**, 139 - 151 (2011).
135. Theodorou, D.N., Suter, U.W. Atomistic modeling of mechanical properties of polymeric glasses. *Macromolecules* **19**, 139-154 (1986).
136. Reddy, A.S., Sastry, G.N. Cation [m = h^+, li^+, na^+, k^+, ca^{2+}, mg^{2+}, nh_4^+, and nme_4^+] interactions with the aromatic motifs of naturally occurring amino acids: A theoretical study. *Journal of Physical Chemistry A* **109**, 8893-8903 (2005).
137. Montero, A., Mann, E., Chana, A., Herradón, B. Peptide-biphenyl hybrids as calpain inhibitors. *Chemistry & Biodiversity* **1**, 442-457 (2004).
138. Zhang, Q., Tian, M., Wu, Y., Lin, G., Zhang, L. Effect of particle size on the properties of $mg(oh)_2$-filled rubber composites. *Journal of Applied Polymer Science* **94**, 2341-2346 (2004).
139. Nakamura, Y., Yamaguchi, M., Okubo, M., Matsumoto, T. Effects of particle size on mechanical and impact properties of epoxy resin filled with spherical silica. *Journal of Applied Polymer Science* **45**, 1281-1289 (1992).
140. Inc., A.S. Discovery studio modeling environment, release 2.1 (Accelrys Software Inc., San Diego; 2007).
141. Bubnis, W.A., Ofner, C.M. The determination of epsilon-amino groups in soluble and poorly soluble proteinaceous materials by a spectrophotometric method using trinitrobenzenesulfonic acid. *Analytical Biochemistry* **207**, 129-133 (1992).
142. Reinhard Schrieber, H.G. (ed.) Gelatine handbook: Theory and industrial practice. (Wiley-VCH, 2007).
143. Miller, M.H., Némethy, G., Scheraga, H.A. Calculation of the structures of collagen models. Role of interchain interactions in determining the triple-helical coiled-coil conformation. 2. Poly(glycyl-prolyl-hydroxyprolyl). *Macromolecules* **13**, 470-478 (1980).

144. Inc., A.S. Material studio modeling environment, release 4.3. (Accelrys Software Inc., San Diego; 2008).
145. Arvanitoyannis, I., Nakayama, A., Aiba, S.-I.A. Edible films made from hydroxypropyl starch and gelatin and plasticized by polyols and water. *Carbohydrate Polymers* **36**, 105-119 (1998).
146. Heuchel, M., Hofmann, D., Pullumbi, P. Molecular modeling of small-molecule permeation in polyimides and its correlation to free-volume distributions. *Macromolecules* **37**, 201-214 (2003).
147. Hofmann, D., Entrialgo-Castano, M., Lerbret, A., Heuchel, M., Yampolskii, Y. Molecular modeling investigation of free volume distributions in stiff chain polymers with conventional and ultrahigh free volume: Comparison between molecular modeling and positron lifetime studies. *Macromolecules* **36**, 8528-8538 (2003).
148. Flory, P.J., Rehner, J. Statistical mechanics of cross-linked polymer networks i rubberlike elasticity. *Journal of Chemical Physics* **11**, 512-520 (1943).
149. Bubnis, W.A., Iii, C.M.O. The determination of amino groups in soluble and poorly soluble proteinaceous materials by a spectrophotometric method using trinitrobenzene sulfonic acid. *Analytical Biochemistry* **207**, 129 (1992).
150. Bordwell, F.G., Mccallum, R.J., Olmstead, W.N. Acidities and hydrogen bonding of phenols in dimethyl sulfoxide. *The Journal of Organic Chemistry* **49**, 1424-1427 (1984).
151. Pinhas, M.F., Blanshard, J.M.V., Derbyshire, W., Mitchell, J.R. *Therm. Anal. Calorim.* **47**, 1499 (1996).
152. Pezron, I., Djabourov, M. X-ray diffraction of gelatin fibers in the dry and swollen states. *J Polym Sci, Part B* **28**, 1823 (1990).
153. Itoh M, Okawa Y. , Kobayashi H., Ohno T., Okamoto Y., T., K. The effect of the thermal history on the gelation of gelatin solution. *Journal of Photographic Science* **42**, 14-17 (1994).
154. Brodsky, B., Thiagarajan, G., Madhan, B., Kar, K. Triple-helical peptides: An approach to collagen conformation, stability, and self-association. *Biopolymers* **89**, 345-353 (2008).
155. Courty, S., Gornall, J.L., Terentjev, E.M. Mechanically induced helix-coil transition in biopolymer networks. *Biophysical Journal* **90**, 1019-1027 (2006).
156. Rivero, S., García, M.A., Pinotti, A. Correlations between structural, barrier, thermal and mechanical properties of plasticized gelatin films. *Innovative Food Science & Emerging Technologies* **11**, 369-375 (2010).
157. Sarti, B., Scandola, M. Viscoelastic and thermal properties of collagen/poly(vinyl alcohol) blends. *Biomaterials* **16**, 785-792 (1995).
158. Lorén, N., Hermansson, A.-M. Phase separation and gel formation in kinetically trapped gelatin/maltodextrin gels. *International Journal of Biological Macromolecules* **27**, 249-262 (2000).
159. Gomez-Estaca, J., Montero, P., Fernandez-Martin, F., Gomez-Guillen, M.C. Physico-chemical and film-forming properties of bovine-hide and tuna-skin gelatin: A comparative study. *Journal of Food Engineering* **90**, 480 (2009).
160. Pinhas, M.F., Blanshard, J.M.V., Derbyshire, W., Mitchell, J.R. The effect of water on the physicochemical and mechanical properties of gelatin. *Journal of Thermal Analysis and Calorimetry* **47**, 1499-1511 (1996).
161. Pezron, I., Djabourov, M., Bosio, L., Leblond, J. X-ray diffraction of gelatin fibers in the dry and swollen states. *Journal of Polymer Science Part B: Polymer Physics* **28**, 1823-1839 (1990).
162. Löbus, A. Processing and characterization of hydroxyapatite/gelatin bioresorbable composite for bone tissue engineering. *Diploma thesis* Friedrich-Schiller-Universität

Jena (Oberflächen-und Grenzflächentechnologien)/GKSS Forschungszentrum für Biomaterialien (Teltow) (Feb. 2010).
163. Neffe, A.T., Löbus, A., Zaupa, A., Stoetzel, C., Müller, F.A., Lendlein, A. Gelatin functionalization with tyrosine derived moieties to increase the interaction with hydroxyapatite fillers. *Acta Biomaterialia* **7**, 1693-1701 (2011).
164. Tampieri, A., Celotti, G., Landi, E., Sandri, M., Roveri, N., Falini, G. Biologically inspired synthesis of bone-like composite: Self-assembled collagen fibers/hydroxyapatite nanocrystals. *Journal of Biomedical Materials Research Part A* **67A**, 618-625 (2003).
165. Teng, S., Shi, J., Peng, B., Chen, L. The effect of alginate addition on the structure and morphology of hydroxyapatite/gelatin nanocomposites. *Composites Science and Technology* **66**, 1532-1538 (2006).
166. Young, A.M., Ho, S.M., Abou Neel, E.A., Ahmed, I., Barralet, J.E., Knowles, J.C., Nazhat, S.N. Chemical characterization of a degradable polymeric bone adhesive containing hydrolysable fillers and interpretation of anomalous mechanical properties. *Acta Biomaterialia* **5**, 2072-2083 (2009).
167. Peroglio, M., Gremillard, L., Eglin, D., Lezuo, P., Alini, M., Chevalier, J. Evaluation of a new press-fit in situ setting composite porous scaffold for cancellous bone repair: Towards a "Surgeon-friendly" Bone filler? *Acta Biomaterialia* **6**, 3808-3812 (2010).
168. Hofmann, D., Entrialgo-Castano, M., Kratz, K., Lendlein, A. Knowledge-based approach towards hydrolytic degradation of polymer-based biomaterials. *Advanced Materials* **21**, 3237-3245 (2009).
169. Kirkpatrick, C., Bittinger, F., Wagner, M., Köhler, H., Kooten, T.V., Klein, C., Otto, M. Current trends in biocompatibility testing. *Proceedings of the Institution of Mechanical Engineers. Part H, Journal of engineering in medicine* **212**, 75-84 (1998).
170. Hanks, C.T., Wataha, J.C., Sun, Z. In vitro models of biocompatibility: A review. *Dental Materials* **12**, 186-193 (1996).
171. Maple, J.R., Hwang, M.-J., Jalkanen, K.J., Stockfisch, T.P., Hagler, A.T. Derivation of class ii force fields: V. Quantum force field for amides, peptides, and related compounds. *Journal of Computational Chemistry* **19**, 430-458 (1998).
172. Cöulfen, H., Borchard, W. Determination of the partial specific volumes of thermoreversible gelatin/water and kappa-carrageenan/water gels. *Macromolecular Chemistry and Physics* **195**, 1165-1175 (1994).
173. Berendsen, H.J.C., Postma, J.P.M., Van Gunsteren, W.F., Dinola, A., Haak, J.R. Molecular dynamics with coupling to an external bath. *The Journal of Chemical Physics* **81**, 3684-3690 (1984).
174. Andersen, H.C. Molecular dynamics simulations at constant pressure and/or temperature. *The Journal of Chemical Physics* **72**, 2384-2393 (1980).
175. Hofmann, D., Weigel, P., Ganster, J., Fink, H.P. Rdf investigations on concentrated-solutions of poly(para-phenylene-1,3,4-oxadiazole) in sulfuric-acid. *Polymer* **32**, 284-289 (1991).
176. Belmares, M., Blanco, M., W. A. Goddard, I., Ross, R.B., Caldwell, G., Chou, S.H., Pham, J., Olofson, P.M., Cristina, T. Hildebrand and hansen solubility parameters from molecular dynamics with applications to electronic nose polymer sensors. *Journal of Computational Chemistry* **25**, 1814-1826 (2004).
177. Lendlein, A., Schmidt, A.M., Langer, R. Ab-polymer networks based on oligo(é›-caprolactone) segments showing shape-memory properties. *Proceedings of the National Academy of Sciences of the United States of America* **98**, 842-847 (2001).
178. Maple, J.R., Dinur, U., Hagler, A.T. Derivation of force fields for molecular mechanics and dynamics from ab initio energy surfaces. *Proceedings of the National Academy of Sciences of the United States of America* **85**, 5350-5354 (1988).

179. Wilson, V.E.B., Decius, J.C., Cross, P.C. Molecular vibrations: The theory of infrared and raman vibrational spectra. (Courier Dover Publications, New York; 1980).
180. Verlet, L. Computer experiments on classical fluids. I. Thermodynamical properties of Lennard-Jones molecules. *Physycal Review* **159**, 98-103 (1967).
181. Hoover, W.G. Canonical dynamics: Equilibrium phase-space distributions. *Journal of Chemical Physics* **31**, 1695--1697 (1985).
182. Flory, P.J. Statistical mechanics of chain molecules, Vol. Chapter III. (Hanser, Munich; 1989).
183. Leach, A.R. Molecular modelling: Principles and applications, Edn. 2nd. (Pearson Education Limited, 2001).